

<b>Non hermetic RF MEMS</b>	<b>Ref: ASP-06-BO/PH/EA-45</b>		
	DATE : 1/03/06	ED/REV :V10	PAGE : 1 / 89

<b>Titre / Title</b>
<b>Final report</b>
<b>ESA contract n°17161/03/NL/PA</b>

<i>Written by</i>	<i>Responsabilité-Société/ Responsibility-Company</i>
A. Crunteanu/P. Blondy	CNRS-IRCOM, RF-MEMS design fabrication and test
O. Vendier	AAS, Technical manager of the contract

ESA Technical Officer : Laurent Marchand

<b>Non hermetic RF MEMS</b>	<b>Ref: ASP-06-BO/PH/EA-45</b>		
	DATE : 1/03/06	ED/REV :V10	PAGE : 2 / 89

## Table of contents

<b>1. INTRODUCTION.....</b>	<b>8</b>
<b>2. SUMMARY .....</b>	<b>8</b>
<b>3. RELIABILITY BACKGROUND.....</b>	<b>9</b>
<b>4. OBJECTIVE OF THE STUDY .....</b>	<b>10</b>
4.1. HYDROPHOBIC SURFACE TREATMENT OF RF MEMS SWITCHES .....	11
4.2. CAPACITIVE SWITCHES WITHOUT DIELECTRICS .....	11
<b>5. POSSIBLE <math>\mu</math>SWITCH MISSION .....</b>	<b>12</b>
5.1. GENERAL OVERVIEW.....	12
5.2. RF MEMS SWITCHES FOR APPLICATION TO MICROWAVE EQUIPMENT .....	13
▪ <i>Redundancy for low level, low noise, high frequency amplification stage</i> .....	13
5.3. APPLICATION TO SPACE SATELLITE ANTENNAS .....	14
▪ <i>Controllable reflect array</i> : .....	15
▪ <i>High power handling capabilities, low-loss phase-shifters</i> : .....	15
5.4. STUDY CASE SPECIFICATION.....	16
▪ <i>Study case 1 : RF MEMS within microwave equipments for redundancy applications</i> .....	16
▪ <i>Study case 2 : RF MEMS within antenna equipments (worst environmental case - GEO mobile spot-)</i> .....	17
<b>6. RELIABILITY CONCERNS.....</b>	<b>18</b>
6.1. RELIABILITY CONCERNS FOR STUDY CASE 1 .....	18
6.2. MAIN ENVIRONMENTAL TESTS USED FOR SPACE MICROWAVE PRODUCTS (GEO SATELLITE) : .....	19
6.3. MAIN ENVIRONMENTAL TESTS USED FOR SPACE ANTENNA PRODUCTS (GEO SATELLITE) : .....	20
6.4. GENERIC MEMS SWITCH FAILURE MECHANISM .....	22
<b>7. DESIGN, LAYOUT CONCEPT AND SIMULATION OF <math>\mu</math>SWITCH INTRODUCTION .....</b>	<b>24</b>
7.1. CAPACITIVE SWITCH .....	25
7.1.1. <i>Mechanical aspects</i> .....	26
7.1.2. <i>Electrical considerations</i> .....	29
7.2. CAPACITIVE SWITCH WITHOUT DIELECTRICS.....	32
7.3. CONCLUSION .....	33
<b>8. DIELECTRIC DEPOSITION SYSTEMS PRINCIPLE AND PRELIMINARY RESULTS .....</b>	<b>34</b>
8.1. THIN FILM DEPOSITION USING PULSED LASER ABLATION FOR RF AND MICROWAVE COMPONENTS .....	34
8.1.1. <i>Principle of Pulsed Laser Deposition</i> .....	34
8.1.2. <i>Basic experimental arrangement</i> .....	35
8.1.3. <i>Specificities of PLD compared to other deposition processes</i> .....	35
8.1.4. <i>Film deposition</i> .....	35
8.1.5. <i>Deposition of alumina films at room temperature</i> .....	36
8.1.6. <i>Deposition of CARBON (tetrahedral carbon - ta-C) films at room temperature</i> .....	36
8.2. THIN FILMS OBTAINED BY PLASMA ENHANCED CHEMICAL VAPOR DEPOSITION .....	38
8.3. EXPERIMENTAL RESULTS .....	40
8.3.1. <i>Results for PLD deposition</i> .....	40
8.3.2. <i>Results for PECVD deposition</i> .....	42
<b>9. RF MEMS MANUFACTURING OVERALL ASSESSMENT .....</b>	<b>45</b>
9.1. METAL BRIDGE DEPOSITION TECHNIQUES .....	45
9.2. OVERALL STATUS ON NEW DIELECTRIC DEPOSITION TECHNIQUES AND THEIR IMPACT ON RELIABILITY .....	53
9.3. DIELECTRICLESS CAPACITIVE SWITCH PROCESS EVOLUTION AND PERFORMANCE ASSESSMENT .....	57

<b>Non hermetic RF MEMS</b>	<b>Ref: ASP-06-BO/PH/EA-45</b>		
	DATE : 1/03/06	ED/REV :V10	PAGE : 3 / 89

9.4. OPTIMIZATION SCHEME USED AND DEVICE STATUS AVAILABLE FOR RELIABILITY TESTING ..... 59

**10. RELIABILITY ASSESSMENT..... 61**

10.1. SAMPLE AND DEVICE AVAILABILITY FOR TESTING ..... 61

10.2. TEST PLAN..... 62

    10.2.1. *Static S parameter measurements* ..... 64

    10.2.2. *Dynamic S parameter measurement* ..... 64

    10.2.3. *CV curves*..... 64

10.3. RELIABILITY TEST RESULTS..... 70

    10.3.1. *Thermal cycle tests*..... 71

    10.3.2. *Thermal storage tests*..... 72

    10.3.3. *Electrical endurance tests*..... 74

    10.3.4. *Total dose radiation test* ..... 78

10.4. CONCLUSION ON RF MEMS SWITCH RELIABILITY ASSESSMENT AND PERSPECTIVES ..... 85

**11. GENERAL CONCLUSION ..... 88**

<b>Non hermetic RF MEMS</b>	<b>Ref: ASP-06-BO/PH/EA-45</b>		
	DATE : 1/03/06	ED/REV :V10	PAGE : 4 / 89

## List of figures

FIGURE 1 : SCHEMATIC CROSS SECTION OF A SHUNT MEMS SWITCH .....	10
FIGURE 2 : CROSS SECTION OF TYPICAL CAPACITIVE SWITCH FABRICATED BY IRCOM.....	10
FIGURE 3 : CAPACITIVE $\mu$ SWITCH WITH CORRUGATED MEMBRANE.....	11
FIGURE 4 : MULTIMEDIA PAYLOAD TYPICAL BLOCK DIAGRAM .....	13
FIGURE 5 : SCHEMATICS OF ONE RF CHAIN WITH 2:1 REDUNDANCY.....	14
FIGURE 6 : CONTROLLABLE MEMS-BASED REFLECT ARRAY UNDER INVESTIGATION WITHIN ALCATEL SPACE .....	15
FIGURE 7 : SPDT IN 'FAIL-SAFE' DESIGN (SPST UNBIASED) .....	19
FIGURE 8 : MAIN CAPACITIVE SWITCH FAILURE MECHANISM.....	22
FIGURE 9 - SWITCH CROSS SECTION .....	25
FIGURE 10 – ON AND OFF STATE AND TOP VIEW OF THE SWITCH.....	26
FIGURE 11 - EVOLUTION OF THE SPRING CONSTANT AS A FUNCTION OF THE BRIDGE LENGTH.....	27
FIGURE 12 – STUDIED CONFIGURATION FOR THE CALCULATION OF THE RESTORING FORCE AND SIMULATION RESULTS FOR SEVERAL SACRIFICIAL LAYER THICKNESS .....	27
FIGURE 13 - INFLUENCE OF THE RESIDUAL STRESS ON THE PULL DOWN VOLTAGE ( $G_0=2\mu\text{m}$ ).....	28
FIGURE 14 - OFF STATE CAPACITANCE VALUE VERSUS BRIDGE HEIGHT, FOR DIFFERENT BRIDGE AREAS .....	30
FIGURE 15 - THEORETICAL ON/OFF RATIO OF THE SWITCH .....	30
FIGURE 16 - BASIC MASK CELL USED FOR THE SWITCH FABRICATION USING $\text{Al}_2\text{O}_3$ AS A DIELECTRIC ( $L =$ BRIDGE LENGTH, $w =$ BRIDGE WIDE, $W =$ CONTACT AREA LENGTH) .....	31
FIGURE 17 : PRINCIPLE OF THE CAPACITIVE AIR SWITCH.....	32
FIGURE 18 : CROSS SECTION OF THE STRUCTURE IN THE DOWN STATE .....	33
FIGURE 19: PLD PRINCIPLE.....	34
FIGURE 20 : FAST PHOTOGRAPH OF BST PLASMA PLUME .....	35
FIGURE 21 : SUBSTRATE OFF-AXIS ROTATION FOR UNIFORM SAMPLE COVERAGE .....	36
FIGURE 22: RESISTIVITIES OF TA AND NI DOPED CARBON FILMS.....	37
FIGURE 23: 5% NI-DOPED TA-C RESISTANCE.....	37
FIGURE 24 : PRINCIPLE OF PECVD DEPOSITION IN A POST-DISCHARGE CONFIGURATION .....	39
FIGURE 25 : CROSS SECTION OF AN $\text{Al}_2\text{O}_3$ FILM ON SI SUBSTRATE SHOWING THE COLUMNAR GROWTH (SCANNING ELECTRON MICROSCOPY IMAGE) .....	40
FIGURE 26: IMAGE OF THE PECVD DEPOSITION SYSTEM HIGHLIGHTING RELEVANT EXPERIMENTAL PARAMETERS. ....	42
FIGURE 27 : SURFACE ROUGHNESS (CALCULATED FROM AFM IMAGES) FOR TWO $\text{Al}_2\text{O}_3$ FILMS DEPOSITED IN DIFFERENT EXPERIMENTAL CONDITIONS: A) SAMPLE 4 ( $T = 300^\circ\text{C}$ , $p = 1 \text{ PA}$ ) WITH RA ROUGHNESS= 1.9NM AND B) SAMPLE 5 ( $T = RT$ , $p = 5 \text{ PA}$ ) WITH RA ROUGHNESS= 60.4 NM .....	43
FIGURE 28 : SCHEMATIC PICTURE A MEMS-RF DIELECTRIC SWITCH DESCRIBING THE COMPONENTS OF THE METALLIC MEMBRANE (CR IS USED HERE AS AN ALTERNATIVE TO TI, SEE BELOW) .....	45
FIGURE 29 : FABRICATION STEPS FOR MANUFACTURING THE MEMS-RF SWITCHES .....	46
FIGURE 30 : AFM MEASUREMENTS ( $2 \mu\text{m}^2$ -AREA AT LEFT AND $1 \mu\text{m}^2$ -AREA AT RIGHT) FOR A 150 NM-THICK EVAPORATED AU LAYER: A) AS-DEPOSITED AND B) AFTER AR-PLASMA TREATMENT FOR 10 MIN. ....	47
FIGURE 31 : RF MEASUREMENTS OF SWITCHES WITH PECVD ALUMINA (Cr/Au/Cr – 15/550/15 NM MEMBRANE, 8Hz, 70 V ACTUATION FREQUENCY AND VOLTAGE, SINUSOIDAL WAVEFORM).....	48
FIGURE 32 : RF MEASUREMENTS OF SWITCHES WITH PLD ALUMINA (Cr/Au/Cr – 15/550/15 NM MEMBRANE, 10Hz, 70 V ACTUATION FREQUENCY AND VOLTAGE, SINUSOIDAL WAVEFORM).....	48
FIGURE 33 : SHAPE OF THE MEMBRANE SECTIONS OBTAINED BY OPTICAL PROFILOMETRY FOR A 1.5 $\mu\text{m}$ -THICK GOLD ELECTROPLATED MEMBRANE WITH Cr/ Au (10/ 100 NM) SEED LAYERS. ....	49
FIGURE 34 : SHAPES OF MEMBRANE SECTIONS OBTAINED BY OPTICAL PROFILOMETRY FOR A 1.5 $\mu\text{m}$ -THICK GOLD ELECTROPLATED MEMBRANE WITH Ti/ Au (5/ 60 NM) SEED LAYERS. ....	49
FIGURE 35 : OPTICAL MICROSCOPY PICTURE OF MEMS SWITCHES WITH DIFFERENT DIMENSIONS (A) AND SCANNING ELECTRON MICROGRAPH (SEM) OF A TYPICAL METALLIC MICRO-MEMBRANE (B) WITH A CLOSER VIEW OF THE SUSPENDED BRIDGE OVER THE ACTUATION ELECTRODE (C) .....	50
FIGURE 36 : SHAPE OF THE METALLIC MEMBRANE SECTIONS OBTAINED BY OPTICAL PROFILOMETRY MEASUREMENTS.....	51
FIGURE 37 : MECHANICAL RESONANT FREQUENCY EVOLUTION WITH TEMPERATURE FOR A $240 \times 160 \mu\text{m}^2$ - AREA Ti/AU / Ti MEMBRANE. ....	52

<b>Non hermetic RF MEMS</b>	<b>Ref: ASP-06-BO/PH/EA-45</b>		
	DATE :	ED/REV :V10	PAGE :
	1/03/06		5 / 89

FIGURE 38 : TYPICAL LOADING-UNLOADING CURVES (APPLIED FORCE AS A FUNCTION OF THE MEMBRANE DEFORMATION) OBTAINED FROM NANOINDENTATION EXPERIMENTS FOR SPRING CONSTANT CALCULATIONS. .... 52

FIGURE 39 : ELECTROMECHANICAL SIMULATIONS USING ANSYS SHOWING DEFORMATION AND STRESS VALUES WHEN APPLYING A MECHANICAL FORCE IN THE CENTRE OF THE MEMBRANE. .... 53

FIGURE 40 : MIM-TYPE CAPACITANCES IMPLEMENTED IN A MICROWAVE COPLANAR WAVEGUIDE (CPW) LINE. .... 54

FIGURE 41 : CURRENT VERSUS APPLIED FIELD FOR A MIM-TYPE CAPACITANCE MADE OF ALUMINA/ TA-C (220/ 20 NM) SANDWICHED BETWEEN GOLD ELECTRODES..... 54

FIGURE 42 : FOURRIER TRANSFORMED IR (FT-IR) TRANSMISSION SPECTRUM OF A 1  $\mu\text{M}$ -THICK  $\text{Al}_2\text{O}_3$  FILM OBTAINED BY PLD AT ROOM TEMPERATURE; IT IS NOTICED THE ABSENCE OF OH- ABSORPTION BANDS BETWEEN 3400 AND 3600  $\text{cm}^{-1}$  ..... 55

FIGURE 43 : FOURRIER TRANSFORMED IR (FT-IR) TRANSMISSION SPECTRUM OF 200 NM-THICK  $\text{Al}_2\text{O}_3$  FILMS OBTAINED BY PECVD IN THE EXPERIMENTAL CONDITIONS DESCRIBED IN TABLE 2; IT IS NOTICED FOR THE "A-" AND "C-TYPE" SAMPLES THE PRESENCE OF ABSORPTION BANDS BETWEEN 3400 AND 3600  $\text{cm}^{-1}$  CORRESPONDING TO THE -OH GROUP ..... 56

FIGURE 44 : PRINCIPLE OF THE 2 STAGE SWITCH..... 58

FIGURE 45 : PROOF OF CONCEPT OF 2 STAGE AIR SWITCH ..... 58

FIGURE 46 : TYPICAL MEMS-RF SWITCH USED FOR S PARAMETERS MEASUREMENTS (LENGTH-280  $\mu\text{M}$ , WIDTH- 80  $\mu\text{M}$ , BOTTOM ELECTRODE WIDTH-120  $\mu\text{M}$ )..... 59

FIGURE 47 :  $S_{21}$  PARAMETER EVOLUTION DURING SWITCH ACTUATION WITH A SINUSOIDAL BI-POLAR WAVEFORM AT 5 Hz (SWITCH S35, 400 NM-THICK ALUMINA PECVD DIELECTRIC) ALONG WITH THE SIMULATED  $S_{21}$  RESPONSES IN THE UP- AND DOWN STATES. .... 59

FIGURE 48 :  $S_{21}$  PARAMETER EVOLUTION DURING SWITCH ACTUATION WITH A SINUSOIDAL BI-POLAR WAVEFORM AT 5 Hz (SWITCH S35, 400 NM-THICK ALUMINA PLD DIELECTRIC) ALONG WITH THE SIMULATED  $S_{21}$  RESPONSES IN THE UP- AND DOWN STATES. .... 60

FIGURE 49 :  $S_{21}$  PARAMETER EVOLUTION IN THE ACTUATED, DOWN STATE (SWITCH S35, 200 NM-THICK ALUMINA PLD DIELECTRIC) AND THE SIMULATED  $S_{21}$  RESPONSE. .... 61

FIGURE 50 : EXAMPLE OF MEASURED S PARAMETERS ON 400 NM  $\text{Al}_2\text{O}_3$  SWITCHES, BIPOLAR 5 KHz, AMPLITUDE 100 Vpp, AMBIENT ATMOSPHERE. GREEN CURVE IS IN DOWN POSITION, RED CURVE IS UP POSITION ..... 64

FIGURE 51 : THE HIGH ELECTRIC FIELDS APPLIED ON THE DIELECTRIC LAYERS DURING SWITCH ACTUATION CAN INDUCE CHARGING OR EVEN ELECTRICAL TRAP GENERATION WITHIN THE LAYER..... 65

FIGURE 52 : CHARGING INDUCED BUILT-IN POTENTIAL OPPOSING THE APPLIED ACTUATION VOLTAGE..... 65

FIGURE 53 : C(V) TEST SET-UP FOR RF-MEMS RELIABILITY. .... 66

FIGURE 54 : C(V) CHARACTERISTICS FOR A 200 NM-THICK DIELECTRIC  $\text{Al}_2\text{O}_3$  PLD SWITCH ACTUATED WITH A TRIANGULAR WAVEFORM (35 V AMPLITUDE, 270 Hz): A) DRIVING VOLTAGE AND DETECTED POWER VERSUS ACTUATION TIME, B) XY-TYPE CURVE OF THE DETECTED POWER VS. APPLIED VOLTAGE AND C) THE EQUIVALENT GRAPH SHOWING CAPACITANCE VARIATION VS; APPLIED VOLTAGE. .... 67

FIGURE 55 : C(V) CURVES TO BE USED AS AN EVALUATION TOOL FOR THE SWITCH DIELECTRIC (BLACK CURVE=REF, BLUE CURVE=AFTER  $10^6$  CYCLES)..... 67

FIGURE 56 : IMPACT OF CONTACT TIME IN DOWN STATE POSITION; EVOLUTION OF V PULL-IN AND PULL-OUT VS CONTACT TIME..... 68

FIGURE 57 : IMPACT OF FREQUENCY AND BIASING WAVEFORM ON 400 NM  $\text{Al}_2\text{O}_3$  PECVD, 39 V AMPLITUDE, BIPOLAR AND AMBIENT ATMOSPHERE AT VARIOUS FREQUENCIES. RIGHT SIDE SINUSOIDAL WAVEFORM, RIGHT SIDE TRIANGULAR WAVEFORM ..... 69

FIGURE 58 : HOMOGENEITY OF THE RESULTS FOR SWITCHES TAKEN FROM THE SAME WP3.4 REF. S54, S64, BIASING CONDITIONS : BIPOLAR +/-45 V ..... 70

FIGURE 59 : IMPACT OF 500 CYCLES (-55; 125  $^{\circ}\text{C}$ ) ON S PARAMETER OF SWITCH REF. S65 FROM WP3.1 TAKEN AT 2 LOCATIONS. BEFORE AGEING (RED (UP STATE), GREEN (DOWN STATE)) AND AFTER AGEING (GREY (UP STATE), BLUE (DOWN STATE))..... 71

FIGURE 60 : IMPACT OF 500 CYCLES (-55; 125  $^{\circ}\text{C}$ ) ON S PARAMETER OF SWITCH REF. S55 FROM WP3.1 TAKEN AT 2 LOCATIONS. BEFORE AGEING (RED (UP STATE), GREEN (DOWN STATE)) AND AFTER AGEING (GREY (UP STATE), BLUE (DOWN STATE))..... 72

FIGURE 61 : IMPACT OF 260 HRS STORAGE AT 125  $^{\circ}\text{C}$  ON S PARAMETER OF SWITCH REF. S65 FROM WP3.3 TAKEN AT 2 LOCATIONS. BEFORE AGEING (RED (UP STATE), GREEN (DOWN STATE)) AND AFTER AGEING (GREY (UP STATE), BLUE (DOWN STATE))..... 73

<b>Non hermetic RF MEMS</b>	<b>Ref: ASP-06-BO/PH/EA-45</b>		
	DATE :	ED/REV :V10	PAGE :
	1/03/06		6 / 89

FIGURE 62 : : IMPACT OF 260 HRS STORAGE AT 125 °C ON SWITCH REF. S55 FROM WP3.3 TAKEN AT 2 LOCATIONS. BEFORE AGEING (RED (UP STATE), GREEN (DOWN STATE)) AND AFTER AGEING (GREY (UP STATE), BLUE (DOWN STATE)) ..... 74

FIGURE 63 : AGING TEST APPLIED ONTO DIELECTRICLESS SWITCHES FROM WP4.1 ..... 75

FIGURE 64 : TYPICAL DIELECTRICLESS MEMS CAPACITIVE SWITCH (WP4.1) ..... 76

FIGURE 65 : 1/C(V) CHARACTERISTICS OF WP4.1 (DIELECTRIC LESS SWITCH) BEFORE AND AFTER ENDURANCE ON/OFF TESTING ..... 76

FIGURE 66: LIFE TIME DETERMINATION ON 400 NM AL<sub>2</sub>O<sub>3</sub> PECVD, 39 V AMPLITUDE, SQUARE WAVEFORM, BIPOLAR AND AMBIENT ATMOSPHERE AT VARIOUS FREQUENCIES. DETERMINATION OF LIFE TIME I.E. C<sub>MIN</sub> (C UP) AND C<sub>MAX</sub> (C DOWN) EVOLUTION VS NUMBER OF CYCLES ..... 77

FIGURE 67 : PICTURE OF THE WP READY TO BE IRRADIATED ..... 78

FIGURE 68 : BACKSIDE VIEW OF THE ESTEC Co SOURCE RADIATION CHAMBER ..... 79

FIGURE 69 : BIASING CONFIGURATION DURING IRRADIATION PHASE ..... 80

FIGURE 70 : 1/C(V) OF SWITCH REF. S35 WITH ALUMINA PECVD (WP2.2) (400 NM) – IRRADIATED WITH A TOTAL DOSE OF 43KRAD, UNBIASED CONDITIONS, TEST PERFORMED WITHOUT ANNEALING ..... 82

FIGURE 71 : 1/C(V) OF SWITCH REF. S35 WITH ALUMINA PLD (WP1.1) (400 NM) – IRRADIATED WITH A TOTAL DOSE OF 47KRAD, UNBIASED CONDITIONS, TEST PERFORMED WITHOUT ANNEALING ..... 83

FIGURE 72 : 1/C(V) OF DIELECTRICLESS SWITCH (WP4.1) REF. S63 IRRADIATED WITH A TOTAL DOSE OF 33 KRAD, UNBIASED CONDITIONS, TEST PERFORMED WITHOUT ANNEALING ..... 84

FIGURE 73 : 1/C(V) CURVES BEFORE AND AFTER SEVERAL TOTAL DOSE IRRADIATION STEPS OF 400 NM THICK AL<sub>2</sub>O<sub>3</sub> PECVD BASED SWITCHES ..... 87

FIGURE 74 : 1/C(V) CURVES BEFORE AND AFTER SEVERAL TOTAL DOSE IRRADIATION STEPS OF 400 NM THICK AL<sub>2</sub>O<sub>3</sub> PLD BASED SWITCHES ..... 87

FIGURE 75 : EXAMPLE OF SWITCH RECOVERY AFTER ANNEALING (168 H 25°C) AND FAILURE NOTICED AFTER 47 KRAD TOTAL DOSE ..... 88

<b>Non hermetic RF MEMS</b>	<b>Ref: ASP-06-BO/PH/EA-45</b>		
	DATE : 1/03/06	ED/REV :V10	PAGE : 7 / 89

### List of tables

TABLE 1 : SINE VIBRATION LEVELS .....	21
TABLE 2 : ACOUSTIC LOADS .....	22
TABLE 3 : OPERATION (CYCLING) CONDITIONS FOR FUTURE RF MEMS IN STUDY CASE 1 (*).....	23
TABLE 4 : OPERATION (CYCLING) CONDITIONS FOR FUTURE RF MEMS FOR USE IN STUDY CASE 2.....	23
TABLE 5 : OPERATION (CYCLING) CONDITIONS FOR FUTURE RF MEMS FOR USE IN STUDY CASE 2' .....	24
TABLE 6 : MICRO SWITCH DIMENSIONS .....	33
TABLE 7 : EXPERIMENTAL CONDITIONS AND RESULTS FOR PECVD ALUMINA FILMS.....	43
TABLE 8 : EXPERIMENTAL CONDITIONS AND RESULTS FOR PECVD-DEPOSITED AL <sub>2</sub> O <sub>3</sub> FILMS .....	44
TABLE 9 : BREAKDOWN VOLTAGE FOR AL <sub>2</sub> O <sub>3</sub> LAYERS OF DIFFERENT THICKNESS OBTAINED BY PLD AND PECVD .....	57
TABLE 10 : S35 MECHANICAL CHARACTERISTICS.....	82
TABLE 11 : EVOLUTION OF THE $V_{PULL-IN}/V_{PULL-OUT}$ VALUES (S35 SWITCH).....	82
TABLE 12 : EVOLUTION OF THE $V_{PULL-IN}/V_{PULL-OUT}$ VALUES (S35 SWITCH): .....	83
TABLE 13 : EVOLUTION OF THE $V_{PULL-IN}/V_{PULL-OUT}$ VALUES ( DIELECTRICLESS SWITCH REF 63):.....	84

<b>Non hermetic RF MEMS</b>	<b>Ref: ASP-06-BO/PH/EA-45</b>		
	DATE : 1/03/06	ED/REV :V10	PAGE : 8 / 89

## 1. INTRODUCTION

MEMS (Microelectromechanical Systems) technology plays a key role in the ongoing miniaturization of electronic modules and systems in the future telecommunications, earth observation and space exploration satellites and probes. While MEMS operating in the low-frequency region are currently being employed e. g. as acceleration sensors in automotive applications, the field of RF (radio frequency) MEMS is still in a state of research and early development. RF MEMS switches exhibit excellent RF properties as low insertion loss, low power consumption and high isolation. In addition, MEMS can very straightforwardly be integrated into RF submodules to achieve a higher degree of functionality, for example in phase shifters or power routing networks.

Space environment is a harsh environment as such, so that packaging constraints are applicable to the RF MEMS components. This constraints can then challenge the overall performance and life time of the device. Compliance with a large temperature range, mechanical vibrations and shock etc. has to be achieved not only by the single MEMS device but also by the packaged subsystems. Adapted packaging technology and reliability are one of the key issues for the application of MEMS technology in the aforementioned fields.

## 2. SUMMARY

This final report describes first the context of RF MEMS application within satellite payloads, followed by the specifications and conceptual design of the  $\mu$ switches to be fabricated within the study. It also presents the capacitive switch design methodology based on two approaches. The first one depends on standard shunt capacitive switches on coplanar wave (CPW) transmission lines using stiff bridges and various dielectrics. The dielectrics are deposited using two deposition system processes pulsed laser deposition (PLD) for Teflon, diamond like carbon (DLC) and  $Al_2O_3$ , and plasma enhanced chemical vapor deposition (PECVD) for  $Al_2O_3$ . Another approach which is very innovative was also used to realize dielectricless capacitive switches for which reliability concerns, such as dielectric charging shall be suppressed. Another section is also dedicated to overall RF MEMS process assessment, in order to clearly explain which dielectric and/or process sequence is applicable or not. This section is then ended by a table of RF-MEMS devices useable for preliminary reliability assessment. A test plan is presented and applied to the relevant RF MEMS switches. This test plan includes thermal storage, thermal cycling, accelerated aging and radiation total dose testing. Except for the radiation testing, focus was put on the most promising RF MEMS structures : dielectricless capacitive switches. Reliability results are then discussed. Finally, we have drawn up some conclusions and perspectives based on this study achievements.

<b>Non hermetic RF MEMS</b>	<b>Ref: ASP-06-BO/PH/EA-45</b>		
	DATE : 1/03/06	ED/REV :V10	PAGE : 9 / 89

### 3. RELIABILITY BACKGROUND

Electrical components with a mechanical functionality can have many failure modes not present in purely electrical components. Although a lot is known about failure modes in electrical systems, and ways of investigating them, this is not the case for micro-mechanical components. This is not only due to the relative recentness of the field of MEMS (micro-electromechanical systems), but also due to some inherent differences between electrical and mechanical failures. Most electrical failures are thermally activated, i.e. they will occur faster at elevated temperatures. This is a very convenient property of electrical failures, as increasing the temperature will accelerate the degradation, and therefore tests don't have to take too long. Also, the lifetime can be calculated rather easily. For most of the failure modes relevant to MEMS Arrhenius law usually do not apply. For example, mechanical failures are often not so temperature dependent. Accelerating the conditions in which a certain failure may occur may even decrease the failure rate of other failures. Some failures cannot be accelerated at all. This means that the field of mechanical reliability is, in a way, even more complex and demanding than that of electrical failures.

A lot of failure modes may cause a MEMS device to cease operation. However, some failures are more common to certain types of devices or structural parts than others, and therefore a prediction of the important failure modes can certainly be made. But before, we have to separate "process related" failure modes and «device related» failure modes. One have to pay attention that this 2 types of failure mode may interfere with each other. This is one of the big challenge of assessing the reliability of quite new technology. This fact somewhat justifies to have a first phase of technology assessment before we go into a more formal reliability test plan.

A literature survey conveys that there are four major players that govern the initial reliability of a metal micro-machined product in use: **stiction, creep, charging of dielectrics** and **electromigration**. Note that metal fatigue is not in the list; observations of Texas Instruments have made clear that metal fatigue due to long term mechanical stress cycling of micro-structures is not normally observed. Observed is only short-cycle fatigue the fracturing of metal parts under large mechanical stress within a relatively small number of cycles (usually less than a thousand). Other effects, inherent to the microscopic properties of MEMS devices, like some of those listed above, are more severe than we would expect from macroscopically known behavior.

Assuming a low level application for a space use of capacitive MEMS switch, stiction and charging of the dielectrics are the main failure modes noticed on the components that we have been able to test so far. These 2 failure modes will be addressed in this study through technological improvements such as :

- Hydrophobic surface treatment (teflon, DLC,...) and improved dielectric material intrinsic properties (Alumina, diamond like carbon,..),
- Contact less capacitive switch

With these 3 approaches we hope to improve the hardness of capacitive MEMS switch with regards to constraints related to thermal stress, voltage endurance and radiations.

<b>Non hermetic RF MEMS</b>	<b>Ref: ASP-06-BO/PH/EA-45</b>		
	DATE : 1/03/06	ED/REV :V10	PAGE : 10 / 89

#### 4. OBJECTIVE OF THE STUDY

As stated in the proposal, we propose to study one of the most popular shunt type switch and to apply either the 'right post treatment' to it, keeping a high level of performance, or to study a slight modification of its structure to remove the dielectric. In both cases, we hope to reduce required level of packaging needed to achieve a long lifetime of operation. We will not remove the need for a packaging, but we hope to reduce the constraint on this package. It could mean that a near hermetic packaging approach, using epoxy or any other high performance organic sealing materials could be acceptable, instead of having to go through a fully hermetic package.

A simplified cross section of the structure is shown below:

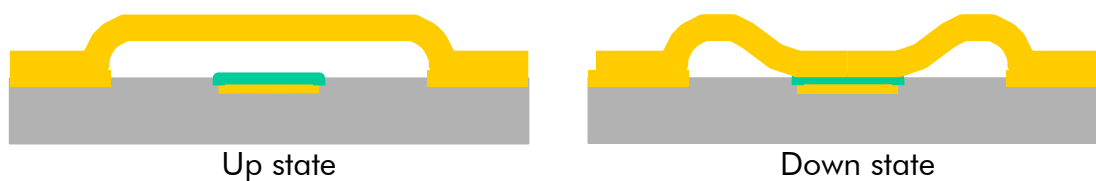


**Figure 1 : Schematic cross section of a shunt MEMS switch**

This type of switch is made on a CPW line where a metal bridge is laid over the structure, with an air gap between the center conductor and the bridge. When a voltage is applied between the bridge and the center conductor, the bridge closes down to the line (Down state), separated from the signal line by a thin dielectric layer. The large capacitance between the bridge and the line shorts the signal to the ground at high frequencies. The electrical and surface properties of the dielectric material under the bridge are of prime importance in the lifetime and the microwave performance of the switch. Work performed within this study will be focused on this dielectric layer.

For this study, we define as standard technology at IRCOM, the following switch as depicted in the following figure :

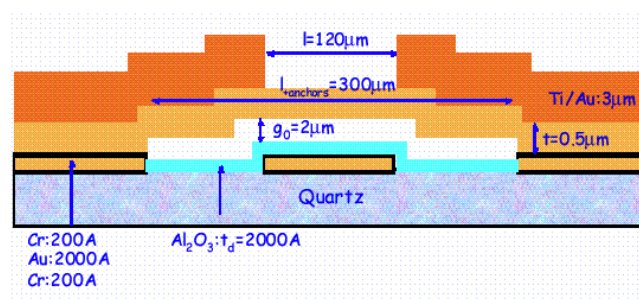


**Figure 2 : Cross section of typical capacitive switch fabricated by IRCOM**

This  $\mu$ switch technology consists in clamped-clamped beam approach, that uses a mixture of evaporated and plated gold to give membrane with tensile residual stresses. The dielectric

<b>Non hermetic RF MEMS</b>	<b>Ref: ASP-06-BO/PH/EA-45</b>		
	DATE : 1/03/06	ED/REV :V10	PAGE : 11 / 89

material used is alumina deposited either by laser ablation or PECVD. These switches can be processed either on high resistivity silicon or quartz.

We propose to study two approaches to enhance the lifetime of capacitive switches in non hermetic packages :

#### **4.1. HYDROPHOBIC SURFACE TREATMENT OF RF MEMS SWITCHES**

The layer is deposited using a Pulsed Laser Deposition system from a Teflon target, and results in a durable patternable hydrophobic layer. The second possibility is to use a thin Diamond Like Carbon coating which has interesting properties both for hydrophobia and wear resistance. Our approach is discussed in the following :

We will first fabricate MEMS switches with and without the hydrophobic treatments. Both teflon coated and DLC coated switches will be tested at microwave frequencies and compared with results obtained on a reference batch which uses only alumina as a dielectric. Conclusions will be drawn on the effects of the hydrophobic layer on the switch performance.

Next, the same two sets of switches will be tested in a laboratory environment with a significant level of humidity. At the same time, the non protected switches will be tested in a high vacuum environment.

The switch will be cycled up. The non-protected switches should fail quickly in humidity environment, but we will see the protected switches performances and will compare them with the same switches in a high vacuum environment. We should be able to conclude on the effects of the protection on the durability of the electrostatic actuated switches.

#### **4.2. CAPACITIVE SWITCHES WITHOUT DIELECTRICS**

In this part of the project we will study a corrugated version of the capacitive switch, that will allow to maintain a small air gap on between the bridge and the bottom electrode. With the standard, teflon coated and DLC coated  $\mu$ switch, this new approach will constitute another capacitive switch configuration addressed in this study. The structure is presented below.

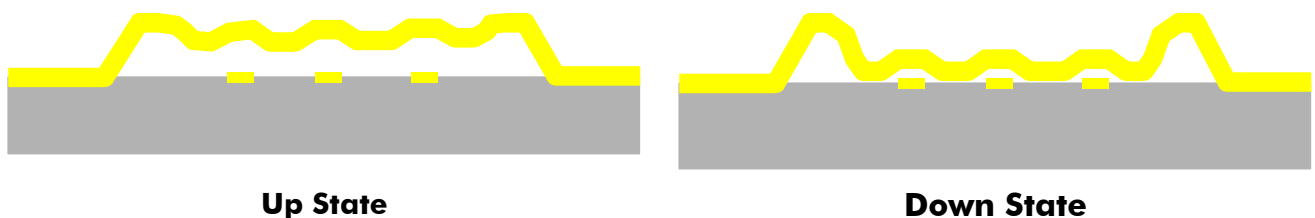


**Figure 3 : Capacitive  $\mu$ switch with corrugated membrane**

<b>Non hermetic RF MEMS</b>	<b>Ref: ASP-06-BO/PH/EA-45</b>		
	DATE :	<b>ED/REV :V10</b>	<b>PAGE :</b>
	1/03/06		12 / 89

The idea is to use the same techniques that are used to define small contacts points in an ohmic switch to create small corrugations in the bridge. When the bridge is down, there is a small air gap between the electrode and the bottom plate. In such a device, the up to down capacitance ratio will be less than the one obtained on a conventional switch. Note that for the best capacitive  $\mu$ switch with silicon nitride as a dielectric this ratio ranges from 40 to 100. Still, preliminary mechanical computations suggest that a ratio between 15 and 25 can be obtained, that could be sufficient to create high contrast MEMS switches. The main advantage of the structure is that it does not suffer from charging because it has no dielectric. Regarding stiction, it is reduced because the contact area is limited to the pillar area. Moreover this corrugated membrane could have an interesting mechanical behaviour that could make it less sensitive to temperature variations. Thus, the corrugation acts as a stress relaxation spring which compensate for thermally induced stresses.

At the end of the study, we will discuss the 4<sup>th</sup> proposed solutions analyzing their drawbacks and advantages, and comparing them with other solutions described in the literature.

## **5. POSSIBLE $\mu$ SWITCH MISSION**

### **5.1. GENERAL OVERVIEW**

In the last years, first in U.S., then in Europe, a high interest has raised about "RF-MEMS" in the Microwave & Antennas community, and a growing effort has been put on RF MEMS technology in academies and in several industrial companies involved in the Microwave market. Indeed, it has been proven, at first for switching applications, that MEMS technology could gather both advantages:

- of electro-mechanical devices: low insertion loss, high isolation, no DC consumption in steady-states (except very small one during short transient phases)....
- and those of micro-electronics: high compactness, manufacturing process derived from that of Integrated Circuits, so expected very low-cost when thousands of devices or sub-assemblies will be produced at large wafers level.

The RF-switch is the basis of many sub-assemblies: controllable phase-shifters, redundancy matrices, variable oscillators .... Besides, it has been quickly discovered that removing some thicker parts of the substrate (typically silicon), allows to create small cavities (basis for high-frequency filters), and air-suspended lines (inducing much lower RF-loss than other planar circuits).

So, combining switches and other passive low-loss and high-Q components, open the way to very compact, while performant, MEMS microwave assemblies.

## 5.2. RF MEMS SWITCHES FOR APPLICATION TO MICROWAVE EQUIPMENT

In the case of next generation of multimedia satellite payloads, as illustrated in the figure below, the need for « transparent » (in size and electrical performance) redundancy component is very critical since it might have strong constraints at subsystem level where high integration, high performance and low power consumption are put at a premium.

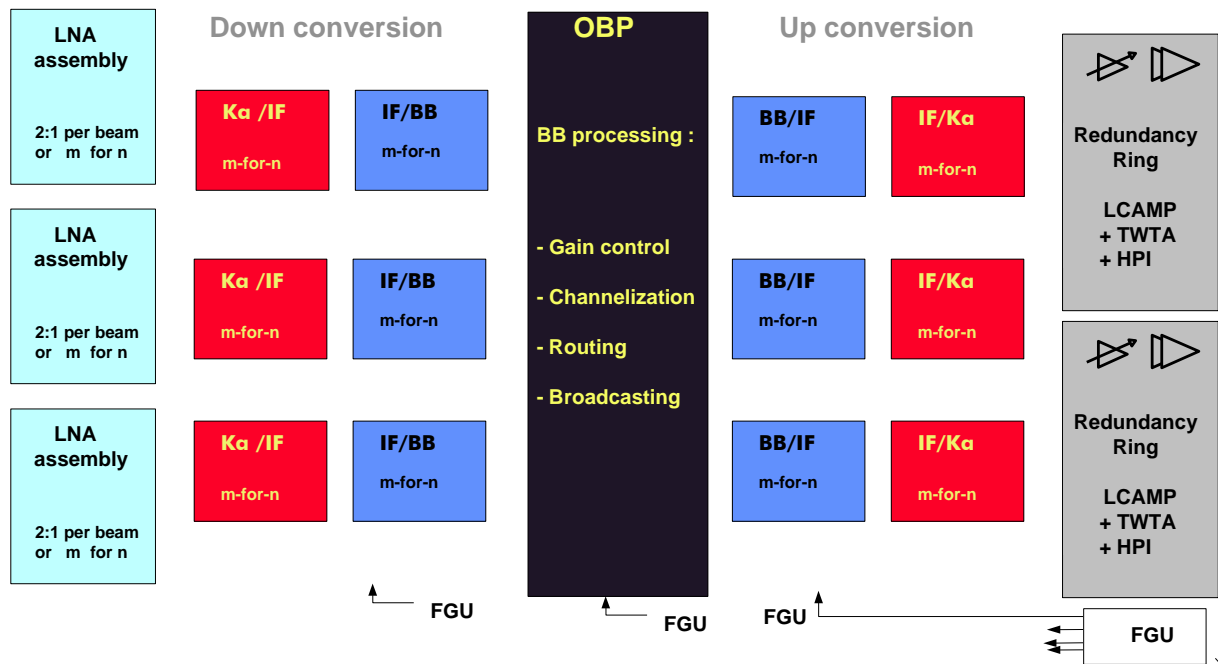


**Figure 4 : Multimedia payload typical block diagram**

- **Redundancy for low level, low noise, high frequency amplification stage**

One application where we have more experience for now, is related to 2 :1 redundancy scheme of LNA module for RX FAFR (Focal array fed reflector). It is linked to the lower constraints applied to the RF MEMS element since very low power is applied to it.

The RF chain for the LNA module is depicted in the figure below. It consists of the MEMS based SPDTs, one LNA filter (that could be distributed to match stringent constraints on the rejection level) and typically 2 LNA per signal path to achieve the dedicated gain in Ka or V band (respectively 30 GHz and 50 GHz).

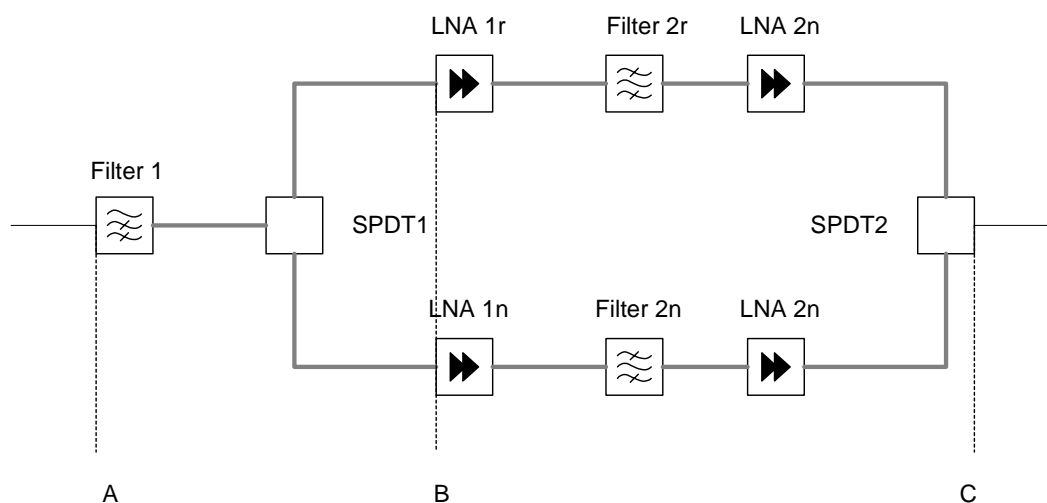


**Figure 5 : Schematics of one RF chain with 2:1 redundancy.**

To minimize the power constraints on the user segment, very strong constraint on  $G/T$  ratio are usually specified.

It results in very low insertion loss for the A to B section of the above figure. As a consequence, this constraint will induce the following optimization scheme at LNA module level:

- Low insertion loss of the SPDT
- Optimized packaging
- Short interconnect

With this basic discussion it is shown here that limiting the interconnect and microwave transition related to the protection of the RF MEMS switch, such as using a non hermetic wafer level package, will considerably help minimizing the insertion loss budget of the RF chain before the first LNA. Technology wise, this approach also applies to low level redundancy rings and  $\mu$ switch based matrices.

This application will be referred, in the following, as study case 1.

### **5.3. APPLICATION TO SPACE SATELLITE ANTENNAS**

As all controllable antennas need numerous identical RF-chains, they are one of the first applications field of MEMS technology but also one the most challenging due to strong environmental constraints (radiation, temperature,...) because they are located outside the spacecraft.

If performant controllable antennas can be produced at moderate cost, they could be largely used, especially in the field of Satellite Systems, either in the form of phased arrays, or of active focal arrays in reflector antennas. Indeed, from year to year, higher performances are required.

For future generation of telecom, observation and science satellites, it could be of interest :

<b>Non hermetic RF MEMS</b>	<b>Ref: ASP-06-BO/PH/EA-45</b>		
	DATE : 1/03/06	ED/REV :V10	PAGE : 15 / 89

-to re-optimize the antenna beams during the long life of geostationary spacecrafts; sometimes to scan quickly one or several beams: beam-hopping on GEO Communication satellite,

-to track fixed Earth stations for moving spacecrafts dedicated to Earth or Sky/stars Observation,

-to provide a constant on-ground foot-print for LEO constellations providing worldwide fast multimedia access

The most promising option for RF MEMS switches within antenna equipments that are currently investigated within Alcatel Space, are described in the following paragraphs.

- **Controllable reflect array :**

-It is either acting as a wide-scanning Direct Radiating Array with medium gain (for LEO Communications, or Data Transmission related to Earth Observation or remote Scientific missions)

-Or used as a re-configurable sub-reflector, within a high-gain dual-reflector antenna (for a GEO telecom satellite to match its coverage to the traffic evolution, or change in orbital position; or for compensating distortions of the main reflector in very high frequency applications).

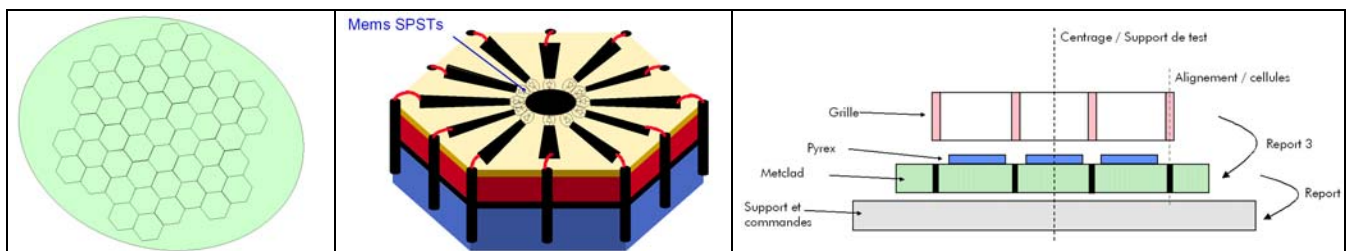


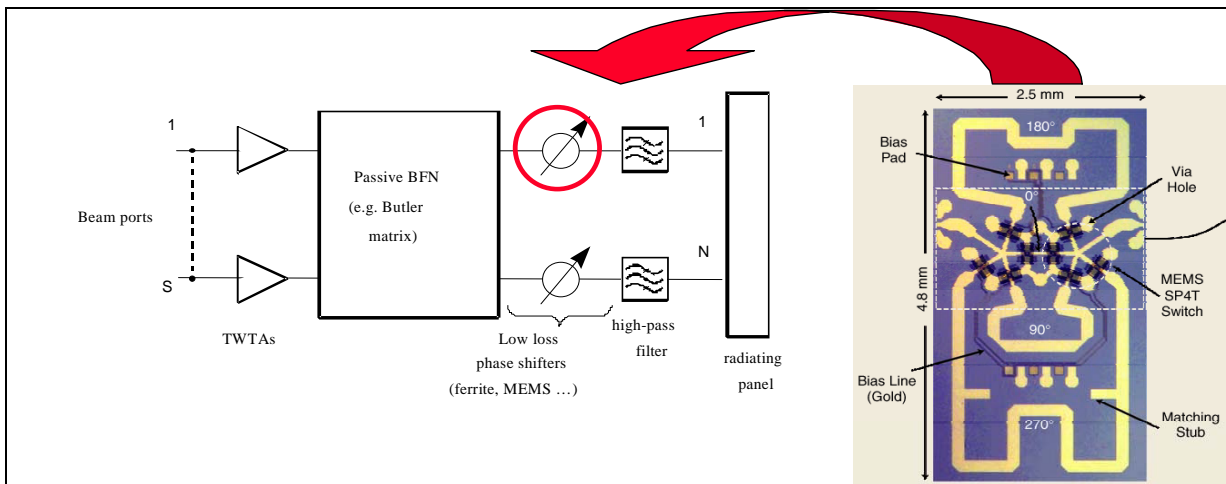
**Figure 6 : Controllable MEMS-based reflect array under investigation within Alcatel Space**

This application will be referred, in the following, as study case 2 (reconfigurable telecom, GEO mission) and 2' (Observation radar, LEO mission)

- **High power handling capabilities, low-loss phase-shifters :**

It is used for electronic self-pointing of a transmit Direct Radiating Array, providing the down-link from Satellite, for a mission providing numerous directive beams: as required in recent high rate Communication Systems at high frequency (Ku, Ka or Q bands).

Note that in this case, the phase shifters are located after the TWTA as illustrated in the following figure. As a result, strong RF power handling capability are needed for the RF MEMS switches. Activity in this area is still in preliminary stage within Alcatel Space, because of limited power handling capabilities of existing RF MEMS devices.



#### 5.4. STUDY CASE SPECIFICATION

According to the RF MEMS technology available through IRCOM, RF MEMS switches will be limited to low level application for the microwave and antenna equipments.

Note also that, since the study which is more technology driven, it was decided not to concentrate on electrical performance and frequency band of the  $\mu$ switch but more on the dielectric coating and specific bridge structure (corrugations).

The table below, gives design goal for the various performance criteria. Objective is trying to keep performance stable with new  $\mu$ switch coating and structuring, together with improved life time under harsh environmental conditions..

▪ **Study case 1 : RF MEMS within microwave equipments for redundancy applications**

Criteria	Design goals	Observation
Frequency band	F0=20 GHz, $\Delta f=1$ GHz	
Insertion loss	< 0.2 dB @20 GHz	On wafer measurement, including access lines
Isolation in off state	25 dB	
Pmax	100 mW	Need to handle overdrive specifications
Switching speed	10-100 $\mu$ s	Not critical at this point
Actuation voltage	+6/-6 or <40 V	Check stability of biasing bus
Temperature range	Operating : -25/70°C Non operating : -55/125°C	With active cooling -65/30 °C
Hermeticity	165 h, 85 °C 85 % RH, Accel. Law of Sinnadurai (1), with a confidence factor of 1.5	Specified to achieve specified ground clean room storage of 3 years max

<b>Non hermetic RF MEMS</b>	<b>Ref: ASP-06-BO/PH/EA-45</b>		
	DATE : 1/03/06	ED/REV :V10	PAGE : 17 / 89

Radiation	Max 300 krad total dose	Geo mission, worst case
Life time	18 years	

This study case 1 is of interest since quite a few study RF MEMS related projects already use similar approach (« MIPA » EC funded project, «  $\mu$ switch for TCS21 payload » CNES funded project ,...)

But at this stage, no evaluation formal approach has been conducted.

(1) F. N. Sinnadurai, « the accelerated ageing of semiconductor devices in environments containing a high vapor pressure of water », *Microelectronics & Reliability*, vol 13, 1974, pp. 23-27.

▪ ***Study case 2 : RF MEMS within antenna equipments (worst environmental case - GEO mobile spot-)***

Criteria	Design goals	Observation
Frequency band	F0=20 GHz, $\Delta f=1$ GHz (TBC)	
Insertion loss	< 0.2 dB at 20 GHz (TBC)	On wafer measurement including access lines
Isolation in off state	25 dB	
Pmax	100 mW	Need to handle overdrive specifications
Switching speed	10-100 $\mu s$	Not critical at this point
Actuation voltage	+6/-6 or <40 V	Check stability of biasing bus
Temperature range	Operating : -100/120°C Non operating : up to -150/150 °C	Temperature range is very antenna architecture and mission dependant
Hermeticity	165 h, 85 °C 85 % RH, Accel. Law of Sinnadurai, with a confidence factor of 1.5	Specified to achieve specified ground clean room storage of 3 years max
Radiation	Max 300 Mrad total dose	Geo mission, total dose received by a radiating panel, worst case
Life time	18 years	

Note that between study case 1 & 2 (2') environmental constraints (temperature range & radiation level) change due to different location of the RF MEMS within the satellite. Electrical design goal for both study cases are limited to available technology and design for the present contract more focused on the technological aspects.

<b>Non hermetic RF MEMS</b>	<b>Ref: ASP-06-BO/PH/EA-45</b>		
	DATE : 1/03/06	ED/REV :V10	PAGE : 18 / 89

## **6. RELIABILITY CONCERNS**

Reliability and testing is treated unitedly in this section, because most of the reliability specifications are actually defined by a testing procedure. Therefore, in many cases assessment of reliability means specification of testing and vice versa.

Existing testing procedures mainly address reliability on the subsystem and system level. These procedures can be used to assess the reliability of MEMS packages and subsystem mounting technologies. An expensive and formal evaluation/qualification plan cannot be applied as such, within the present study, because of budget and time limitation. Today, there are no testing procedures for the long-term reliability of MEMS switches. Although certain failure modes are known, it is not clear to which extent they apply to a certain switch concept and switch design. The investigation of (dominant) failure modes for MEMS switches within the specific space environments is already put forward in this study which consist of stiction and dielectric charging phenomenon. The test plan proposed is supposed to address mainly this 2 degradation mechanisms.

### **6.1. RELIABILITY CONCERNS FOR STUDY CASE 1**

This paragraph is showing how design and application dependant needs to be the reliability test plan to be representative.

In a space satellite telecommunication mission, life time is specified to be up to 18 years. In the case of a redundancy switch (study case 1), the worst specification is a SPST that would be in OFF or ON state (depending upon the configuration of the SPDT) during 17.5 years and that would need to be actuated in the last six month of the mission. What would happen ?

Since both degradation mechanisms and corresponding accelerated tests are not known yet, it is impossible to give standards for test procedures as it is done for electronic component where degradation mechanisms are mostly temperature activated and accelerated.

This is one of the key issues for MEMS devices to be solved.

An important aspect of the redundancy SPDT is that in case of one point failure (for example SPDT power supply), the nominal (N) line needs in operating configuration while the redundant line (R) bring an open circuit. This is depicted in figure 6. This means that the SPDT is asymmetrical. It can be either constituted by one serie and one shunt SPST, or with 2 shunt SPST which combines quarter wavelength for one SPST to emulate a series switch with the inconvenience of extra insertion losses.

<b>Non hermetic RF MEMS</b>	<b>Ref: ASP-06-BO/PH/EA-45</b>		
	DATE : 1/03/06	ED/REV :V10	PAGE : 19 / 89

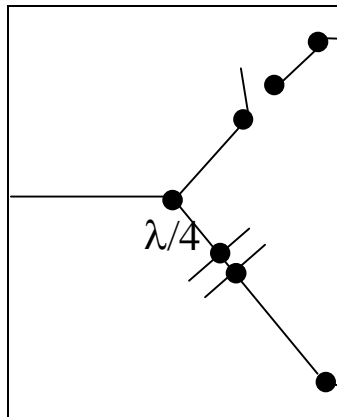


**Figure 7 : SPDT in 'fail-safe' design (SPST unbiased)**

In this configuration, it is shown that parallel shunt switch and serie switch are combined to use them in their idle mode in nominal operation (serie switch is normally off and parallel is normally on) to improve reliability related to stiction problems.

## 6.2. MAIN ENVIRONMENTAL TESTS USED FOR SPACE MICROWAVE PRODUCTS (GEO SATELLITE) :

- **High Temperature storage :**

Corresponding standard : (ESA PSS-01-612 / Mil STD 883 – Method 1008, "B")  
Evaluation stage : 2000h @ 125°C.

- **Thermal cycling :**

Corresponding standard : (ESA PSS-01-612 / Mil STD 883 – Method 1010, "B")  
Evaluation stage : 500 cycles : -55/+125°C

- **Moisture resistance :**

Corresponding standard : (ESA PSS-01-612 / Mil STD 883 – Method 1004)  
Evaluation stage : 10 cycles 25/65°C 85% RH

- **Mechanical Shock :**

Corresponding standard : (ESA PSS-01-612 / Mil STD 883 – Method 2002, "C")  
Qualification stage : 3000g peak / 0.3 ms (5 cycles in the 5 defined directions)

- **Vibration :**

Corresponding standard : (ESA PSS-01-612 / Mil STD 883 – Method 2007, "B")  
Qualification stage : 50g peak - 20/2000Hz (4 cycles in the 3 defined directions)  
(Instead of the classical sinusoidal variation from the MIL STD, we often prefer random

<b>Non hermetic RF MEMS</b>	<b>Ref: ASP-06-BO/PH/EA-45</b>		
	DATE : 1/03/06	ED/REV :V10	PAGE : 20 / 89

variation with 60 to 80g RMS)

- **Specificity for hermetic package :**

Hermeticity of the package can be assessed using the following standard :

MIL-STD 883

Method 1014.9 "Seal"

Method 1018.2 "Internal Water-Vapor Content" related to RGA

If non hermetic sealing is done, then one has to perform these extra tests :

- HAST (JESD22\_A110\_b)  
96h @ 130°C/85% RH with bias  
264h @ 110°C/85% RH with bias
- THB (JESD22\_A101\_b)  
1000h @ 85°C/85% RH with bias

- **Radiation :**

Radiation environment is strongly dependant on the mission. In this study where the idea is to try to understand the mechanism that will affect the reliability, we will limit our study to available timing and facilities available at ESA. Main focus will be total dose radiation with a target of 100 krad ,which is already quite representative of what can be seen in a GEO mission (15 years) on badly located equipments.

### **6.3. MAIN ENVIRONMENTAL TESTS USED FOR SPACE ANTENNA PRODUCTS (GEO SATELLITE) :**

To specify the below, we make the hypothesis that the antenna module will be mounted on the Earth panel of the satellite, which is the top panel in launch configuration. The mounting plane is parallel to the satellite XY plane, while the perpendicular to the mounting plane is parallel to the satellite Z axis.

- **Thermal cycling :**

For passive antenna product, main environmental tests are focused to temperature cycling, and mechanical test (vibration,...). When the equipment are passive temperautre range could be as large as -150 °C to 150 °C. Usually with proper passive thermal control (MLI and white color painting) this temperature range could be reduced with minor change in term of thermal control to -100 to +125 °C. Compared to microwave equipment specifications, the number of cycle to comply with is also larger, because of changing solar condition during one day of revolution (GEO).

<b>Non hermetic RF MEMS</b>	<b>Ref: ASP-06-BO/PH/EA-45</b>		
	DATE : 1/03/06	ED/REV :V10	PAGE : 21 / 89

**Thermal cycles** : 1000 Cycles –150 °C +125°C (Rapid thermal cycling, 10°/min ramps)

▪ ***Mechanical aspects***

Frequency requirements :

In stowed configuration, the frequencies of the global modes of the volume shall comply with the following requirements :

- First lateral (X or Y) mode frequency shall be higher than **60 Hz**
- First longitudinal (Z) mode frequency shall be higher than **100 Hz**

In deployed configuration the frequencies of the global modes of the volume shall comply with the following requirements :

- First lateral (X or Y) mode frequency shall be higher than **5 Hz**

Quasi-static

It should comply with the following :

- Whole module longitudinal load (satellite Z axis):  $\pm 15 \text{ g Z} \pm 5 \text{ g X}$  and  $\pm 15 \text{ g Z} \pm 5 \text{ g Y}$
- Whole module lateral load:  $\pm 25 \text{ g}$  (any direction in satellite XY plane, worst case direction to be identified)

Vibrations

These sine vibration levels are applicable to the complete module, and are given in the following table

<b>Perpendicular to the mounting plane (Satellite Z axis)</b>		<b>Parallel to the mounting plane (Satellite X and Y axis)</b>	
Frequency (Hz)	level	Frequency (Hz)	level (G)
0 - 10	$\pm 10 \text{ G}$	0 - 10	$\pm 10 \text{ G}$
10 - 25	$\pm 10 \text{ G}$	10 - 45	$\pm 10 \text{ G}$
25 - 50	$\pm 7 \text{ G}$	45 - 80	$\pm 3 \text{ G}$
50 - 60	$\pm 3 \text{ G}$	80 - 100	$\pm 2 \text{ G}$
60 - 80	$\pm 7.5 \text{ G}$		
80 - 100	$\pm 6.5 \text{ G}$		

**table 1: Sine vibration levels**

In addition, the antenna module shall withstand without any degradation the acoustic loads defined in the following table :

Octave Band (centre frequency - Hz)	Qualification / PFM level (dB)	Acceptance level (dB)	Test tolerance	
31,5	<b>132</b>	<b>128</b>	-2	+4
63	<b>136</b>	132	-1	+3
125	140	136	-1	+3
250	143	139	-1	+3
500	138	<b>135</b>	-1	+3
1000	135	132	-1	+3
2000	130	127	-1	+3
4000	124	<b>121</b>	-2	+4
8000	123	<b>119</b>	<b>-3</b>	+4
Overall level	146,7	142,9	-1	+3
Test duration	QM = 120 seconds PFM = 60 seconds	FM = 60 seconds		

(Ref : 0 dB = 2 x 10<sup>-5</sup> Pa)

**table 2 : Acoustic loads**

The purpose of the sine test is to verify the stiffness of the overall assembly, to characterize for low frequencies the modal spectrum of the overall assembly and thus to correlate the mechanical mathematical model and finally to verify the good behaviour of the overall assembly for the specified sine levels.

Note that due to the very low mass of the suspended membrane and the intrinsic resonance frequency (about 10-100 kHz for most of the  $\mu$ switches), we anticipate very low impact on the  $\mu$ switch characteristics itself. Nevertheless, one should check the highest acoustic loads which approaches the  $\mu$ switch intrinsic resonance.

This part is given as a reference and will not be treated within the present contract.

#### 6.4. GENERIC MEMS SWITCH FAILURE MECHANISM

The most important of these failure modes have been determined as stiction (mainly caused by water condensation at the bridge/dielectric interface), creep (static deformation of the bridge caused by mechanical stress), dielectric charging/degradation (may cause stiction of the bridge or failure of the dielectric), and electromigration. This is illustrated in the figure below.

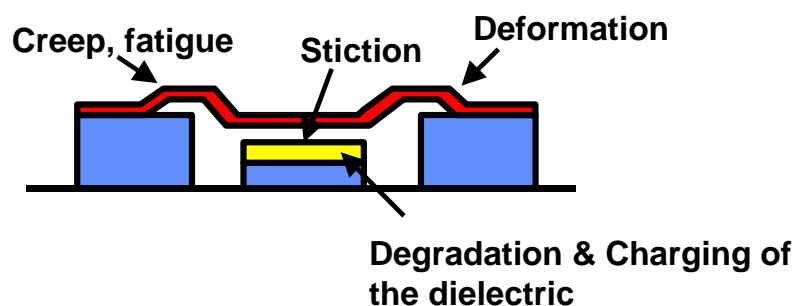


**Figure 8 : main capacitive switch failure mechanism**

<b>Non hermetic RF MEMS</b>	<b>Ref: ASP-06-BO/PH/EA-45</b>		
	DATE :	<b>ED/REV :V10</b>	<b>PAGE :</b>
	1/03/06		23 / 89

As an example, charging of the dielectric caused by charges tunneling into the dielectric cannot easily be evaluated in a thermal stress test, because charge tunneling at high electric fields (Fowler-Nordheim tunneling) is rather weakly dependent on temperature while thermionic (Schottky) injection has a  $\exp(-1/T)$  temperature dependence. Therefore, field strength, barrier height, tunneling and charge transport processes, charge diffusion out of the dielectric, and the impact of charging of the dielectric on the device (sticking of the bridge, dielectric breakdown,...) have to be evaluated in order to design a testing procedure (e.g. with enhanced pull-down voltage on the MEMS device) which is capable of assessing MEMS switch reliability with respect to dielectric charging.

The reliability requirements of a future MEMS-based satellites equipments are characterized by a long operation time, therefore a large number of switching cycles (study case 2), or a long period of idle time (study case 1), a long total lifetime (sum of operation and standby/switched-off times), and demanding environmental conditions (temperature, vibrations, mechanical shock, radiation etc...), in which the device has to operate.

The table below will help establishing the testing condition especially the on/off cycling for each specific study case, defined as such.

total number of switching cycles	10-100 cycles	Range given for 1:2 reduded LNA in FAFR, but also for low level redundancy ring; and including on-ground testing
cycle duration (*)	Months or years	Seconds or minutes for on-ground testing
switching time	1 ms (TBC)	(worst case).
total time of switch pulled down	15 years (worst case)	This criterium is very important because directly related to the dielectric charging degradation mechanism, so sticking risk. It is here considered that the down position for one of the 2 paths is kept during all the mission.

**table 3 : Operation (cycling) conditions for future RF MEMS in study case 1 (\*)**

total number of switching cycles	≈ 6000	Changed Once a day in-flight(Worse Case)
cycle duration (*)	1 day (typical)	Seconds or minutes for on-ground testing
switching time	2-3 μs (goal)	(could be some μs, with very small degradation, if switching the various cells one after the other).
Time Up / Time Down	From 25 to 75% each	Depends on the reflecting element concept (only some of the dipoles or slots are made resonant)
total time of switch pulled down	7-8 years	When non-operating (e.g. storage), membranes are assumed Up, to limit sticking risks, and because the driving voltage is then null.

**table 4 : Operation (cycling) conditions for future RF MEMS for use in study case 2**

note that for Study case 1 and 2, a GEO mission is intended giving in term of life time, 18 years, including 3 years on earth in storage conditions .

<b>Non hermetic RF MEMS</b>	<b>Ref: ASP-06-BO/PH/EA-45</b>		
	DATE :	<b>ED/REV :V10</b>	<b>PAGE :</b>
	1/03/06		24 / 89

total lifetime	10 years	sum of operation and non-operation times
operating lifetime	5 years	total time for which the device will be operated (in orbit)
Standby time	80% of each orbit	Spaceborne SAR instruments operate no more than 20% of each orbit
total number of switching cycles	$3 \times 10^6$	
cycle duration	$\approx 10$ seconds	Time between 2 scanning operations (swath change)
switching time	2-3 $\mu$ s (goal)	could be tenths $\mu$ s, for classical SAR modes.
Time Up / Time Down	$\approx 50\%$ each	For phase-shifters at subarray level, On/Off probability are about equal for any bit.
total time of switch pulled down	6 months	50% of total imaging time during satellite life. When non-operating (on-ground or in-flight), membranes are assumed Up, to limit sticking risks, and because the driving voltage is then null.

**table 5 : Operation (cycling) conditions for future RF MEMS for use in study case 2'**

Replacing the DC pull-down voltage with a rectangular (bipolar) AC signal or reversing the polarity of the switching voltage on each successive switching process is an option to reduce charge tunneling into the dielectric. Further, during the standby time (study case 2) a "detrapping" process (e.g. pulling all switches down with reversed and enlarged pull-down voltage) may be employed. This approach could make compliant total dose radiation level assuming that dielectric charging is fully reversible.

The actuation voltage to pull down the switch is typically much higher than the voltage necessary to hold down the actuated switch. If the MEMS bias voltage is reduced after pulling down the switch, the problem of charge injection into the dielectric can further be alleviated.

## **7. DESIGN, LAYOUT CONCEPT AND SIMULATION OF $\mu$ SWITCH INTRODUCTION**

This report presents the design of the switch, for the two versions, with or without dielectrics. The switch that has been developed in this project is as un-original as possible. In other words as standard as possible. It is derived from the original work by goldsmith, published in 1995. This device is a metallic membrane, laid over a CPW line, like an air bridge structure. When a voltage is applied between the membrane and the center conductor, the electrostatic pressure causes the bridge to collapse, short-circuiting the signal to the ground. In the up state, the air capacitance between the signal line and the ground plane is low enough in order to limit the impact of this capacitor on the return loss and the on state loss of the switch.

The design parameters can be listed below:

The on state capacitance and its influence on the on state loss.

The actuation voltage and the associated mechanical parameters of the switch.

The restoring force, large enough to prevent first-order stiction.

The strategy that has been chosen is outlined below:

<b>Non hermetic RF MEMS</b>	<b>Ref: ASP-06-BO/PH/EA-45</b>	
	DATE : 1/03/06	ED/REV :V10
	PAGE : 25 / 89	

The switch combines electroplated gold areas and evaporated structures. The component is made with metal: the temperature behavior will not be very good, since the CTE mismatch between the bridge and the substrate is high ( $CTE_{Si}=4.2 \text{ ppm/}^\circ\text{C}$ ,  $CTE_{Au}=14.2 \text{ ppm/}^\circ\text{C}$ ). The switch is stiff, that is to say that the actuation voltages have not been minimized, but the mechanical resonance frequencies are high, and the parasitic forces, like contact forces have a minimized influence.

### 7.1. CAPACITIVE SWITCH

The switch cross section is presented on Figure 9, with dimensions given on the same figure. The substrate chosen in this example is quartz, but the switch can be fabricated on silicon, or glass without any change in the fabrication process.

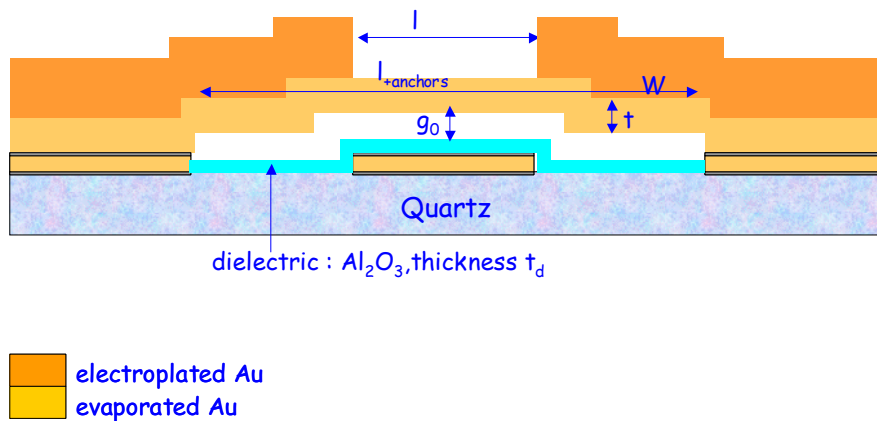
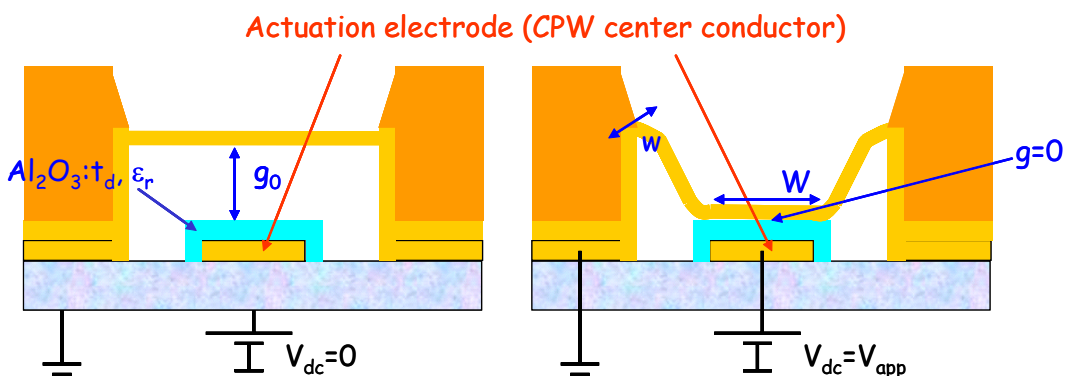


**Figure 9 - Switch cross section**

The signal line is running under the bridge, and it is covered with a thin layer of dielectric that prevents the top electrode from collapsing on the signal line. The structure is a metallic membrane, that is to say its stiffness comes mostly from the build in stress in the evaporated gold layer. This metal has a stress that has been estimated to be around 50-100MPa, on our equipment. These values have been determined from pull-in voltage measurement on fabricated structures. Indeed, by knowing the initial height of the structure, one can determine the spring constant of the bridge from  $V_p$  measurement, which is link to the residual built in stress (see the equation below)



<b>Non hermetic RF MEMS</b>	<b>Ref: ASP-06-BO/PH/EA-45</b>		
	DATE : 1/03/06	ED/REV :V10	PAGE : 26 / 89

Up and down states

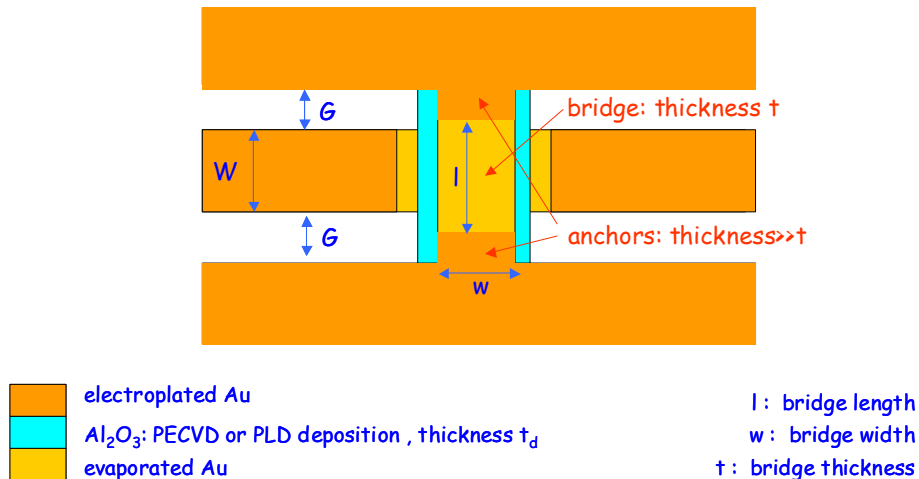


**Figure 10 – On and off state and top view of the switch**

### 7.1.1. Mechanical aspects

The switch has been designed using a linear beam approximation, using analytical formulas or a software from Berkeley, sugar, but still based on semi analytical modeling. The advantage of this approach is to be very fast, and to allow fast optimization and prediction of the bridge properties.

The spring constant  $k$  of a fixed-fixed beam, with a built in stress  $\sigma$  is given below:

$$k \cong \frac{32Ewt^3}{l^3} + \frac{8\sigma(1-\nu)rw}{l}$$

With  $E$ , the Young's modulus,  $w$  its width,  $l$  its length,  $t$  the thickness,  $\sigma$  the tensile stress,  $\nu$  the Poisson's coefficient

In our case, the membrane thickness is  $0.5\mu\text{m}$ , its build in stress is  $50\text{-}100\text{MPa}$ , and the material is gold ( $E=80\text{GPa}$ ,  $\sigma=0.41$ ). The spring constant is estimated at the center of the bridge, and the variations are given below:

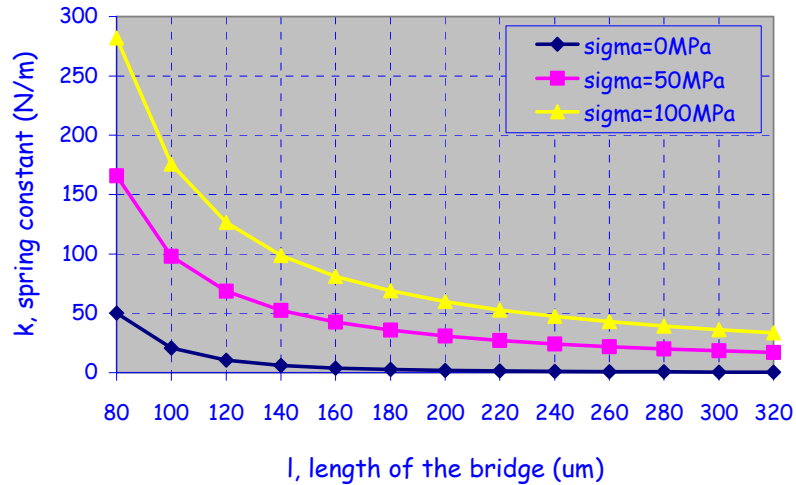


**Figure 11 - Evolution of the spring constant as a function of the bridge length**

The membrane nature of the structure can be seen on this graph, where the spring constant is dominated by stress. The targeted values for the spring constants are between 10 and 50 N/m that correspond to bridge length between 100 and 220  $\mu\text{m}$ . This gives restoring forces between 20 and 100  $\mu\text{N}$  adequate to overcome stiction forces. However, devices with larger dimensions have been added to this targeted group of devices, in order to have a wide range of mechanical structures.

The switch is shown in the down state, on the figure below:

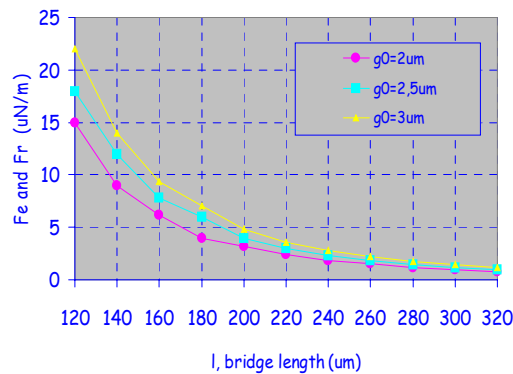
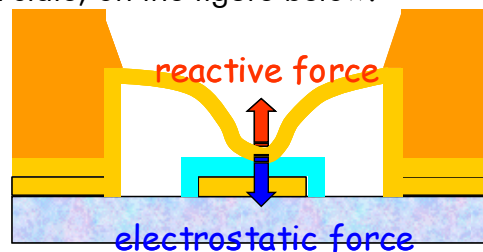


**Figure 12 – Studied configuration for the calculation of the restoring force and simulation results for several sacrificial layer thickness**

<b>Non hermetic RF MEMS</b>	<b>Ref: ASP-06-BO/PH/EA-45</b>		
	DATE : 1/03/06	ED/REV :V10	PAGE : 28 / 89

After the spring constant and the restoring force have been studied, the influence of stress on the pull down voltage has been studied:

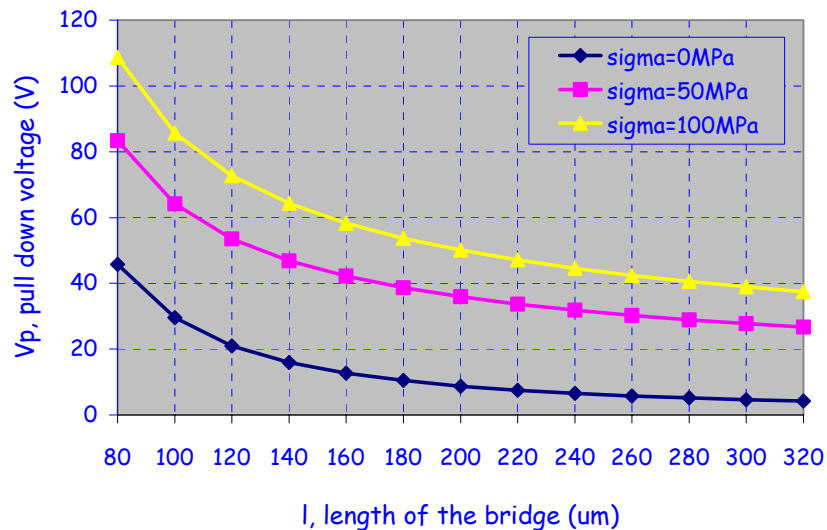


**Figure 13 - Influence of the residual stress on the pull down voltage (go=2μm)**

Again, it can be seen that the built in stress dominates the switch behavior. This is typical for membrane type switches, (a mechanical membrane is a structure with its stiffness given by stress). Most papers in literature show that restoring forces higher than 5μN are required for correct operation of MEMS switches. Below these values, the switch is plagued with surface adhesion related problems. For these values, pull down voltages are around 40 Volts that corresponds to bridge length between 100 and 300 μm.

The above graphs ( fig. 4 & 5) present the variations of the switch parameter as a function of dimensions. However, the equipments, and the process facilities that are available at the lab restrict many of these parameters.

The sacrificial layer thickness varies from 2 μm up to 3 μm, while the membrane built in stress is hard to predict. For a given sets of evaporation conditions, the stress varies between 50MPa and 100MPa. We have therefore chosen to use a large set of different switches in order to maximize the number of functional structures.

<b>Non hermetic RF MEMS</b>	<b>Ref: ASP-06-BO/PH/EA-45</b>		
	DATE : 1/03/06	ED/REV :V10	PAGE : 29 / 89

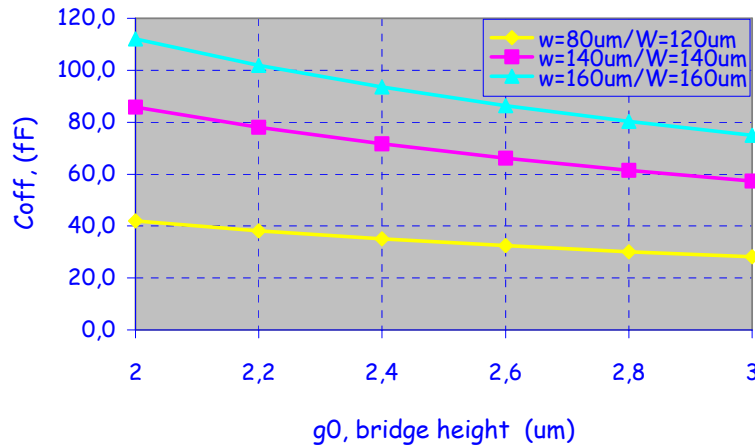
L $\mu\text{m}$	w $\mu\text{m}$	W $\mu\text{m}$	K1 N/m	K2 N/m	Vp1 Volts	Vp2 Volts	Fr1 $\mu\text{N}$	Fr2 $\mu\text{N}$	Fm1 KHz	Fm2 KHz
80	80	80	97	140	64	83	194	334	126	166
100	80	80	70	125	54	72	140	251	96	128
120	80	120	54,5	100	39	53	109	202	77,3	105
140	80	80	45	85	43	59,5	90	169	65	89
160	80	120	38	73	32	45	76	146	56	76
180	80	160	33,3 5	64	26	37	67	129	49	68
200	80	120	29,6	57	29	40	59	115	44	61,5
220	160	160	53	103	23	33	107	208	40	55
240	80	200	24	47	20	28	48	95	36	51
240	80	120	24	47	26	36	48	95	36	51

Table 1: Summary of dimensions of the fabricated switches, with their computed characteristics.

L: Bridge Length, w: Bridge Width, W: Electrode width, K1: computed spring constant ( $\sigma=50\text{Mpa}$ ), K2: computed spring constant ( $\sigma=100\text{Mpa}$ ), Vp1: computed pull-down voltage ( $\sigma=50\text{Mpa}$ ), Vp2: computed pull-down voltage ( $\sigma=100\text{Mpa}$ ), Fr1: computed restoring force ( $\sigma=50\text{Mpa}$ ), Fr2: computed restoring force ( $\sigma=100\text{Mpa}$ ), Fm1: computed mechanical resonance frequency ( $\sigma=50\text{Mpa}$ ), Fm2: computed mechanical resonance frequency ( $\sigma=100\text{Mpa}$ ),

### ***7.1.2. Electrical considerations***

The switch performances are dominated by the contrast between the on and off states, or the ratio between the capacitance in the up state and the down state. We have performed a parametric analysis, again using simple analytical formulas in order to get an approximate initial guess of the switch behavior.



**Figure 14 - Off state capacitance value versus bridge height, for different bridge areas**

It can be seen on Figure 14 that the switch off state capacitance is low enough for common switch areas. Indeed, a capacitance to the ground less than 150 fF has a very limited influence on the switch performance up to frequencies higher than 25 GHz.

For two types of dielectrics available at the lab, BST (Barium Strontium Titanate ) and  $Al_2O_3$  have been studied for the theoretical computation of the on to off ratio of the switch. Since BST has a dielectric constant two times higher than  $Al_2O_3$  (18 vs. 9.8), the on to off ratio increases sharply if this dielectric is being used. Also, the performance of the switch is improved if the dielectric thickness is decreased. Based on previous experience, we will not use a dielectric thinner than  $0.2 \mu m$ , that is enough to obtain high on-off values, at least theoretically. Indeed, lower thickness result in really huge electric field in the dielectric and problems like step coverage, sensitivity to small defects in the film reduces dramatically the yield and reliability of the switch.

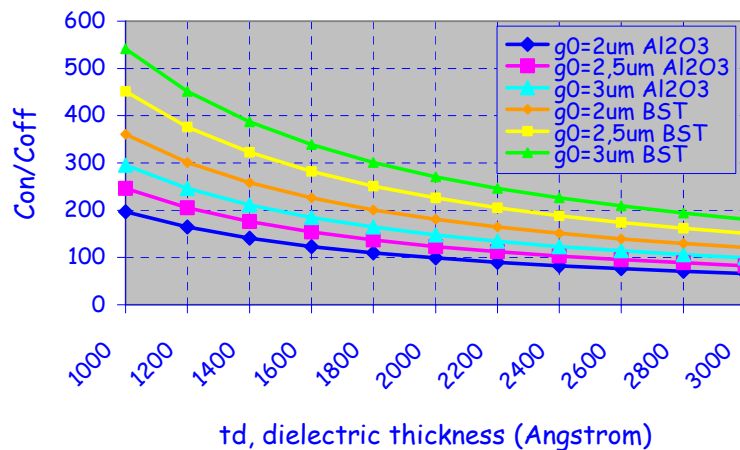


**Figure 15 - Theoretical On/Off ratio of the switch**

<b>Non hermetic RF MEMS</b>	<b>Ref: ASP-06-BO/PH/EA-45</b>		
	DATE : 1/03/06	ED/REV :V10	PAGE : 31 / 89

As discussed before and in order to overpass the problems linked to the unknown parameters appearing in the fabrication process (roughness, membranes stress) we have fabricated structures with different dimensions. They are summarized below:

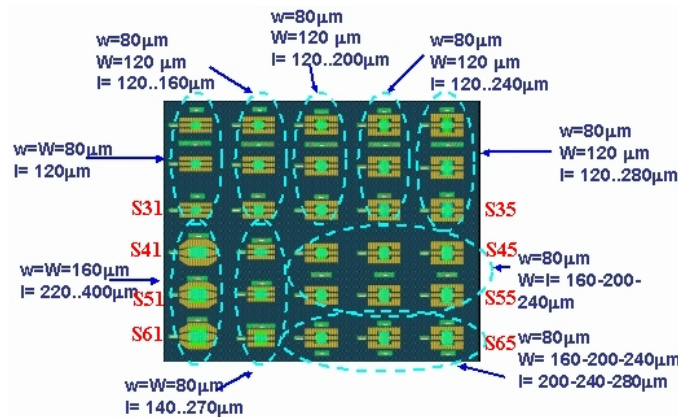


**Figure 16 - Basic mask cell used for the switch fabrication using Al<sub>2</sub>O<sub>3</sub> as a dielectric (l = bridge length, w= bridge wide, W= contact area length)**

In practice, we have optimized the roughness of the metal and of the dielectrics to obtain a good On/Off ratio. Applying a 15 min. Ar plasma in the PECVD system can drastically reduce the roughness of the metal. Still, the most critical parameters are linked to the properties of the dielectric layer. The films should be obtained under the following conditions :

- Use of low temperature deposition for compatibility with switch fabrication technology
- Be thick enough to withstand high breakdown voltages
- Not too thick, otherwise the down-state capacitance will be reduced (~200 nm is a good compromise)
- Present a low roughness for an efficient surface contact (and high down-state capacitance)
- Present low density of charge trapping centers on the surface (low surface OH chemical bonds).

In order to optimize all these properties we varied the experimental conditions involved in the deposition methods used for obtaining the dielectric layers (PECVD – Plasma Enhanced Chemical Vapour Deposition or PLD – Pulsed Laser Deposition). For example, in the case of the PECVD we investigated the influence of the temperature, total pressure, substrate polarization and plasma-substrate distance on the deposition rate, roughness, OH concentration and dielectric constant of the obtained films. This allowed us to identify a set of optimum deposition parameters, which will be further refined. This work is being further detailed in TN3.1.

<b>Non hermetic RF MEMS</b>	<b>Ref: ASP-06-BO/PH/EA-45</b>		
	DATE : 1/03/06	ED/REV :V10	PAGE : 32 / 89

## 7.2. CAPACITIVE SWITCH WITHOUT DIELECTRICS

In the case of the switch presented before, the dielectric layer separating the metal membrane from the bottom electrode is subject to charging caused by the high electric field applied on this layer. This may result in drift in the  $1/C(V)$  characteristic of the switch. However, this can be strongly reduced by using a bipolar actuation voltage, and lifetime of billions of cycle can be demonstrated for these components. Another approach is to use a small air gap instead of a dielectric film. Bipolar actuation voltage makes the biasing network more complex than standard DC voltage, but this is not impossible to implement within TM/TC of microwave satellite equipment. The reason is that no current is generated and that relatively slow ramp is being used (few tens of  $\mu s$  vs ns for solid state electronics).

A mechanical movement is used to achieve a contrast as high as possible between a high gap and low gap positions of the designed switch, as shown Figure 17. The advantage is that the device will not suffer from dielectric charging and it will be less sensitive to radiations when used in space environment. It has also no metal-to-metal contact susceptible to degradation. Moreover, with appropriated corrugation dimensions, switch contact surfaces will be very small reducing the effect of the parasitic contact forces. Although the On to Off ratio of the switch can be seen too low because air is used as a dielectric in both positions, this ratio can be further improved by reducing the air gap in the down state to increase the capacitance.

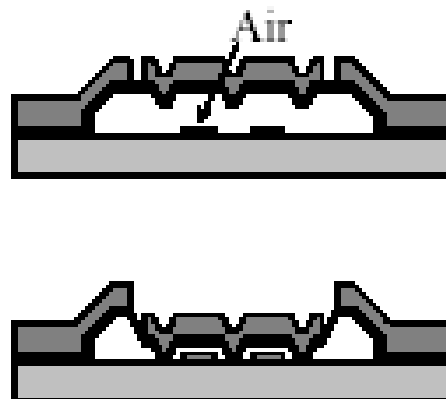


**Figure 17 : Principle of the capacitive air switch**

The design is based on the computation of the spring constant in the up state and in the down state. In the up state, the switch is dominated by the spring constant of the non-electroplated areas that can be approximated as a switch of length  $2.L$  with a thickness  $t$ . Again, in order to maximize the number of functional structures, we choose to vary the dimensions of the fabricated switches ( $L$ ,  $l$ -the length and width of the non-electroplated area,  $w_f$ - width of the corrugations,  $g_d$ - height of the air gap). The electrode is made of 6 lines running in parallel. The spacers are in contact with the substrate in this area and they prevent top electrode from being in contact with the bottom electrode as shown in Figure 17 and Figure 18.

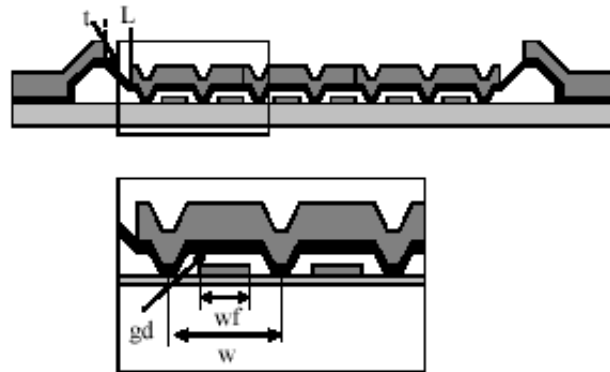


**Figure 18 : Cross section of the structure in the down state**

For the dimensions given on the table below the spring constant is of about 15 to 20 N/m depending of the membrane stress. The resulting theoretical pull down voltage is between 35 to 40 Volts, depending on the height taken into account, with or without the corrugations.

wf	20 $\mu\text{m}$
L (length)	300 $\mu\text{m}$
l (width)	300 $\mu\text{m}$
gd	0.3 $\mu\text{m}$
Ho (initial height)	3.2 $\mu\text{m}$
w	40 $\mu\text{m}$

**table 6 : Micro switch dimensions**

When the switch is in down position, the computed pull down voltage of the membranes used as air capacitance for off state, is higher than 1000 volts, thanks to the large thickness of the electroplated gold. Time domain simulation of the mass-spring reduced model of switch pull down movement, have shown that these dimensions prevent any complete pulling down of the switch.

### **7.3. CONCLUSION**

<b>Non hermetic RF MEMS</b>	<b>Ref: ASP-06-BO/PH/EA-45</b>		
	DATE : 1/03/06	ED/REV :V10	PAGE : 34 / 89

This section presented the design of shunt capacitive switches expected to operate with somewhat limited packaging constraints. Two approaches have been studied:  
 A switch (with dielectric contact layer) stiff enough to prevent contact stiction troubles.  
 A switch without dielectric contact layer, to prevent stiction induced by dielectric charging.

For both designs, the switch mechanical behavior has been studied and parametric analyses have been done to find the appropriated switch dimensions and reach the desired pull down voltage, restoring force and mechanical frequency. An electrical analysis has been also done to optimize the switch performances in both states and reach a high capacitance ratio ( $C_{on}/C_{off}$ ). Thus, several couples of dimension have been outlined and we have chosen to use a large set of different switches in order to maximize the number of functional structures. Now we focus on the optimization of experimental conditions for the dielectric deposition to improve the switch performance (dielectric roughness and purity). For switches designed without dielectric, corrugation dimensions will be optimized to reach higher capacitive impedance ratio.

## 8. DIELECTRIC DEPOSITION SYSTEMS PRINCIPLE AND PRELIMINARY RESULTS

The goal of this section is to describe the equipment used in the study to deposit dielectric materials at SPCTS used to fabricate capacitive micro switches. It consists in two deposition systems:

- Pulsed laser ablation
- PECVD

### 8.1. THIN FILM DEPOSITION USING PULSED LASER ABLATION FOR RF AND MICROWAVE COMPONENTS

#### 8.1.1. Principle of Pulsed Laser Deposition

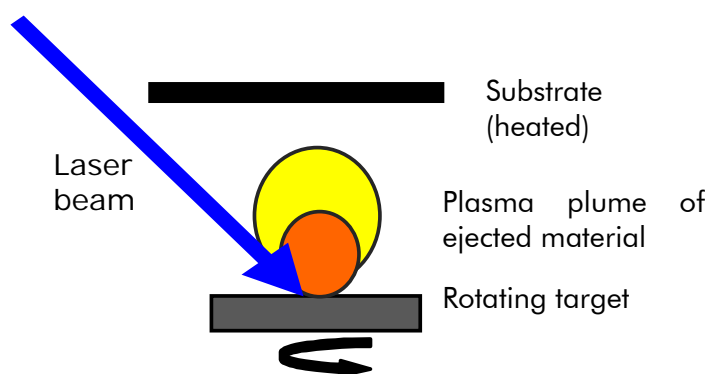


**Figure 19: PLD principle**

<b>Non hermetic RF MEMS</b>	<b>Ref: ASP-06-BO/PH/EA-45</b>		
	DATE : 1/03/06	ED/REV :V10	PAGE : 35 / 89

### ***8.1.2. Basic experimental arrangement***

The laser beam (here KrF 248 nm, 15 ns pulse duration) is focused on the target surface, in an ultra high vacuum cell. The impact size and the laser energy on the target are chosen in order to define the required laser fluency.

### ***8.1.3. Specificities of PLD compared to other deposition processes***

- Possibility of a complex chemical composition transport from the target to the substrate without modification - High kinetic energies and high instantaneous flux of impinging particles on the substrate
- Deposited thickness resolution (0.1 to 1 Å per laser pulse)
- Deposition in one step, using a single multitarget device, of multilayer materials, doped materials or materials with well-controlled composition gradients; possibility of new (artificial) materials synthesis- Possibility to induce reactive phenomena during transport of ejected particles by introducing gas in vacuum cell (as example the effect of oxygen pressure on plume expansion on Fig 2) ; doping.

**Figure 20 : Fast photograph of BST plasma plume**

### ***8.1.4. Film deposition***

The angular particle flux distribution may be approximated by:

$$J(\theta) d\Omega \approx \cos^n(\theta) d\Omega$$

Consequently, the thickness distribution of the deposited film is:

$$T(\theta) d\Omega \approx \cos^{n+3}(\theta) d\Omega = \cos^p(\theta) d\Omega$$

Films with uniform thickness (5%) can be obtained by off-axis rotation of the substrate (Fig.3) up to 6 inches in diameter.

<b>Non hermetic RF MEMS</b>	<b>Ref: ASP-06-BO/PH/EA-45</b>		
	DATE : 1/03/06	ED/REV :V10	PAGE : 36 / 89

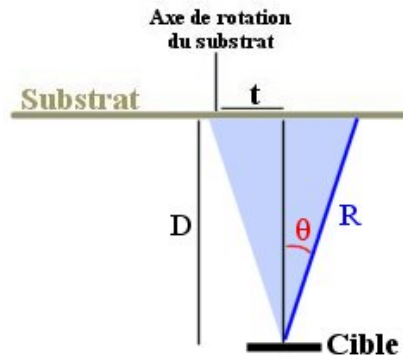


**Figure 21 : Substrate off-axis rotation for uniform sample coverage**

### ***8.1.5. Deposition of alumina films at room temperature***

Properties of PLD deposited "aluminium oxide" films:

Amorphous, transparent with a refractive index of 1.68, composition Al/O  $\approx$  2/3 (RBS), permittivity  $\epsilon = 9,4$ , resistivity :  $5 \cdot 10^7 \Omega \cdot \text{cm}$ , breakdown electric field  $> 3 \cdot 10^6 \text{ V/cm}$ .

The interesting electrical properties make this material, deposited at room temperature (with no substrate heating), a good candidate for dielectric insulation between electrodes in MEMS devices.

According to low mass density ( $3.9 \text{ g/cm}^3$ ) and high Young modulus (300 GPa) of alumina, these films can also be used as structural material (cantilever or bridge), allowing a reduction of component size.

### ***8.1.6. Deposition of CARBON (tetrahedral carbon - ta-C) films at room temperature***

Carbon films are deposited at room temperature from high purity grade graphite targets under high vacuum with high laser fluencies. They are hydrogen free and constituted of C atoms mainly hybridized  $sp^3$  ( $> 70\%$ ) with an amorphous structure.

<b>Non hermetic RF MEMS</b>	<b>Ref: ASP-06-BO/PH/EA-45</b>		
	DATE : 1/03/06	ED/REV :V10	PAGE : 37 / 89

Their properties are:

- *Mechanical properties:* Hardness: 45 GPa measured using nanoindentation. For comparison the crystalline diamond hardness is between 80 et 100 GPa.

Young modulus: > 650 GPa (crystalline diamond ≈ 1200 GPa).

Surface roughness: < 1 nm for films of 300 nm in thickness deposited on Si wafers (estimated by AFM)

- *Electrical properties:* Conduction mechanisms in TA-C involve very complex phenomena. As example, the resistivity, without bias, is of about  $10^8 \Omega \cdot \text{cm}$  and becomes about  $4 \cdot 10^4 \Omega \cdot \text{cm}$  under applied electric fields larger than  $10 \text{ V}/\mu\text{m}$ .

- *Optical properties:* Good transmission in the visible spectrum and very good in the infra-red.

- *Thermal properties:* diffusivity between  $2.2 \cdot 10^{-6} \text{ m}^2/\text{s}$  and  $8 \cdot 10^{-6} \text{ m}^2/\text{s}$ , corresponding to values of thermal conductivity ranging between 4 and 14 W/m.K, and Cp of about 510 J/kg.K and a specific mass of  $3500 \text{ kg}/\text{m}^3$  (depending on deposition conditions), to be compared to thermal conductivity of 1.4 W/m.K for fused silica.

- *Large chemical inertness*

Using multitarget laser ablation, metal-doped ta-C films can be deposited, giving materials with very well defined resistivity (Figure 22) allowing realization of microresistances (Figure 23).

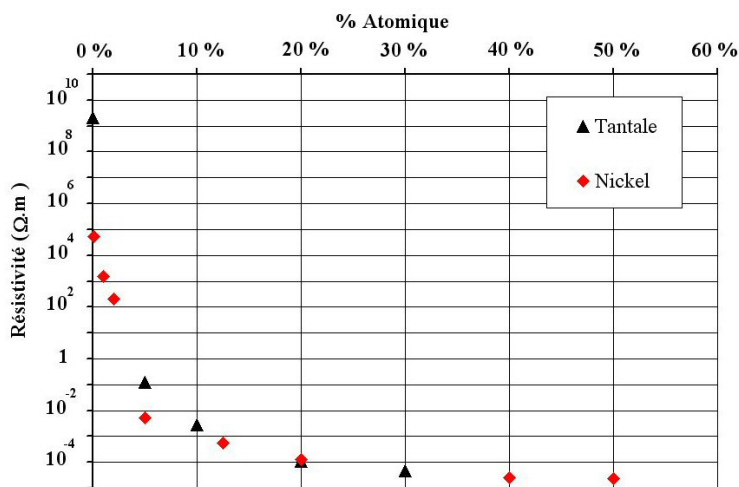


**Figure 22: Resistivities of Ta and Ni doped carbon films**

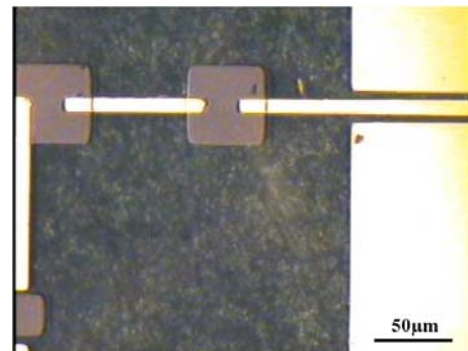


**Figure 23: 5% Ni-doped ta-C resistance**

<b>Non hermetic RF MEMS</b>	<b>Ref: ASP-06-BO/PH/EA-45</b>		
	DATE : 1/03/06	ED/REV :V10	PAGE : 38 / 89

## **8.2. THIN FILMS OBTAINED BY PLASMA ENHANCED CHEMICAL VAPOR DEPOSITION**

The PECVD process (Plasma Enhanced Chemical Vapor Deposition) is based on the decomposition of a gaseous compound near the substrate surface, similar to the related epitaxy and CVD (Chemical Vapor Deposition). One of the reaction products is a solid matter, which precipitates onto the surface such that a new layer is formed.

For technical realization of plasma CVD process, two parts of the deposition system are of great importance, namely, the glow discharge configuration and the gas inlet and distribution system. As a power source, direct current (dc), pulsed dc, radio frequency (rf) or microwaves can be used. Low deposition temperatures (<250°C) along with higher deposition rates can be achieved by PECVD. The lower deposition temperatures might be an advantage for sensitive substrate materials or might cause the formation of metastable phases of the deposit.

The standard equipment for PECVD at SPCTS (Figure 24) used a remote microwave excitation (2.45 MHz, RMPECVD process) and is based on a post discharge configuration (separation between plasma and deposition areas) in which only one gas is exited /dissociated. The substrate is immersed in the post-discharge chamber and can be RF polarized which results in a better control of the bombardment/deposition. The plasma volume reactions are very complex because of the large number of different species and possible reaction channels. One very important process is the decomposition of the polyatomic carrier gas by electron impact dissociation. The energetic electrons generate some free radicals and ions also, which are able to decompose the neutral carrier gas and polyatomic radicals by radical-molecule and ion-molecule reactions. The efficiency of the decomposition of the process gas is usually very high. Often, 10-100% of the carrier gas fed into the reactor can be decomposed.

<b>Non hermetic RF MEMS</b>	<b>Ref: ASP-06-BO/PH/EA-45</b>		
	DATE : 1/03/06	ED/REV :V10	PAGE : 39 / 89

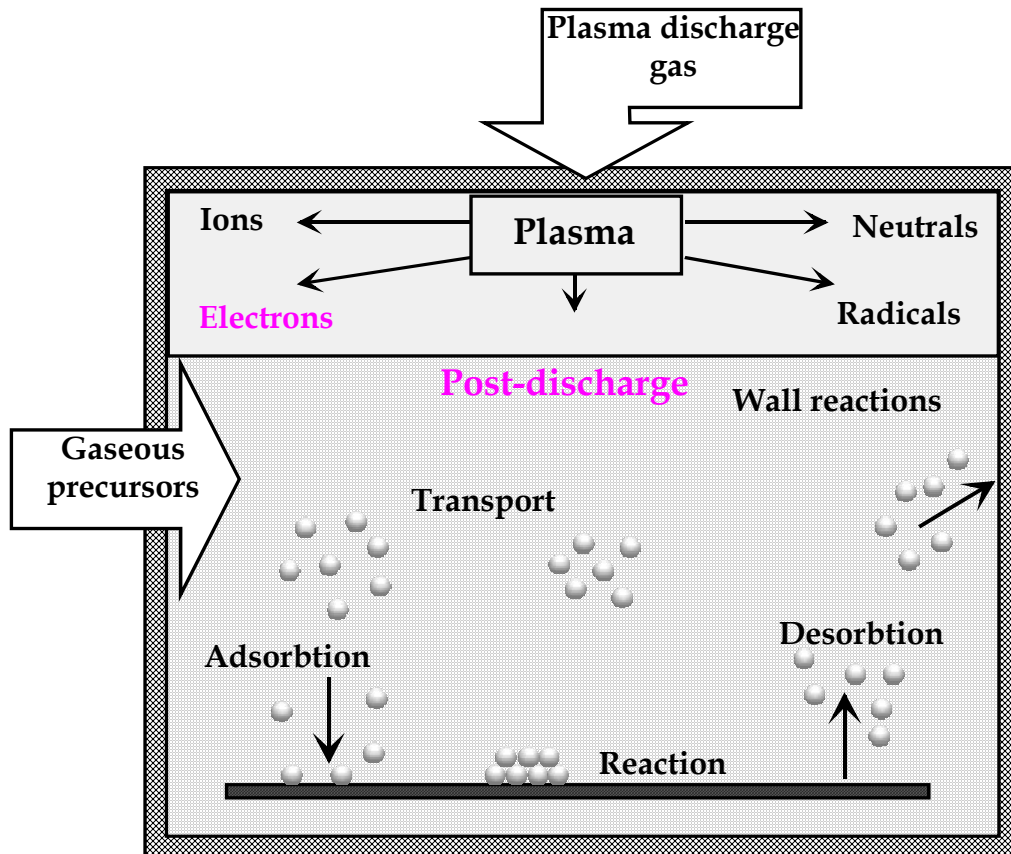


**Figure 24 : Principle of PECVD deposition in a post-discharge configuration**

A large number of parameters can be varied in order to identify the best experimental conditions, which result in high quality films: substrate temperature and polarization, microwave power, gaseous flows, total pressure etc.

For  $\text{Al}_2\text{O}_3$  deposition, trimethylaluminium (TMA) carried by Ar is used as gaseous precursor in an  $\text{O}_2$  plasma discharge. The experimental conditions are:

- oxygen plasma (125 sccm, 1 Pa, 1600 W, 1min30s)
- deposition phase (125/3 sccm, 1-5 Pa, 1600 W, 10 min)

The  $\text{Al}_2\text{O}_3$  thin films characteristics are described below:

- stoichiometry:  $\text{O}/\text{Al} = 1,72$  ( $\text{Al}_2\text{O}_3$ - 1,5), %at. H : 15 %, %at. C : 0,4 %
- density:  $3,0 \pm 0,3 \text{ g/cm}^3$  (density of  $\text{Al}_2\text{O}_3$   $\gamma$  :  $3,6 \text{ g/cm}^3$ ) columnar growth (Figure 28)amorphous, as indicated by XRD measurementslarge area deposition (up to 10 cm diameter)deposition rates between 50 and 500 nm/min

<b>Non hermetic RF MEMS</b>	<b>Ref: ASP-06-BO/PH/EA-45</b>		
	DATE : 1/03/06	ED/REV :V10	PAGE : 40 / 89

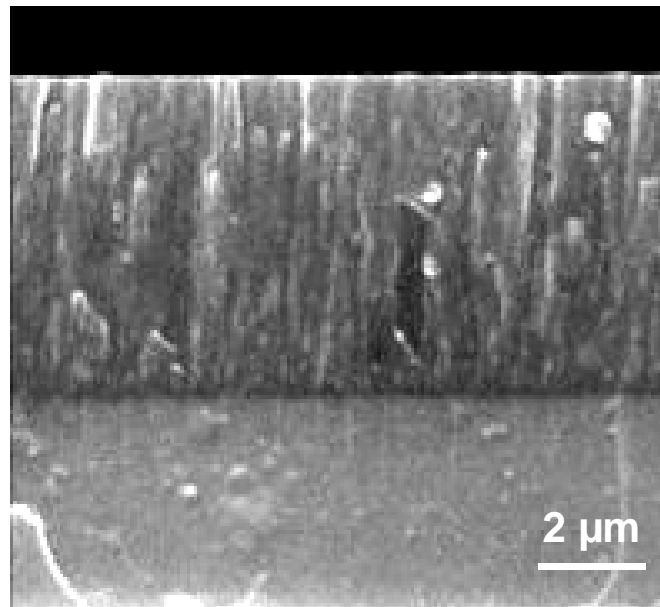


**Figure 25 : Cross section of an Al<sub>2</sub>O<sub>3</sub> film on Si substrate showing the columnar growth (scanning electron microscopy image)**

### **8.3. EXPERIMENTAL RESULTS**

The deposition of high-quality dielectric layers is a critical step in the realization of the switches. Alumina (Al<sub>2</sub>O<sub>3</sub>) was chosen because it can stand high breakdown voltage for relatively thin layers (~2000 Å), shows less charging effects (compared with other dielectrics like SiO<sub>2</sub> or Si<sub>3</sub>N<sub>4</sub>) and it can be deposited under low temperature (even at room temperature) without losing its main properties, both by PLD and PECVD methods.

If we refer to the deposition methods, we expect some differences between the films obtained by PLD compared with those obtained by PECVD, either at the compositional or morphological level. This came from the nature of the mechanisms involved in each deposition process. Thus, a certain amount of hydrogen can be incorporated in the alumina-PECVD films (from TMA precursor decomposition) while the alumina-PLD films are hydrogen-free. Nevertheless our goal is to obtain, in both cases, dielectric films with low surface roughness -for a high surface contact (and high C<sub>down</sub>), with low density of -OH chemical bonds -which acts as charge traps and can potentially lead to the switch failure.

#### ***8.3.1. Results for PLD deposition***

Using the **PLD technique** we deposited several types of dielectric structures, namely:

- **Alumina (2500 Å)** – from high-purity alumina target under high-vacuum (~5x10<sup>-6</sup> mbar total pressure), at 10 Hz laser repetition rate and off-axis rotation geometry for

<b>Non hermetic RF MEMS</b>	<b>Ref: ASP-06-BO/PH/EA-45</b>		
	DATE : 1/03/06	ED/REV :V10	PAGE : 41 / 89

uniform coverage of the samples (see Fig. 3); very resistant (etching rate in buffered HF acid is  $\sim 240$  nm/min), it can stand high electric fields, of  $\sim 100$  kV/cm;

- **Alumina (2500 A) covered by a thin, hydrophobic layer to protect against stiction in humid environments:**
  - **alumina (2500 A) + Teflon (500 A)** – the results are not conclusive since the Teflon layer is deposited with high roughness which can potentially be transmitted in the sacrificial layer, hence, geometrical non-uniformity of the switch membrane, so, poor characteristics;
  - **alumina (2500 A) + Diamond Like Carbon (DLC) (or ta-C) (200 A)** – only one wafer was processed so far with unexpected results: the DLC layer behaves like a field emitter although isolated from the down electrode by the dielectric layer;
- **Diamond Like Carbon (DLC) (or ta-C) (1000 A)** – for comparing with the pure alumina results: as expected, field emission from the coating, good correlation with the low threshold field emission properties of DLC, which induced destruction of the switches.

<b>Non hermetic RF MEMS</b>	<b>Ref: ASP-06-BO/PH/EA-45</b>		
	DATE : 1/03/06	ED/REV :V10	PAGE : 42 / 89

### **8.3.2. Results for PECVD deposition**

Concerning the **PECVD experiments** we were interested in finding out which are the most influential deposition parameters on the morphological and dielectric properties of the coating. We identify several experimental parameters for optimizing the alumina coating properties. These are sketched in the Figure 26 and their values were modified as below:

- Temperature of the substrate holder (room temperature (RT) and 300°C)
- Total pressure ( 1 and 5 Pa)
- RF polarization of the substrate holder (0 and 150 V)
- Distance between TMA precursor injector and substrate holder, IS (4 and 8 cm)

Under these conditions, we search to optimise several films parameters, namely: thickness, deposition rate, relative permittivity of the films, roughness, -OH content.

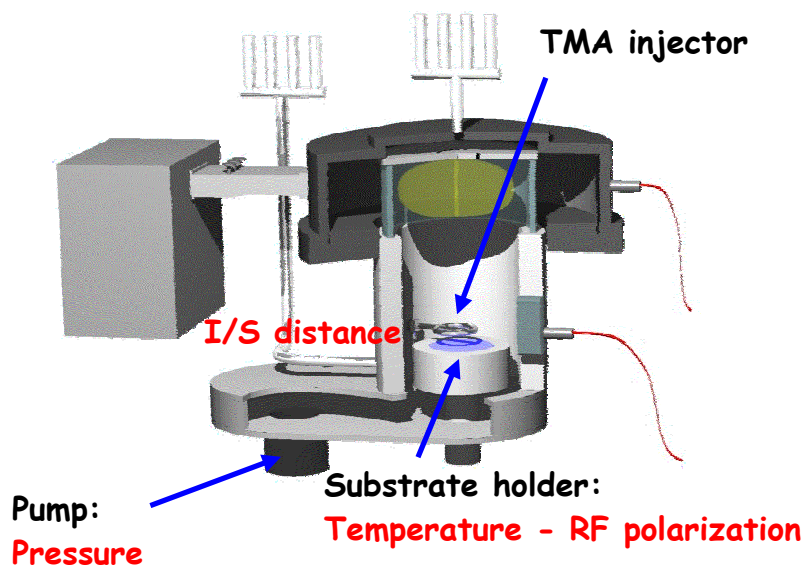


**Figure 26: Image of the PECVD deposition system highlighting relevant experimental parameters.**

The experimental conditions for the deposited alumina coatings along with the results are described in Table 1.

<b>Non hermetic RF MEMS</b>	<b>Ref: ASP-06-BO/PH/EA-45</b>		
	DATE : 1/03/06	ED/REV :V10	PAGE : 43 / 89

**table 7: Experimental conditions and results for PECVD alumina films**

N° exp	Temp	Pressure	polar	I/S	duration	thickness	Dep. rate	$\epsilon$	Ra mean	OH
	°C	Pa	Volts	cm	min	nm	nm/min		nm	A cm <sup>-1</sup>
1	300	5	150	4	2,50	245	98,0	4,7	4,3	82
2	RT	5	150	4	2,50	245	98,0	7,3	4,3	53
3	RT	1	150	8	5,00	350	70,0	8,9	2,4	20
4	300	1	0	8	5,00	390	78,0	10,4	1,9	77
5	RT	5	0	8	4,66	301	64,6	10,5	60,4	60
6	300	1	150	4	2,50	423	169,2	10,8	9,3	12
7	300	5	0	8	5,00	325	65,0	9,0	11,2	65
8	RT	1	0	4	1,66	362,5	218,4	9,7	1,4	72
9	300	1	150	8	5,00	361,5	72,3	10,1	2,3	6
10	RT	5	150	8	5,00	214	42,8	5,0	7,2	65

The results depicted in the table were obtained by using profilometry (for thickness and deposition rate measurements), Atomic Force Microscopy –AFM (roughness), FT-IR spectroscopy (–OH density) and RF measurements of MIM capacitors (for relative permittivity). It can be seen that the characteristics of the films are highly influenced by the experimental conditions. An example is given in Figure 27 which shows roughness evolution for two samples obtained in different temperature and pressure conditions.

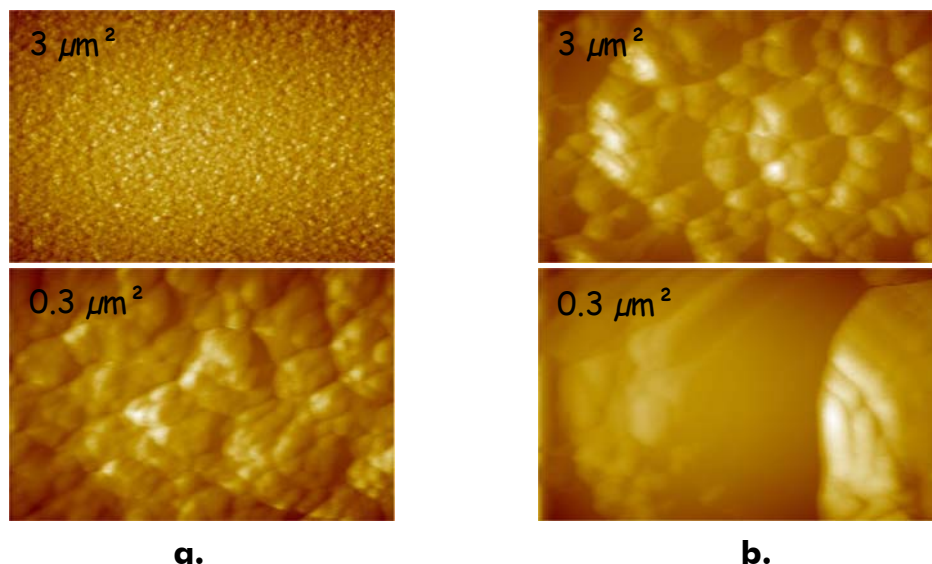


**Figure 27 : Surface roughness (calculated from AFM images) for two Al<sub>2</sub>O<sub>3</sub> films deposited in different experimental conditions: a) sample 4 (T= 300°C, p=1 Pa) with Ra roughness= 1.9nm and b) sample 5 (T= RT, p=5 Pa) with Ra roughness= 60.4 nm**

<b>Non hermetic RF MEMS</b>	<b>Ref: ASP-06-BO/PH/EA-45</b>		
	DATE : 1/03/06	ED/REV :V10	PAGE : 44 / 89

These preliminary results allowed us to extract the optimum parameters for the PECVD films deposition, as follows:

- total pressure of 1 Pa (at low pressure all films characteristics are better for MEMS applications)
- IS distance of 8 cm (for optimum deposition rate)
- Temperature – its influence being not fully conclusive we will use both RT or 300°C
- RF polarisation – still to optimise, between 0 and 150 V.

Based on these findings the final switches with PECVD-alumina as dielectric were realized using a total pressure of 1 Pa and an IS distance of 8 cm. We varied the deposition temperature (RT and 300°C) and RF polarisation of the substrate (0 and 150 V). The thickness and deposition rate for the 4 experimental conditions combinations are described in table 8.

**table 8 : Experimental conditions and results for PECVD-deposited Al<sub>2</sub>O<sub>3</sub> films**

No.	Temp °C	Polarization V	Time min	Thickness nm	Dep. rate nm/min
<b>a1</b>	<b>RT</b>	<b>0</b>	<b>4.5</b>	<b>215</b>	<b>47.78</b>
<b>b1</b>	<b>RT</b>	<b>150</b>	<b>4.5</b>	<b>202</b>	<b>44.88</b>
<b>c1</b>	<b>300</b>	<b>0</b>	<b>4.5</b>	<b>210.5</b>	<b>46.78</b>
<b>d1</b>	<b>300</b>	<b>150</b>	<b>4.5</b>	<b>230</b>	<b>51.11</b>

Although the samples were not fully characterized, we already observed that the films b1 and d1 are tougher, having a much lower etching rate in diluted HF solution (10% HF) than samples a1 and c1 (~10 nm/s compared to ~70 nm/s).

Indeed, the FT-IR spectra of samples a1 and c1 show large bands centred at ~3500 cm<sup>-1</sup> (not present in the FT-IR spectra of samples b1 and d1), characteristic to –OH vibration modes, which implies a higher H content, hence a lower density for these samples.

The results suggest that the RF polarization (applied for samples b1 and d1) is the main parameter that determines the sample's quality. If we recall that our needs go towards dense alumina dielectric films with low surface roughness and low density of -OH chemical bonds it can be seen that samples b1 and d1 meet these requirements. Unlike samples a1 and c1, they are much denser, have very low density of –OH bonds and low roughness (~2.4 nm, measured for samples 3 and 9 in Table 1, obtained in the same conditions as for b1 and d1). Based on these considerations, for the alumina PECVD deposition we will choose the experimental parameters employed for the fabrication of samples b1 and d1.

In conclusion, we may see that experimental deposition conditions have a high influence on films characteristics, which in turns may affect the characteristics and performances of the RF switches. The switches using these different types of dielectrics (Al<sub>2</sub>O<sub>3</sub>- PLD, Al<sub>2</sub>O<sub>3</sub>+DLC- PLD or Al<sub>2</sub>O<sub>3</sub>-(samples b1-d1)- PECVD) have been selected for RF MEMS manufacturing.

<b>Non hermetic RF MEMS</b>	<b>Ref: ASP-06-BO/PH/EA-45</b>		
	DATE : 1/03/06	ED/REV :V10	PAGE : 45 / 89

## 9. RF MEMS MANUFACTURING OVERALL ASSESSMENT

The goal of this section is to review each of the process variation that have been implemented within the present study. It includes work on the metal bridge deposition techniques, results obtained with the various dielectric (Teflon, DLC/AL2O3, Al2O3 PECVD and PLD,...) and dielectricless capacitive switch process evolution and optimization schemes used within the study.

### 9.1. METAL BRIDGE DEPOSITION TECHNIQUES

The electrostatic-actuated metallic membrane which form the bridge of the MEMS-RF switch play an important role in switch actuation: it should be stiff enough to allow the recovery of the initial, up-state position after the electrical actuation but in the mean time it should be actuated with acceptable voltages. A too stiff membrane means high elastic forces, which should be compensated during actuation by a high electrical field, equivalent to high actuation voltages. The parameters influencing the stiffness of the membrane are its thickness, its constituent materials and theirs residual stress developed during deposition. The final biaxial residual stress of the bridge (which depends on the deposition conditions) is quite difficult to control. As mentioned before, for the switch design it was estimated between 50 and 100 MPa for a typical, Ti/Au/Ti (5/500/5nm) multi-layer membrane Figure 28 made by thermally evaporated gold layer sandwiched between two Ti layers (the Ti is used here only for increasing the adhesion of gold on the deposited surfaces).

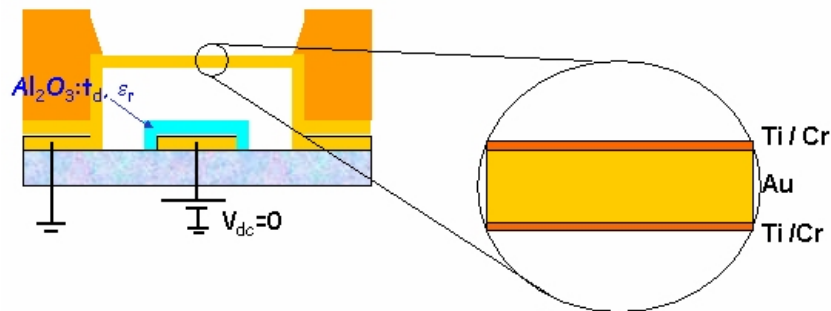


**Figure 28 : Schematic picture a MEMS-RF dielectric switch describing the components of the metallic membrane (Cr is used here as an alternative to Ti, see below)**

In order to validate the choice for a specific metallic membrane we performed a survey scan over several types of membranes: thin, thermally evaporated tri-layers like Ti/Au/Ti, Cr/Au/Cr with overall thickness of  $\sim 500$  nm or thick electroplated gold membranes of  $1.5 \mu\text{m}$  (using thin seeding layers of Ti/ Au or Cr/ Au – 5/ 100 nm). Since the equivalent residual stress of beams composed of different materials is given by  $\sigma_e = \frac{\sum(\sigma_n * t_n)}{\sum t_n}$  (where  $\sigma_n$  is the residual stress of the individual component and  $t_n$  is its thickness), the use of Cr instead of Ti was meant as a solution to compensate the low –tensile stress of the Au layer with the high-tensile stress of Cr (up to 1-2 Gpa).

For testing the actuation behavior of these types of membranes we fabricated MEMS switches by using alumina dielectric obtained either by PECVD or PLD method. The fabrication steps are

<b>Non hermetic RF MEMS</b>	<b>Ref: ASP-06-BO/PH/EA-45</b>		
	DATE : 1/03/06	ED/REV :V10	PAGE : 46 / 89

presented in Figure 29. Briefly, the electrodes (signal and ground lines) were patterned on a 5/150 nm-thick Ti/Au bi-layers made by thermal evaporation on high-resistivity Si or quartz substrates. Then the Al<sub>2</sub>O<sub>3</sub> dielectric layer was deposited either by pulsed laser deposition (PLD) or plasma enhanced chemical vapor deposition (PECVD). A 2.2 μm-thick photoresist layer (Shipley, S1818 or S1828) was spin-coated and lithographically patterned as the sacrificial layer and typically, a 0.5 μm-thick tri-layer Ti/Au/Ti was further evaporated to form the bridge (alternatively, Cr/Au/Cr or thick electroplated membrane were used). The anchors of the bridge and the electrodes were thicken up to ~ 3 -μm using gold electroplating in order to increase the stiffness of the device. The last steps include patterning of the membranes using wet etching followed by releasing of the suspended membranes (by removing the sacrificial layer using acetone and isopropyl alcohol or using a CO<sub>2</sub> critical point drier system).

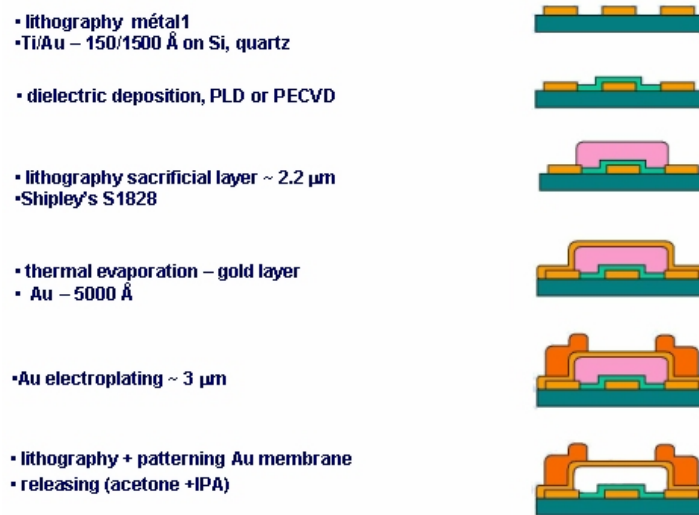


**Figure 29 : Fabrication steps for manufacturing the MEMS-RF switches**

In the case of PECVD, prior to the alumina deposition, the the electrodes (signal and ground lines) were submitted to an Ar plasma treatment (1 Pa total pressure, 150 sccm, 1600 W total power, -150 V RF polarization for 10 minutes) in order to obtain smother metallic surfaces for increasing the dielectric adhesion and obtain a better alumina roughness. After this treatment of the metallic electrodes we observed a reduction of their rms roughness from of ~15-30 nm down to 1.5-3 nm, as indicated by AFM measurements in Figure 30.

<b>Non hermetic RF MEMS</b>	<b>Ref: ASP-06-BO/PH/EA-45</b>		
	DATE : 1/03/06	ED/REV :V10	PAGE : 47 / 89

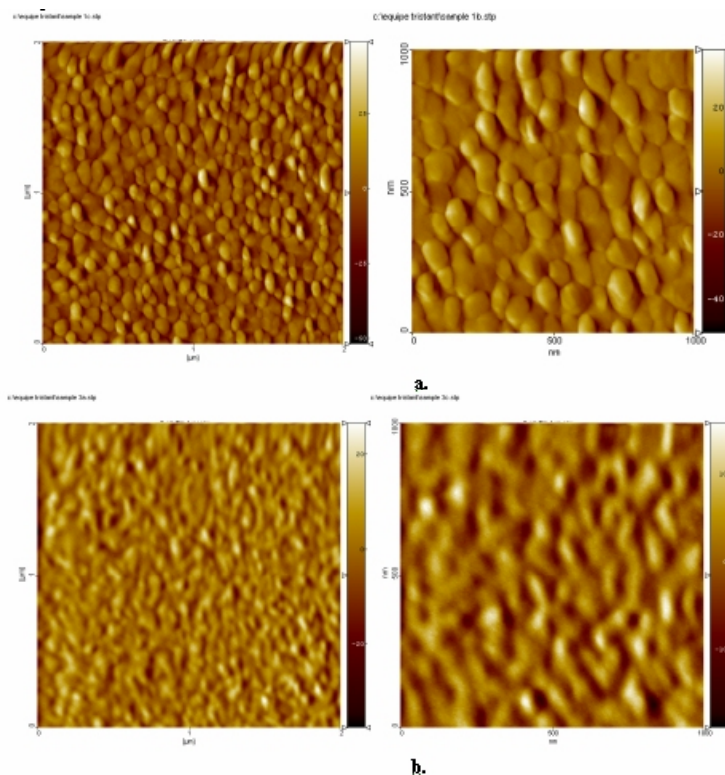


**Figure 30 : AFM measurements (2  $\mu\text{m}^2$ -area at left and 1  $\mu\text{m}^2$ -area at right) for a 150 nm-thick evaporated Au layer: a) as-deposited and b) after Ar-plasma treatment for 10 min.**

RF measurements of the PECVD alumina circuits revealed that there are  $\sim 8$  db of insertion losses (Figure 31). A closer analysis (resistivity measurements of the signal line and between the signal line and the ground lines) revealed that the signal line has a quite low conductivity. The source of this problem comes from the surface preparation procedure of the wafers before alumina deposition in the PECVD reactor. Indeed, the metallic electrodes exposed to Ar plasma are partially etched/ sputtered in the cleaning process inducing low conductivity of the signal line. The circuits realised with alumina PLD does not present these insertion losses, since they were not treated under Ar plasma (Figure 32). Therefore we decided to discard this plasma cleaning step for the future fabrication processes.

<b>Non hermetic RF MEMS</b>	<b>Ref: ASP-06-BO/PH/EA-45</b>		
	DATE : 1/03/06	ED/REV :V10	PAGE : 48 / 89

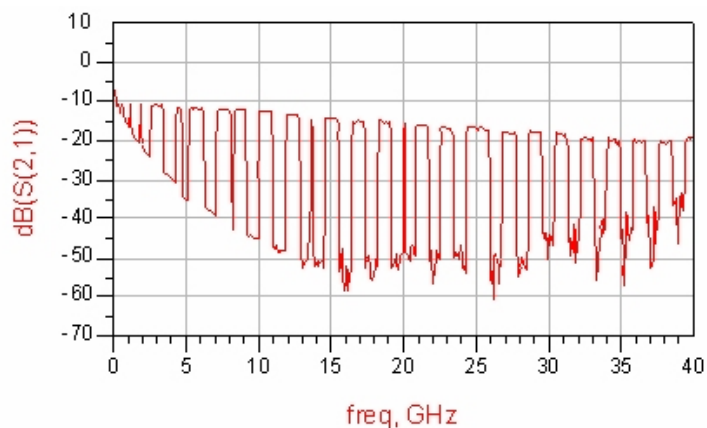


**Figure 31 : RF measurements of switches with PECVD alumina (Cr/Au/Cr – 15/550/15 nm membrane, 8Hz, 70 V actuation frequency and voltage, sinusoidal waveform)**

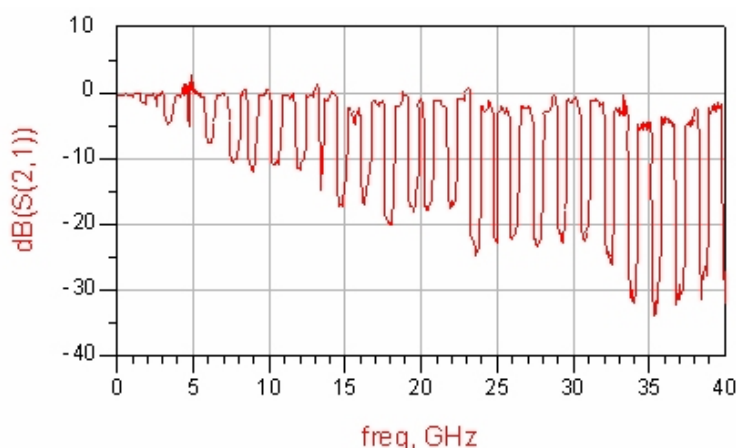


**Figure 32 : RF measurements of switches with PLD alumina (Cr/Au/Cr – 15/550/15 nm membrane, 10Hz, 70 V actuation frequency and voltage, sinusoidal waveform)**

Concerning the fabricated membranes, some of the switches made with the Cr/Au/Cr membranes show good actuation (for voltages between 40 and 60 V) but most of them are sticking on dielectric. In the case of the switches made with the thick electroplated gold membrane (1.5  $\mu\text{m}$  thick), the voltages needed for the actuation are very high (>100 V which makes them incompatible with space use), beyond the maximum voltage we can apply in our vacuum measurement set-up. Investigations made by optical profilometry showed that these membranes are highly stressed and up-curved (see Figure 33). These profiles are a possible consequence of the highly stressed Cr/Au seed layers (10/ 100 nm thick) used for the thick gold electroplating. Indeed, similar electroplated membranes using instead Ti/ Au (5/ 60 nm) seed layers show clear improvement in the membrane shape (Figure 34).

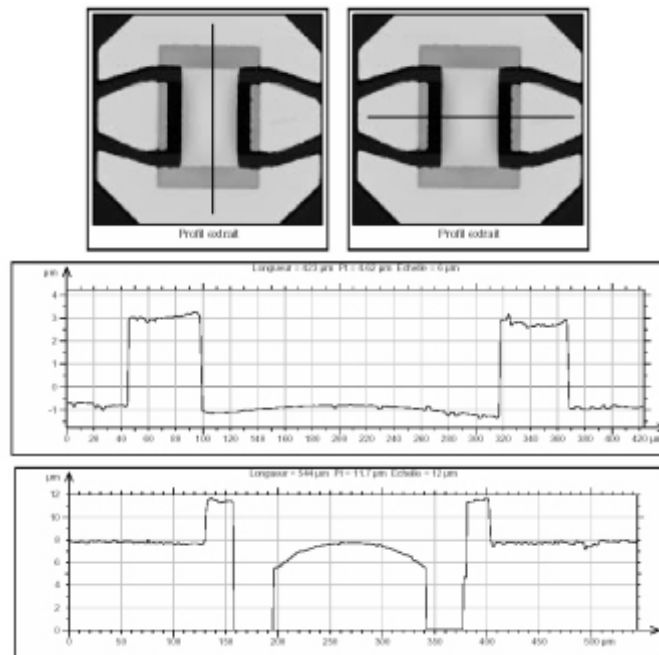


**Figure 33 : Shape of the membrane sections obtained by optical profilometry for a 1.5 μm-thick gold electroplated membrane with Cr/ Au (10/ 100 nm) seed layers.**

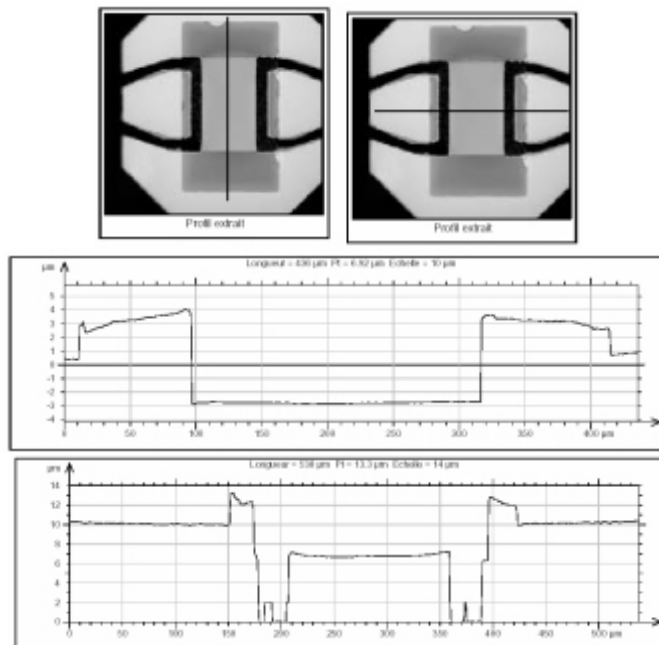


**Figure 34 : Shapes of membrane sections obtained by optical profilometry for a 1.5 μm-thick gold electroplated membrane with Ti/ Au (5/ 60 nm) seed layers.**

Nevertheless, also in this last configuration (Ti/ Au seed layer and thick electroplated membrane) the voltages need for actuated the switches are extremely high (>150 V), beyond our actuation set-up possibilities and their use on satellite platform.

<b>Non hermetic RF MEMS</b>	<b>Ref: ASP-06-BO/PH/EA-45</b>		
	DATE : 1/03/06	ED/REV :V10	PAGE : 50 / 89

We noticed that the use of Cr/ Au/ Cr or of the thick electroplated gold layers combinations do not offer acceptable results in term of actuation behaviour of the switches. Therefore we focused our researches on identifying the experimental deposition parameters, which allows the fabrication of stiff though low actuated metallic membranes in the Ti/ Au/ Ti configuration. Although the first exploratory experiments result in low-stressed membranes resulting in buckling of the bridges when actuated, we managed to identify the conditions for obtaining stiff bridges, which can be actuated at relatively low voltages (20-35 V). Two important parameters are essential for the fabrication of such membranes. One is related to the deposition of the metallic membrane (a suitable choice of the evaporation rate for the gold material) and the other one involves the selection of a proper resist for the sacrificial layer (common photo-resists like Shipley's S1818 or S1828 do not withstand heating during metal evaporation and they are also deformed by the in-plane stress from the metallic layer; they were replaced by a temperature-resistant sacrificial layer – PMGI). Figure 35b and c shows a SEM picture of such a switch obtained by the optimised fabrication process (PMGI sacrificial layer and stiff Ti/ Au/ Ti membranes) having dimensions of 240 x 160  $\mu\text{m}^2$ , which is the largest element of an array (partly showed in Figure 8a) containing 30 membranes with different dimensions (the smallest ones having an area of 120 x 60  $\mu\text{m}^2$ )

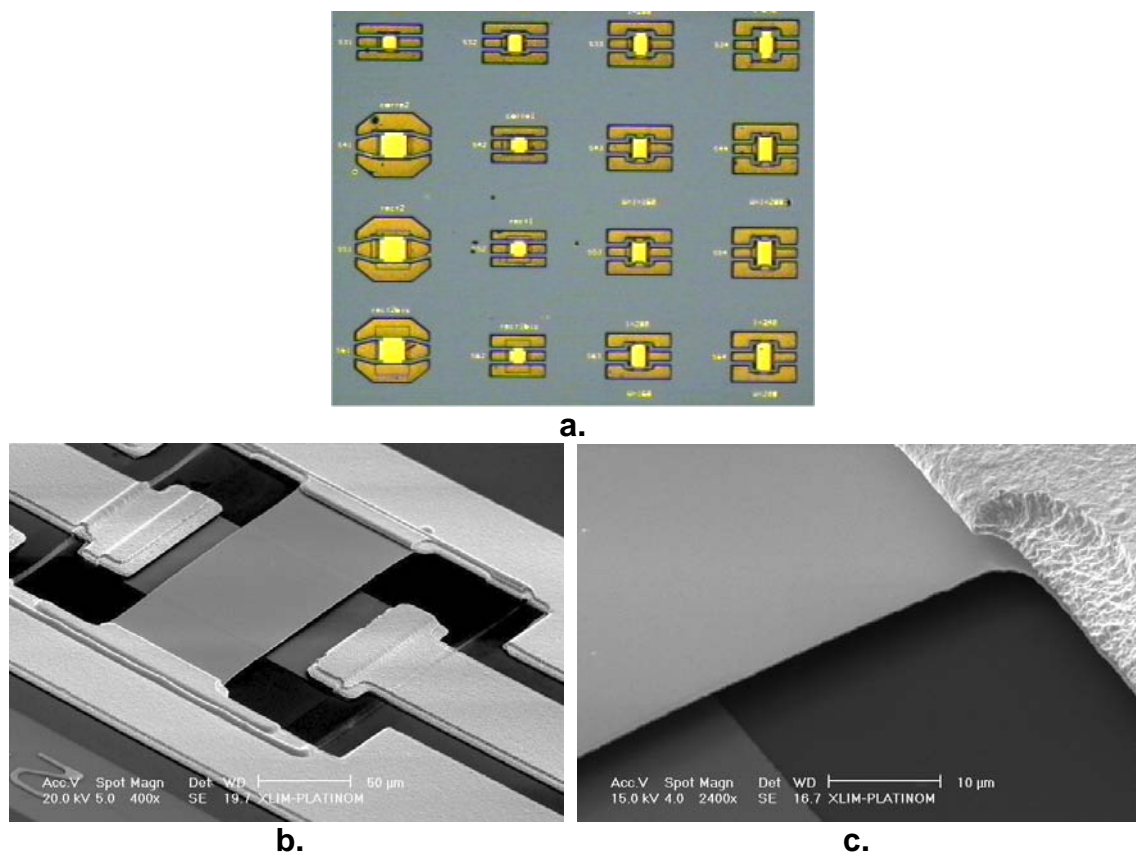


**Figure 35 : Optical microscopy picture of MEMS switches with different dimensions (a) and scanning electron micrograph (SEM) of a typical metallic micro-membrane (b) with a closer view of the suspended bridge over the actuation electrode (c)**

The profile of a typical switch (Figure 36) shows a relatively low-stresses but stiff metallic membrane with slightly up-warded sides in the small-dimension direction.

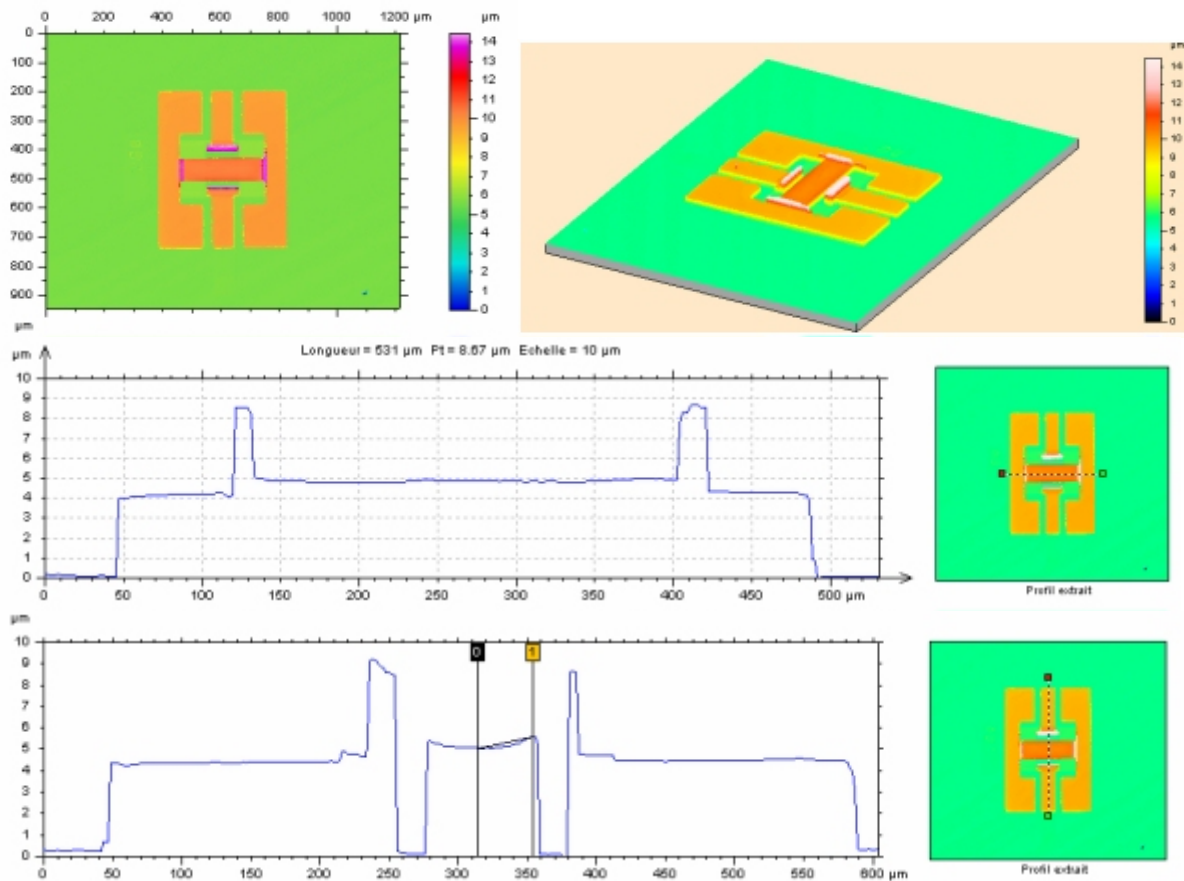


**Figure 36 : Shape of the metallic membrane sections obtained by optical profilometry measurements.**

An important parameter of a MEMS-RF switch is its switching time. This parameter translates into the switching actuation speed, which is determined, in a first-order approximation, by the membrane's mechanical primary resonant frequency. The higher this frequency, the faster is the switching speed.

Depending on the dimensions, the metallic membranes have a relatively high mechanical resonant frequency at room-temperature (RT), ranging from ~ 90 kHz (for the 240 x 160 μm<sup>2</sup>-area membranes) up to 170 KHz (for the 120 x 60 μm<sup>2</sup> ones). Figure 10 shows the temperature evolution of the resonant frequency for a 240 x 160 μm<sup>2</sup>- area mirror undergoing a cooling-heating cycle between RT and liquid-nitrogen (LN<sub>2</sub>) temperature (77 K). During the cooling cycle the resonant frequency is increasing up to 250 KHz but the membrane recovers its mechanical behavior when heating back to RT. Typical switching times ranges between 1 and 3 μs as measured from switching time recordings when applying a square actuation waveform on the switches.

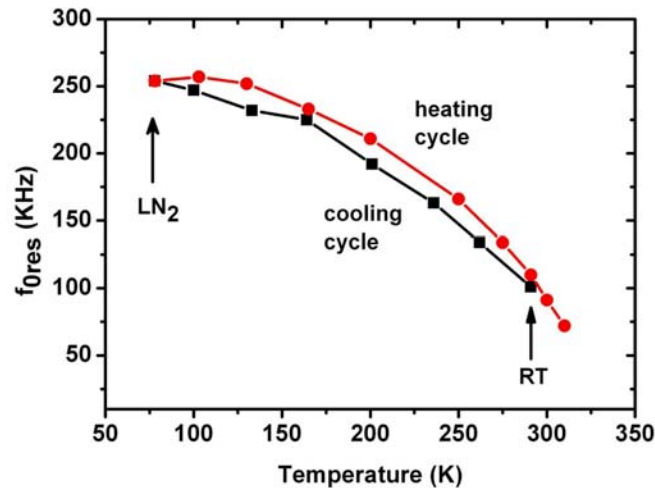


**Figure 37 : Mechanical resonant frequency evolution with temperature for a 240 x 160µm<sup>2</sup>- area Ti/Au / Ti membrane.**

The stiffness of the bridges was evaluated by measuring the spring constants of the membranes using a nanoindentation method. A sharp nanoindenter was applied in the centre of the membranes with a constant speed and the applied force versus the vertical deformation was recorded. The dependence of the force as a function of the deformation (Figure 37) combined with electromechanical simulations of the experiment using Ansys (Figure 38) allows us to obtain the typical values of the spring constants of the membranes which ranges between 20 and 70 N/m, depending on the dimensions.

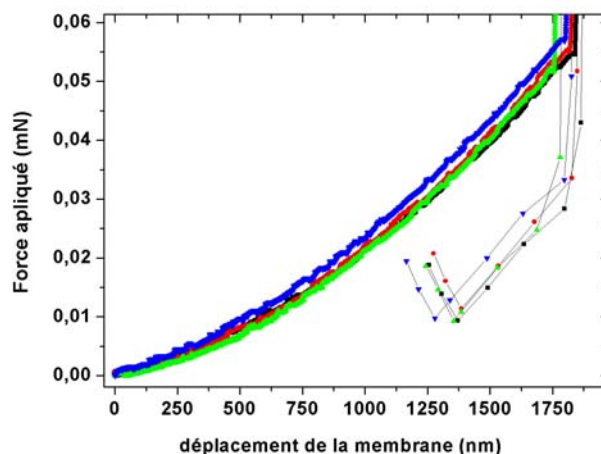


**Figure 38 : Typical loading-unloading curves (applied force as a function of the membrane deformation) obtained from nanoindentation experiments for spring constant calculations.**

<b>Non hermetic RF MEMS</b>	<b>Ref: ASP-06-BO/PH/EA-45</b>		
	DATE : 1/03/06	ED/REV :V10	PAGE : 53 / 89

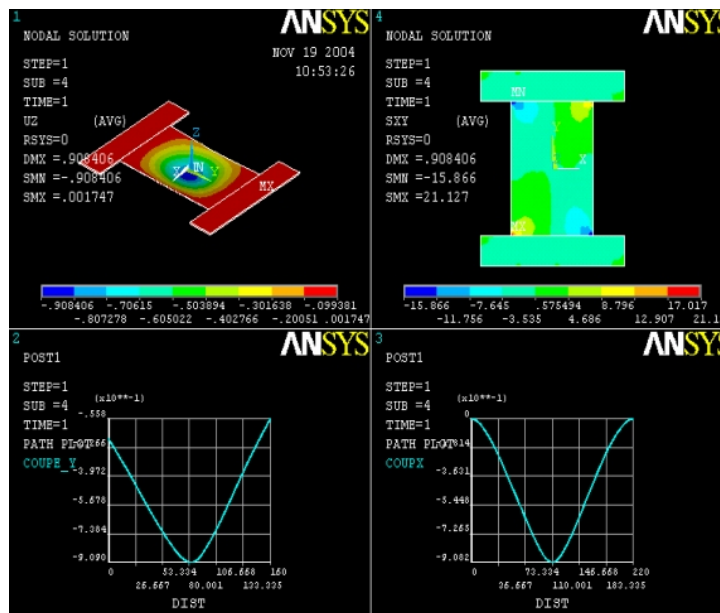


**Figure 39 : Electromechanical simulations using Ansys showing deformation and stress values when applying a mechanical force in the centre of the membrane.**

In conclusion, the fabrication process is thoroughly controlled, the main parameters of the switch (that depends in general on the structural material, dimensions, stress developed during fabrication) being displayed below:

- stiffness - spring constant,  $k \sim 20 - 70 \text{ N/m}$
- pull-in or actuation voltage,  $V_{\text{pull-in}} \sim 15 - 35 \text{ V}$  mechanical resonant frequency,  $f_{\text{res}} \sim 90 - 150 \text{ kHz}$  switching time,  $t_s \sim 2 - 3 \mu\text{s}$

## **9.2. OVERALL STATUS ON NEW DIELECTRIC DEPOSITION TECHNIQUES AND THEIR IMPACT ON RELIABILITY**

### **Protective layers investigation**

In order to investigate the dielectric impact on switch reliability the alumina layer deposition (obtained by PLD or PECVD) was optimized especially from the point of view of thickness and composition (in the case of PECVD deposition). In terms of protective layers thin films of PTFE and tetrahedral carbon (ta-C) were fabricated on top of the alumina layers. They are supposed to increase the hydrophobic characteristics of the alumina dielectric and the switch resistance in humid environments. However, it was noticed that the PTFE layers deposited by PLD presented a high roughness, which could potentially influence- via the sacrificial layer- the membrane shape (which should be as smooth as possible for a perfect contact with the dielectric during on-state actuation). Based on these findings, this PTFE protection coating was then given up.

For the thin ta-C (20 nm) deposited by PLD on top of the alumina layers ( $\sim 220 \text{ nm}$  thickness) it was observed that the fabricated switches were drastically damaged once the actuation voltage is applied. The phenomenon was explained by a strong electrical conduction mechanism in the thin ta-C layer (similar to the field emission from the same type of material)

<b>Non hermetic RF MEMS</b>	<b>Ref: ASP-06-BO/PH/EA-45</b>		
	DATE : 1/03/06	ED/REV :V10	PAGE : 54 / 89

under the strong electrical field applied to the switches. This was verified by including the same type of sandwich layer (alumina+ ta-C) in MIM-type capacitances (with gold electrodes) implemented in a microwave coplanar waveguide (CPW) line (Figure 40) and by performing I(V) measurements on these structures.

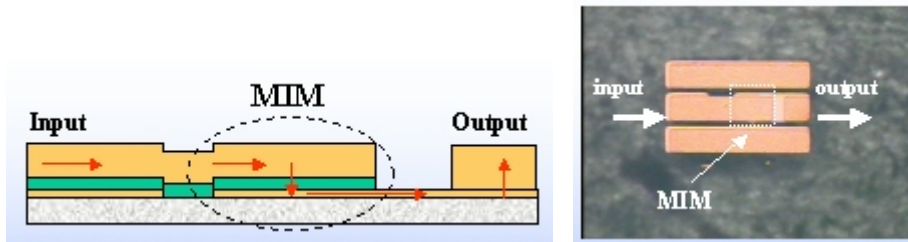


**Figure 40 : MIM-type capacitances implemented in a microwave coplanar waveguide (CPW) line.**

It was noticed that the current through the MIM structure increase constantly with the applied electrical field followed by an abrupt augmentation after a certain value of the electrical field (Figure 41). After reaching a maximum (e.g. ~170 mA) the current decreases to zero even if the voltage is increased. Afterwards the system behaves like a capacitance, without any current flow. This phenomenon could not be explained at this stage. It could be either material related (field emission through a dielectric layer like alumina is still unexplained) or process related (unwanted short (pin holes, step coverage problems) between top and bottom electrode). A more systematic approach (process, thickness or temperature dependence) of this type of MIM capacitances could not be further pursued because of the availability of multi-layer PLD equipment.

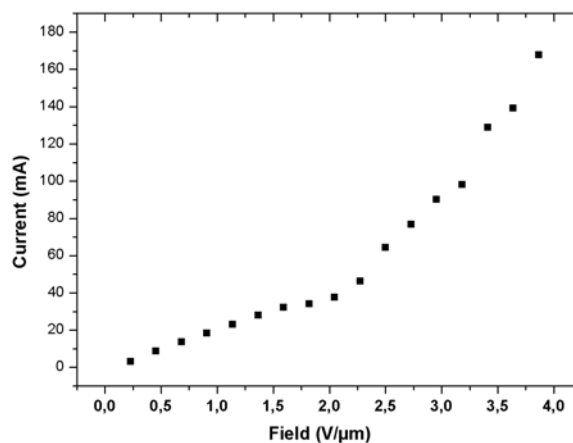


**Figure 41 : Current versus applied field for a MIM-type capacitance made of alumina/ ta-C (220/ 20 nm) sandwiched between gold electrodes.**

The dielectric properties of Al<sub>2</sub>O<sub>3</sub> layers obtained either by PLD or PECVD were studied by applying a.c. signals of different frequencies on the same type of MIM capacitive structures

<b>Non hermetic RF MEMS</b>	<b>Ref: ASP-06-BO/PH/EA-45</b>		
	DATE : 1/03/06	ED/REV :V10	PAGE : 55 / 89

containing the films under investigation. For the frequencies range 50 MHz- 3 GHz the capacitance of the MIM structures was obtained after simulations of the CPW response at MW excitation frequencies. The dielectric constant of the pure alumina is around  $\epsilon_r = 9.8$  for the PLD-obtained layers while for the PECVD-ones this values is slightly lower (8-9) for the entire investigated frequencies domain.

**-OH contamination of the Al<sub>2</sub>O<sub>3</sub> layers**

-OH type groups within Al<sub>2</sub>O<sub>3</sub> could be seen as contaminant which are strongly linked to the reactivity of the Al<sub>2</sub>O<sub>3</sub> with chemicals and environment as well as its density. We could also anticipate some impact on the charging of the dielectric, but this has not been clearly demonstrated within this study.

The PLD-fabricated alumina layers do not show any contamination with -OH-type groups as shown in FTIR spectrum of Figure 42.

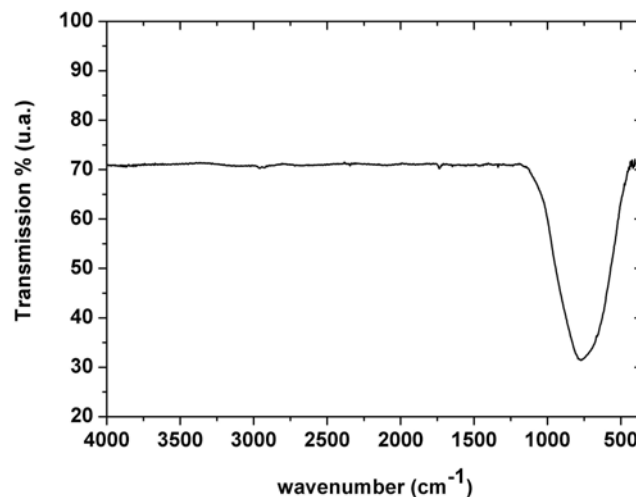


**Figure 42 : Fourier transformed IR (FT-IR) transmission spectrum of a 1 μm-thick Al<sub>2</sub>O<sub>3</sub> film obtained by PLD at room temperature; it is noticed the absence of OH- absorption bands between 3400 and 3600 cm<sup>-1</sup>.**

In the case of the PECVD obtained alumina layers we noticed for the “a-” and “c-type” samples absorption bands in the FT-IR transmission spectra which correspond to the -OH presence while the “b-” and “d-type” alumina samples do not presents such absorption bands (Figure 43).

<b>Non hermetic RF MEMS</b>	<b>Ref: ASP-06-BO/PH/EA-45</b>		
	DATE : 1/03/06	ED/REV :V10	PAGE : 56 / 89

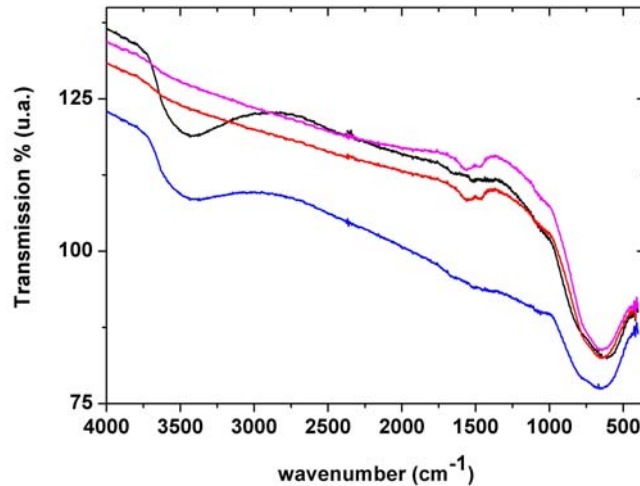


**Figure 43 : Fourier transformed IR (FT-IR) transmission spectrum of 200 nm-thick  $\text{Al}_2\text{O}_3$  films obtained by PECVD in the experimental conditions described in Table 2; it is noticed for the “a-” and “c-type” samples the presence of absorption bands between 3400 and 3600  $\text{cm}^{-1}$  corresponding to the  $-\text{OH}$  groups.**

It was further decided to use only one type of PECVD alumina films, the “d-type” one, since the deposition rate is slightly higher for this type of layers compared with the “b-type ones” and they are more resistant to acid etching in a % HF acid bath (perceived as an element that witness of their higher density).

The roughness of these PECVD  $\text{Al}_2\text{O}_3$  “d-type” layers is quite low, comparable with that of the PLD  $\text{Al}_2\text{O}_3$  films ( $R_a \sim 1-2 \text{ nm}$ ).

### **Breakdown voltage of the $\text{Al}_2\text{O}_3$ layers**

Breakdown voltage (BV) of the dielectric layers is a critical parameter for the optimum functioning of the MEMS-RF device. The BV events in dielectrics are generally explained by a buildup in the dielectric bulk of defects produced by the stress of the high field applied across the film (in the actuated, on-state of the switch). Defect concentration increases up to a critical value corresponding to the onset of a conductive, percolation path joining the lower and the upper (bridge) electrodes. This triggers the breakdown of the dielectric, which loses its insulator characteristics.

In order to investigate the “strength” of the alumina insulators under high electric fields we recorded the breakdown voltage of  $\text{Al}_2\text{O}_3$  layers of different thickness (200 and 400 nm, obtained either by PECVD or by PLD) sandwiched between two gold electrodes (MIM capacitances like those depicted in Figure 40). The results are presented in table 9.

<b>Non hermetic RF MEMS</b>	<b>Ref: ASP-06-BO/PH/EA-45</b>		
	DATE : 1/03/06	ED/REV :V10	PAGE : 57 / 89

Layer	Deposition method	Thickness (nm)	Breakdown voltage (V)	Corresponding electric field MV/cm
Al <sub>2</sub> O <sub>3</sub>	PECVD type d	200	~35-50	~1.7-2.5
Al <sub>2</sub> O <sub>3</sub>	PECVD type d	400	> 100	> 2.5
Al <sub>2</sub> O <sub>3</sub>	PLD	200	~30-40	~1.5-2
Al <sub>2</sub> O <sub>3</sub>	PLD	400	~45-60	~1-1.5

**table 9 : Breakdown voltage for Al<sub>2</sub>O<sub>3</sub> layers of different thickness obtained by PLD and PECVD**

It can be observed, as a general rule, that the thicker the layer the better they resist under the high fields applied across them. For a given thickness, the alumina PECVD layers (especially the 400 nm-thick ones) seem to stand higher voltages than the PLD-obtained films. For the PLD layers there is no direct relationship between the magnitudes of the applied electric field and the breakdown voltage. It seems that the breakdown for this layers does not depends on the thickness but it is rather triggered by its composition and structure (impurities, defects etc.). Since the values of the BV for the 200 nm –thick layers (obtained either by PECVD or PLD) are close enough to the actuation voltage values of the MEMS switches it is suitable to use thicker alumina layers (of 400 nm for example) for the switches meant to be tested (cycling, RF measurements, 1/C(V), irradiations etc.).

### **9.3. DIELECTRICLESS CAPACITIVE SWITCH PROCESS EVOLUTION AND PERFORMANCE ASSESSMENT**

This very innovative approach to realize dielectricless capacitive switches has been assessed and has proven the concept for long time actuation of the switch.

Still, while this technique allows to demonstrate dramatic improvement of the reliability of capacitive RF-MEMS switches, the contrast between the two states is strongly degraded since the two positions are using an air gap separating layer in both states with dielectric constant of 1 versus several tens for standard dielectric.

In order to improve the performances of the switch, a novel structure has been developed to increase the contrast between the two states. The principle of the structure is outlined in the figure below.

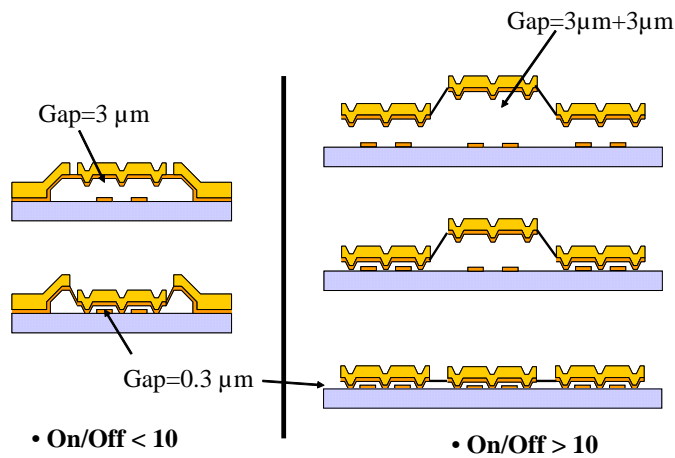
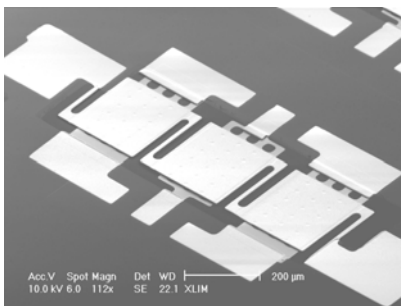
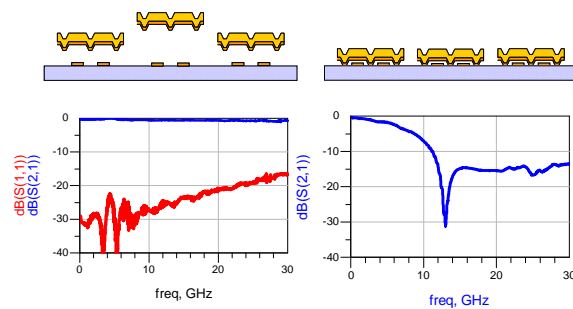


**Figure 44 : Principle of the 2 stage switch**



(a) SEM picture of the RF-MEMS switch



(b) Measured performances in the up state and down states

**Figure 45 : Proof of concept of 2 stage air switch**

Some of the fabricated structures are presented above, along with the measured performances. The structures performances are strongly improved and allow to further integrate dielectricless switches in signal routing applications and lower frequency applications.

In conclusion for this part, the reliability of capacitive switches has been dramatically improved using this technique. Using single layer structures, the switches can achieve contrasts in the range of 8-10, which is very well suited for phase shifting applications or tuning applications. More applications are possible using double layer sacrificial layers, to improve the RF performances. This type of components should be further developed to assess their behaviour and improve lifetime testing of the structures.

<b>Non hermetic RF MEMS</b>	<b>Ref: ASP-06-BO/PH/EA-45</b>		
	DATE : 1/03/06	ED/REV :V10	PAGE : 59 / 89

#### 9.4. OPTIMIZATION SCHEME USED AND DEVICE STATUS AVAILABLE FOR RELIABILITY TESTING

The S-parameters of switches with different dimensions were measured in both up and down state positions. Figure 46 shows one typical measured switch (S35, 280  $\mu\text{m}$  in length, 80  $\mu\text{m}$  in width and with a bottom central electrode width of 120  $\mu\text{m}$ ) fabricated with different types and thickness of alumina dielectric.

The S parameters were recorded during switch actuation with a sinusoidal bi-polar waveform at 5 Hz (Figure 47). The insertion losses ( $S_{21}$ - up state) of the switch fabricated with a 400 nm-thick alumina PECVD dielectric are very low, less than 0.6 dB from 50 MHz to 30 GHz. In the down state position 15 dB isolation is achieved at 20 GHz, and the maximum isolation is about 20 dB at 30 GHz. The  $S_{21}$  curves (in the up- and down-states) were fitted using an equivalent RLC circuit allowing us to obtain the up state and down state experimental capacitances of the switch. The estimated capacitance in the up state is  $\sim 54$  fF while in the down state is  $\sim 1.5$  pF, giving an experimental  $C_{\text{on}}/C_{\text{off}}$  ratio of 28.

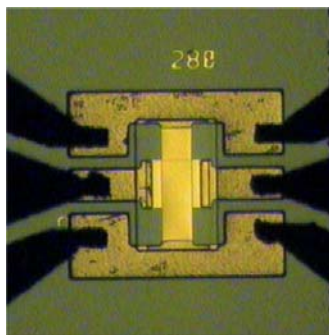


**Figure 46 : Typical MEMS-RF switch used for S parameters measurements (length-280  $\mu\text{m}$ , width- 80  $\mu\text{m}$ , bottom electrode width-120  $\mu\text{m}$ ).**

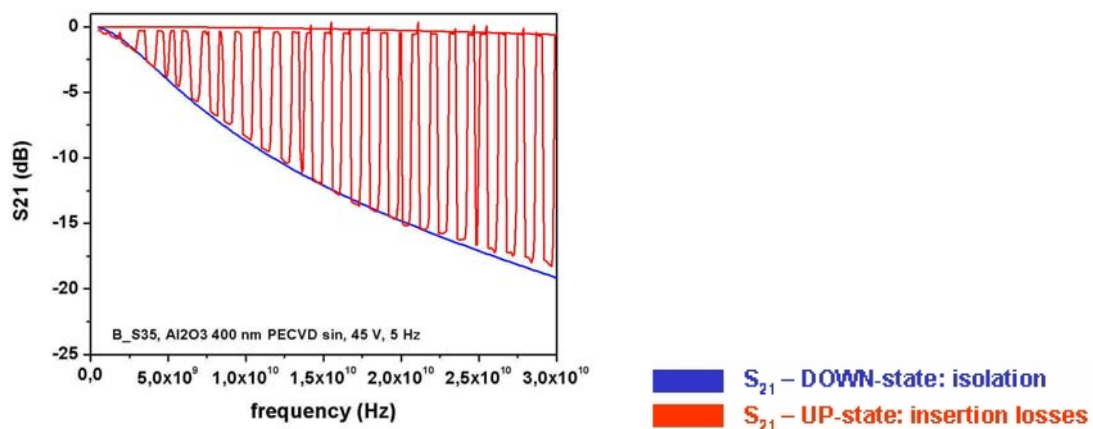


**Figure 47 :  $S_{21}$  parameter evolution during switch actuation with a sinusoidal bi-polar waveform at 5 Hz (switch S35, 400 nm-thick alumina PECVD dielectric) along with the simulated  $S_{21}$  responses in the up- and down states.**

<b>Non hermetic RF MEMS</b>	<b>Ref: ASP-06-BO/PH/EA-45</b>		
	DATE : 1/03/06	ED/REV :V10	PAGE : 60 / 89

A similar evolution of the  $S_{21}$  parameter for the same switch (S35) but fabricated with a 400 nm-thick alumina PLD layer is presented in Figure 48. We noticed isolation better than 15 dB between 18 and 30 GHz and better than 20 dB between 22 and 30 GHz with insertion losses lower than 0.6 dB from 50 MHz to 30 GHz. The measurements were obtained with no deembedding.

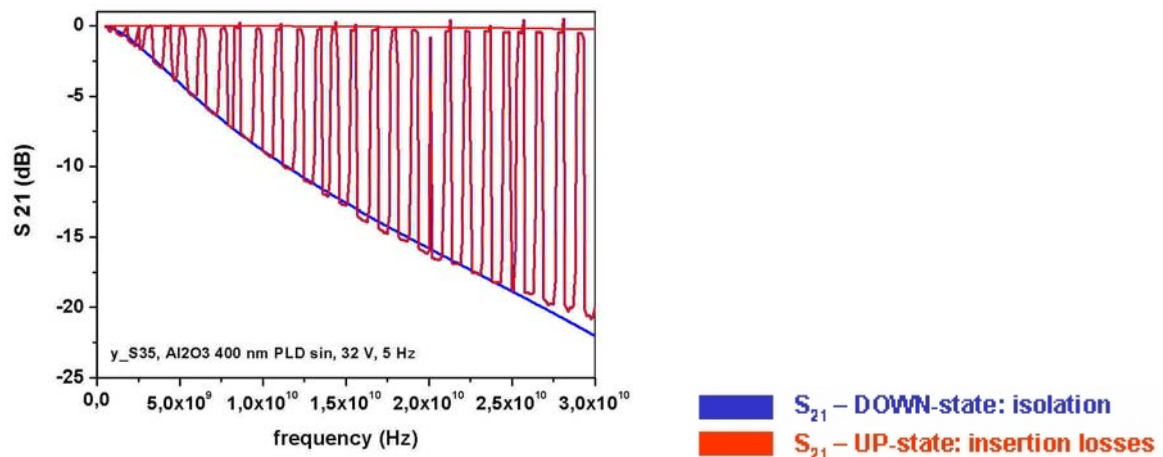


**Figure 48 :  $S_{21}$  parameter evolution during switch actuation with a sinusoidal bi-polar waveform at 5 Hz (switch S35, 400 nm-thick alumina PLD dielectric) along with the simulated  $S_{21}$  responses in the up- and down states.**

The estimated capacitance in the up state is  $\sim 51$  fF while in the down state is  $\sim 1.5$  pF, with an experimental  $C_{on}/C_{off}$  ratio of 29 which is of the same order of magnitude as for the switch with alumina PECVD layer. Figure 49 presents the evolution of the  $S_{21}$  parameter in the down state along with its simulation using an equivalent RLC circuit for an S35-type switch fabricated using 200 nm-thick PLD alumina dielectric. The insertion losses (not shown in the picture) are lower than 0.5 dB from 50 MHz to 30 GHz while the isolation is better than 15 dB from from 14 to 30 GHz and better than 20 dB from 20 to 30 GHz. The estimated capacitance in the up state is  $\sim 45$  fF while in the down state is  $\sim 2$  pF, with an experimental  $C_{on}/C_{off}$  ratio of  $\sim 45$  which is of about 1.5 times higher than for switches fabricated with the 400 nm-thick alumina dielectric.

<b>Non hermetic RF MEMS</b>	<b>Ref: ASP-06-BO/PH/EA-45</b>		
	DATE : 1/03/06	ED/REV :V10	PAGE : 61 / 89

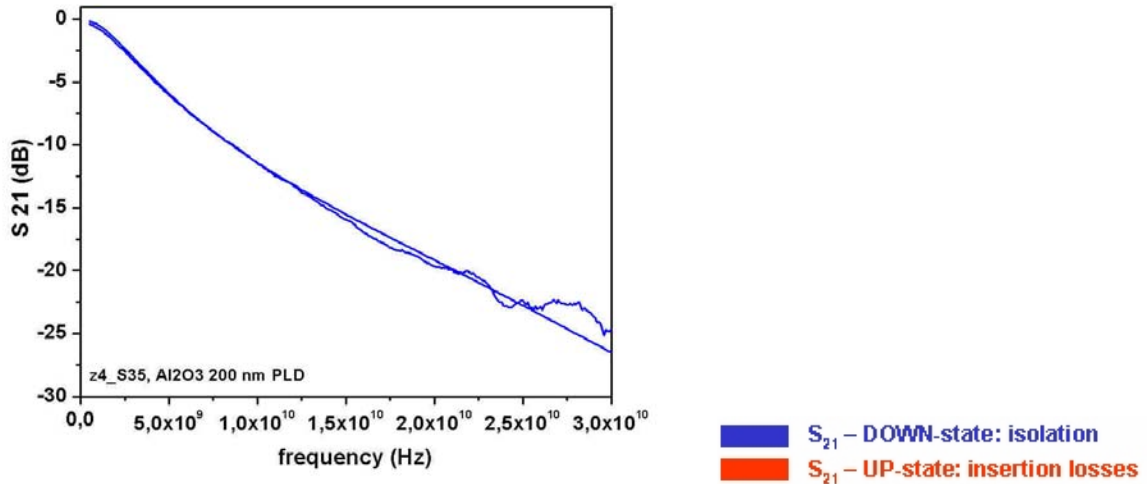


**Figure 49 :  $S_{21}$  parameter evolution in the actuated, down state (switch S35, 200 nm-thick alumina PLD dielectric) and the simulated  $S_{21}$  response.**

We may conclude by saying that the MEMS-RF switches fabricated using alumina dielectric (either by PECVD or PLD) show good RF performances. Although the 200 nm-thick alumina switches have a more limited lifetime (due to their low breakdown voltage they are more likely to suffer from stiction due to charging or to fail due to the dielectric failure) they show, however, an increased  $C_{on}/C_{off}$  ratio. Nevertheless, for reliability investigations it is suitable to use the 400 nm-thick dielectric switches that are more resistant to different failure modes associated with these types of circuits.

## 10. RELIABILITY ASSESSMENT

Based on the elements given in the sections before, we had to adapt our reliability test plan in order to better match with the sample availability, the compliance of the tests to be performed with RF MEMS reliability published results and the time constraints.

Based on our experience, stiction due to dielectric charging, is the main degradation mechanism we have noticed in the technology we assessed. In the following we have focused our study on dielectric charging phenomenon and its evolution total induced dose irradiation on the life time of the RF MEMS switches.

### 10.1. SAMPLE AND DEVICE AVAILABILITY FOR TESTING

For each fabrication batch, we have a min of 2 wafer part (wp) (size : < 1 cm<sup>2</sup>, about 40 devices per wp) including one ref wafer part, so that 1 wp can be left unstressed in standard storage environment when possible and that could follow any handling and transport applied to the wp to be stressed.

The detail of each batch is described below :

Batch 1 : Al<sub>2</sub>O<sub>3</sub> 400 nm PLD, substrate used is high resistivity silicon (1 ref. + wp1.1)

<b>Non hermetic RF MEMS</b>	<b>Ref: ASP-06-BO/PH/EA-45</b>		
	DATE : 1/03/06	ED/REV :V10	PAGE : 62 / 89

Batch 2 : Al<sub>2</sub>O<sub>3</sub> 400 nm PECVD, substrate used is high resistivity silicon (1 ref. + wp2.1 & 2.2)

Batch 3 : Al<sub>2</sub>O<sub>3</sub> 200 nm PECVD, substrate used is high resistivity silicon (1 ref. + wp3.1, wp3.2 wp3.3, wp3.4)

Batch 4 : Dielectric less (wp4.1 : only one piece will be available for this one but with enough functional switches), substrate used is fused silica.

## 10.2. TEST PLAN

Based on our experience in testing RF MEMS devices, we have tried to apply to the available components, representative test flows that are meant to give usefull information for the device life time. Because of dielectric charging problems that are encountered in most capacitive RF MEMS technologies, we thought that total dose radiation testing would be primarily important toward this degradation mechanism. It is also state of the art research, since very few publication are available worldwide.

Thermal stress handling capability is also a quite important issue if RF MEMS want to be used as any electronic component which needs to handle packaging related stresses.

Based on these elements, we have then selected 2 main test flows :

- Flow 1 : Total dose radiation testing up to 100 Krad (with reference taken to H<sub>2</sub>O) where most of the devices will be left unbiased due to limited life time of the devices
- Flow 2 : Thermal testing which consists in thermal storage (125 °C; 260 hrs, without biasing) and Thermal cycles (500 cycles, -55 + 125°C without biasing)

In addition to these quite standard tests, some endurance tests have been performed by IRCOM and AAS on selected switches representative from each batch, giving some results on behavior on long holding time in DC and AC biasing conditions (on dielectricless switch : batch 4), on-off cycling test at low frequency for PECVD 400 nm Al<sub>2</sub>O<sub>3</sub> (mainly on batch 2 because of fast charging mechanisms).

The amended test plan that we used for this contract is presented in the next page. It has been adapted with the switches availability, the representativness of the tests applied according to the technological maturity of the RF MEMS.

Below in this section, we have described each of the methods to be used to assess RF MEMS switch performance with example of measurements taken prior to proceeding with the test plan.

<b>Non hermetic RF MEMS</b>	<b>Ref: ASP-06-BO/PH/EA-45</b>		
	DATE : 1/03/06	ED/REV :V10	PAGE : 63 / 89

Material and technology assessment

**Process optimization and assessment phase**

Endurance tests :  
-on-off cycling  
-DC bias on testing

**Flow 1 : Total dose radiation test**  
4 switches per wafer part (wp) fully monitored

PECVD Al2O3 400 nm	PLD Al2O3 400 nm	PECVD Al2O3 200 nm	dielectricless
-----------------------	---------------------	-----------------------	----------------

Initial testing (C-V), optical observation and S parameter measurements

Total dose : 10 krad, 4 switches biased bipolar, other unbiased

Testing (C-V) and optical observation

Total dose : 23.4 krad

Total dose :10 krad (1)

Testing (C-V) and optical observation

Testing (C-V)

Total dose : 46.7 krad

Total dose :33.3 krad

Testing (C-V) and optical observation

Testing (C-V)

Total dose : Min 87 krad

Total dose :74.3 krad

Final testing (C-V), optical observation and S parameter measurements

**Flow 2 : Thermal tests**  
4 switches per wafer part (wp) fully monitored

PECVD Al2O3  
200 nm

PECVD Al2O3  
200 nm

Initial testing : S parameter measurements

Thermal storage  
125 °C 260 hrs

Thermal cycling  
(-55 °C, +125 °C)  
500 cycles

Final testing : S parameter measurements and optical observation

(1) switch biased in bipolar +/-70 V, 5 Hz

(3) switch biased in monopolar 64 V, 5 Hz

Note that due to high charging defects, PECVD Al2O3 200 nm thick has been given up in the flow 1.

<b>Non hermetic RF MEMS</b>	<b>Ref: ASP-06-BO/PH/EA-45</b>		
	DATE : 1/03/06	ED/REV :V10	PAGE : 64 / 89

### 10.2.1. Static S parameter measurements

Static because the applied biasing of the RF switch is set to a DC setting (or frequency higher than the mechanical response of the membrane) while the s parameters are taken by . If the RF MEMS have a life time compatible with the VNA acquisition system, this is a very accurate way to determine its electrical parameters from which you can deduce physical parameters such as membrane height in up position for shunt capacitive switches based on the reflection coefficient. The capacitance ratio between up and down state can be deduced based on the measured isolation of the switch.

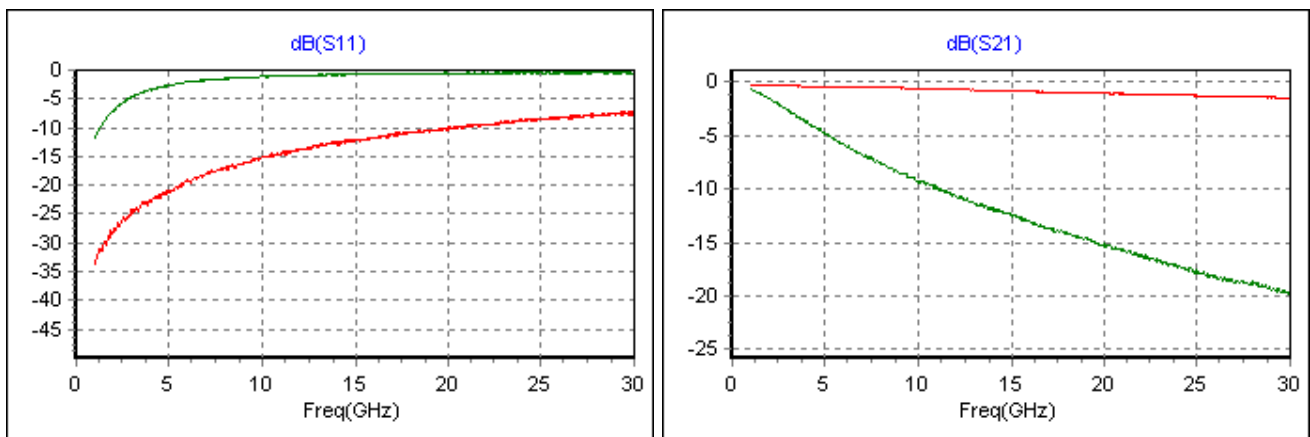


**Figure 50 : Example of measured S parameters on 400 nm Al<sub>2</sub>O<sub>3</sub> switches, bipolar 5 kHz, amplitude 100 Vpp, ambient atmosphere. green curve is in down position, red curve is up position**

### 10.2.2. Dynamic S parameter measurement

To minimize the charging effect on the switch dielectric, s parameter can be taken while modulating the biasing of the RF MEMS switch at a frequency where the switch can mechanically respond. We can then apply this mean on low life time switches to access their S parameters and relevant intrinsic characteristics with minimized impact on their actual lifetime.

### 10.2.3. CV curves

The electric fields applied on the dielectric layer of a RF-MEMS switch are typically higher than 1 MV/cm (> 20 V applied voltage over a ~200 nm-thick layer). At these high values, the dielectric is likely to suffer from charge injection from the metallic electrodes that can be trapped at the surface or even in the volume of the layers (Figure 51). As mentioned before, the high electric fields can even trigger defects generation in the dielectric layer, which may evolves as additional trap sites for electric charges.

<b>Non hermetic RF MEMS</b>	<b>Ref: ASP-06-BO/PH/EA-45</b>		
	DATE : 1/03/06	ED/REV :V10	PAGE : 65 / 89

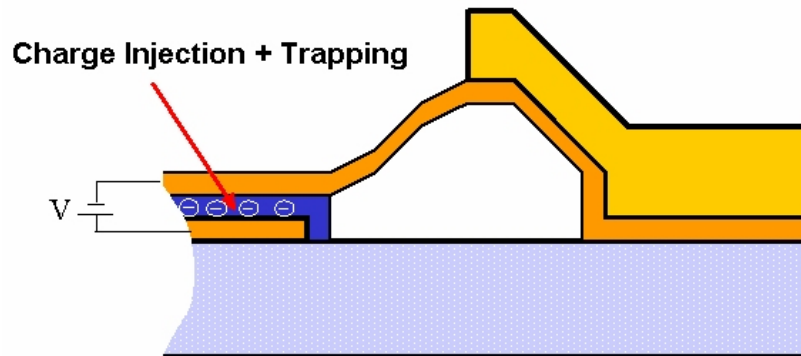


**Figure 51 : The high electric fields applied on the dielectric layers during switch actuation can induce charging or even electrical trap generation within the layer.**

As the charges are progressively trapped in the dielectric they will induce a built-in electrical potential ( $V_{charge}$ ), which can be of opposing sign to the one of the applied electric field over the layer ( $V_{actuation}$ ) (Figure 52). The appearance of a charging-induced electrical force opposing the one due to the actuation voltage of the MEMS switch will cause shifting of the  $V_{pull-in}$  or  $V_{pull-out}$  voltage values.

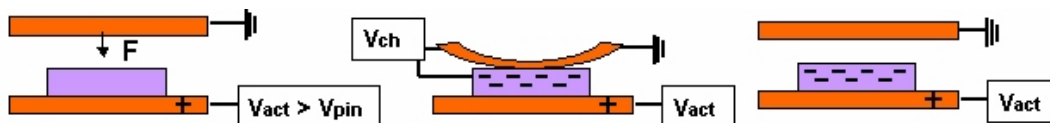


**Figure 52 : Charging induced built-in potential opposing the applied actuation voltage.**

During switch actuation, when the  $V_{actuation} > V_{pull-in}$  voltage is maintained over the electrodes and the opposing built in potential  $V_{charge}$  is higher than  $V_{pull-in}$ , the membrane comes up (possibly to a different up-state, with the off-state capacitance value affected). If  $V_{charge} < V_{pull-in}$ , the stiffest parts of the bridge come up, affecting the on-state capacitance value. When  $V_{actuation}$  is removed, depending on the sign and value of the  $V_{charge}$ , the bridge can remain stacked in the down position (stiction of the membrane) or it can come up, possibly to a different position (in this case, the values of capacitance in the up-state,  $V_{pull-in}$  and  $V_{pull-out}$  are modified). The charges trapped by the dielectric can flow away in time (the discharging time can vary, depending on the dielectric material, from second to days...) or by annealing.

As the dielectric charging was identified to be the main failure mode of the capacitive MEMS switches there is a high interest of the scientific community for identifying the specific charging mechanisms of dielectric layers which, combined with cycling tests under specific stress factors (humidity, temperature, actuation schemes etc.) may lead to switch operation models or lifetime predictions. Although there are currently several charging and lifetime prediction models proposed (usually developed for a specific combination of switch design/ process or dielectric type), the development of specific/ universal standard tests for MEMS-RF type circuits is still lacking.

The variation of the  $V_{pull-in}/V_{pull-out}$  values witnessing charging mechanisms (through electrode-dielectric charge transfer and trapping) of the alumina dielectric MEMS-RF switches were

<b>Non hermetic RF MEMS</b>	<b>Ref: ASP-06-BO/PH/EA-45</b>		
	DATE : 1/03/06	ED/REV :V10	PAGE : 66 / 89

monitored by recording their C(V) characteristic when actuated with different types of voltage waveforms.

The C(V) set-up (presented in Figure 53) allows to apply different polarization waveforms to the RF MEMS switches (sin, square, triangular, square – bi-polar or uni-polar) and to record its C(V) characteristic by recording the evolution of an applied RF signal passing through the MEMS charged coplanar waveguide during switch actuation (the transmitted RF power variation is inversely proportional with the capacitance variation during actuation). The information concerning  $V_{pull-in}$ ,  $V_{pull-out}$ , capacitance variation and their evolution in time allow to obtain an insight of the dielectric charging/ discharging mechanisms.

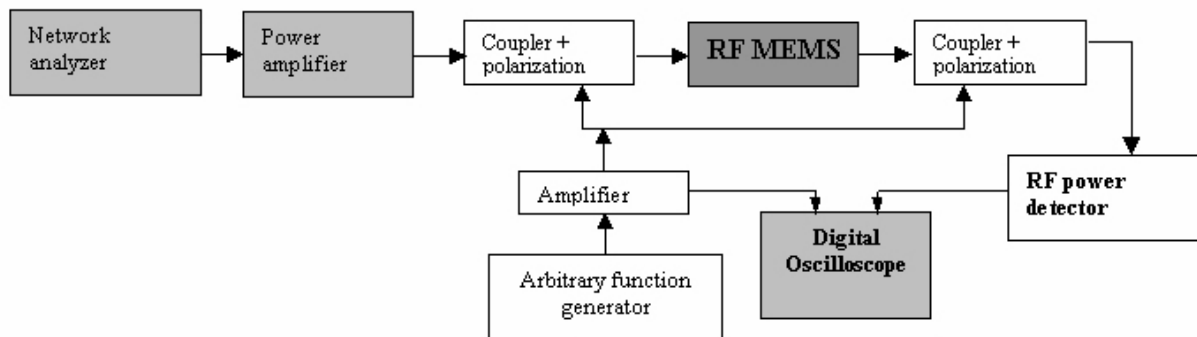
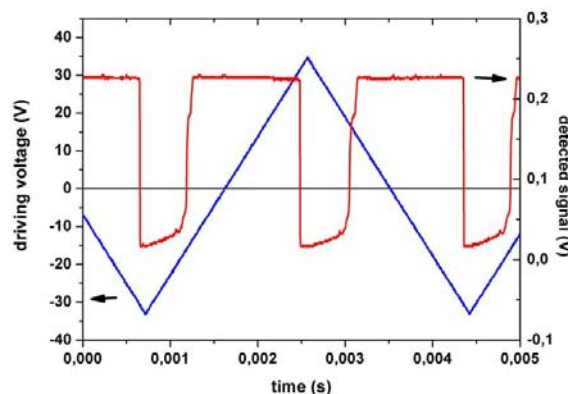
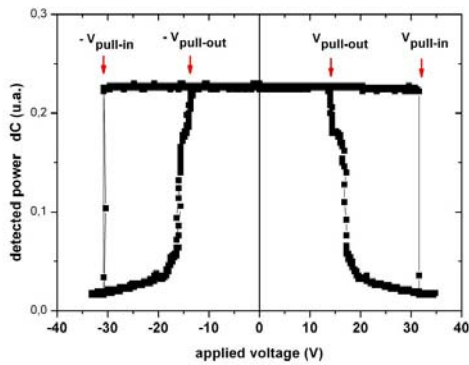


**Figure 53 : C(V) test set-up for RF-MEMS reliability.**

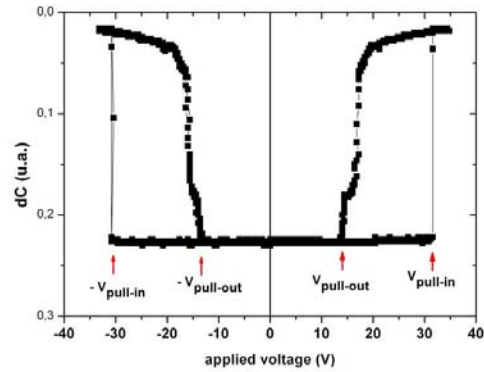
A typical evolution of the signal detected during MEMS switch actuation, proportional with the capacitance variation is given in Figure 54, for a switch (S35- type) realized with a 200 nm-thick Al<sub>2</sub>O<sub>3</sub> PLD on which a triangle waveform (35 V amplitude, 270 Hz) is applied.



**a.**



**b.**



**c.**

**Figure 54 : C(V) characteristics for a 200 nm-thick dielectric Al<sub>2</sub>O<sub>3</sub> PLD switch actuated with a triangular waveform (35 V amplitude, 270 Hz): a) driving voltage and detected power versus actuation time, b) XY-type curve of the detected power vs. applied voltage and c) the equivalent graph showing capacitance variation vs; applied voltage.**

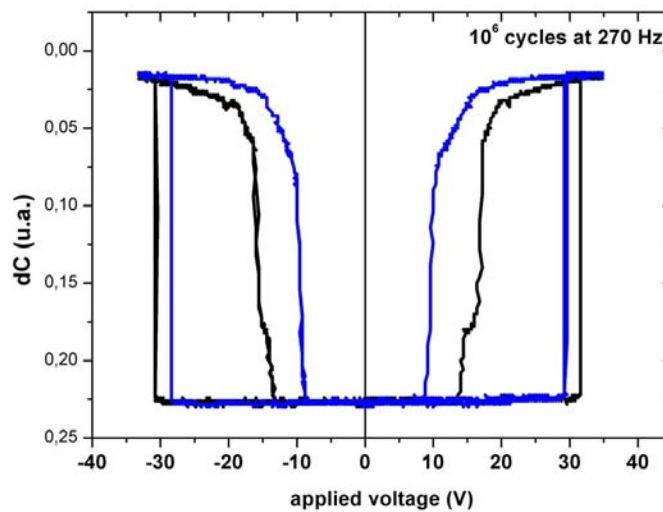


**Figure 55: C(V) curves to be used as an evaluation tool for the switch dielectric (black curve=ref, blue curve=after 10<sup>6</sup> cycles)**

For the same switch (200 nm-thick Al<sub>2</sub>O<sub>3</sub> by PLD) actuated using a triangular waveform of 35 V amplitude and different frequencies (between 15 and 270 Hz) the evolution of the  $V_{pull-in}$ ,  $V_{pull-out}$  and of the difference  $\Delta V = V_{pull-in} - V_{pull-out}$  is presented in Figure 55.

# Non hermetic RF MEMS

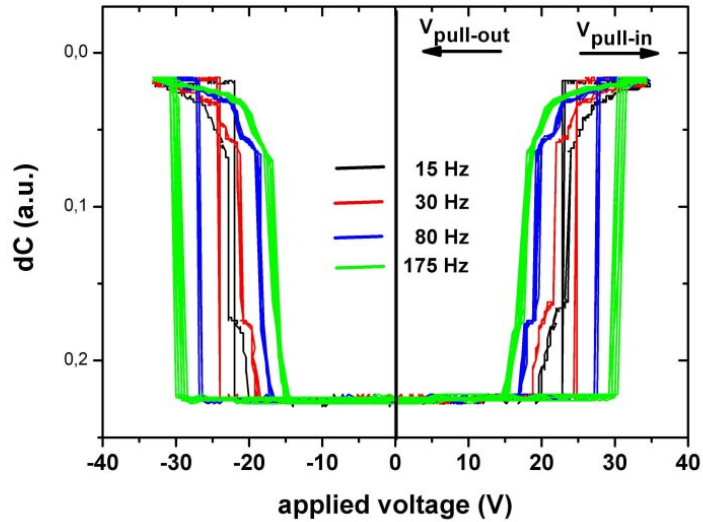
Ref: ASP-06-BO/PH/EA-45

DATE :  
1/03/06

ED/REV :V10

PAGE :  
68 / 89

With this evaluation criteria we will be able to address switch reliability as far as dielectric



charging is concerned.

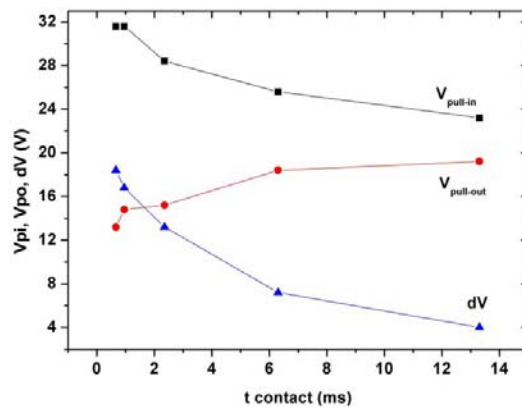
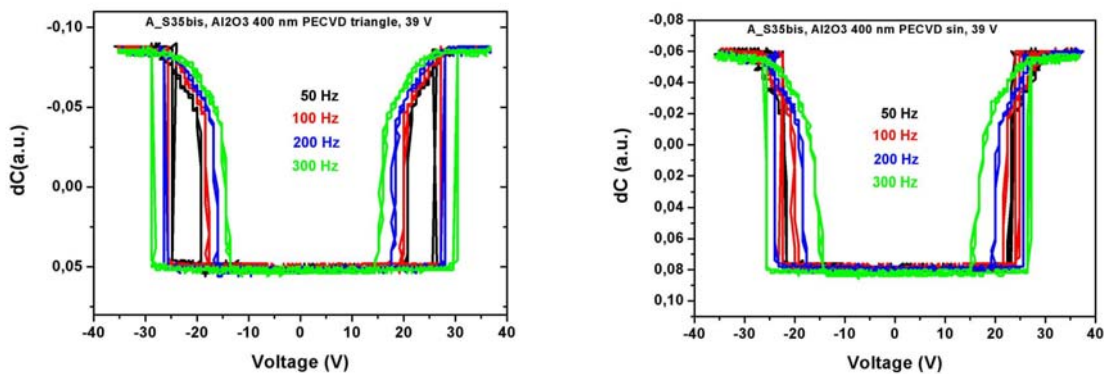


Figure 56 : Impact of contact time in down state position; evolution of V pull-in and pull-out vs contact time



# Non hermetic RF MEMS

Ref: ASP-06-BO/PH/EA-45

DATE :  
1/03/06

ED/REV :V10

PAGE :  
69 / 89

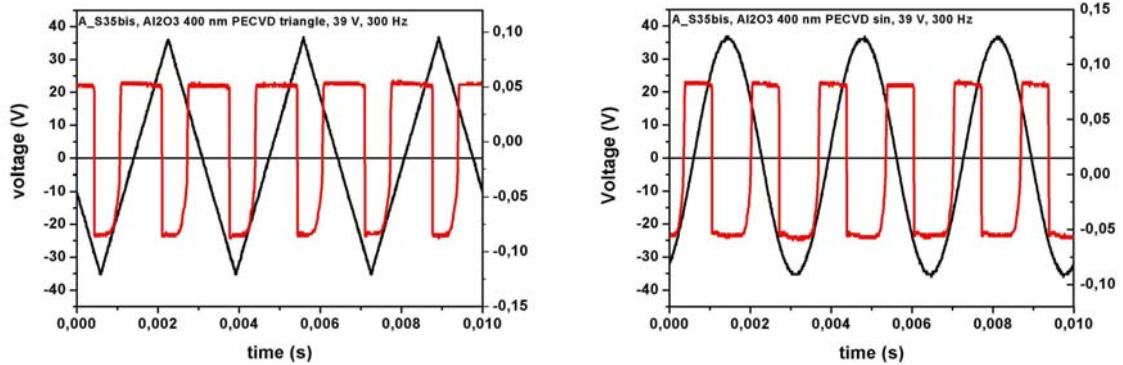


**Figure 57 : Impact of frequency and biasing waveform on 400 nm Al<sub>2</sub>O<sub>3</sub> PECVD, 39 V amplitude, bipolar and ambient atmosphere at various frequencies. Right side sinusoidal waveform, right side triangular waveform**

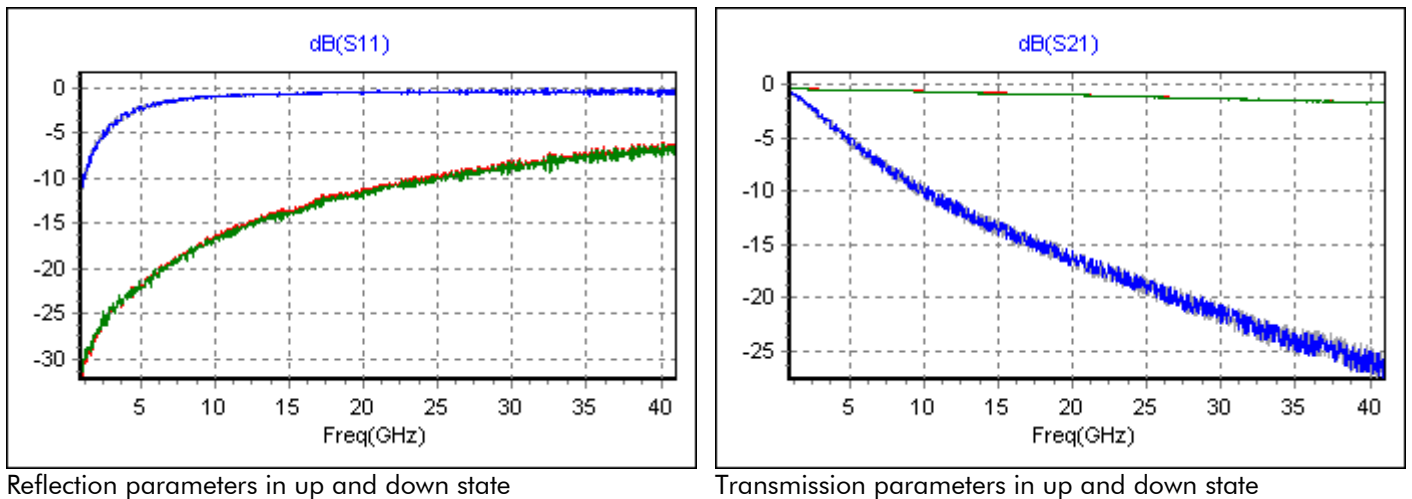
It shows in Figure 57 that the ramp used for the biasing of the component has an effect on the charging of the device.

<b>Non hermetic RF MEMS</b>	<b>Ref: ASP-06-BO/PH/EA-45</b>		
	DATE : 1/03/06	ED/REV :V10	PAGE : 70 / 89

### 10.3. RELIABILITY TEST RESULTS

Excepted for the total dose radiation tests, where both  $Al_2O_3$  dielectric and dielectricless capacitive switches has been used, on all the other tests we had to concentrate on available devices which were  $Al_2O_3$  dielectric capacitive switches.

Based on the above, we have characterized RF MEMS switches before and after ageing. Characterization was done on 200 nm thick  $Al_2O_3$  switches as presented in the test plan. Since the switches were very sensitive to dielectric charging mechanisms, we have used same reference devices from same wafer piece (wp) but at different location so that it is only stressed once. Prior to using this approach, we have shown that same reference device had repeatable s parameter characteristics in on and off state wherever its location on the wp as depicted in Figure 58.



Reflection parameters in up and down state

Transmission parameters in up and down state

**Figure 58 : Homogeneity of the results for switches taken from the same wp3.4 ref. S54, S64, biasing conditions : bipolar +/-45 V**

<b>Non hermetic RF MEMS</b>	<b>Ref: ASP-06-BO/PH/EA-45</b>		
	DATE : 1/03/06	ED/REV :V10	PAGE : 71 / 89

### 10.3.1. Thermal cycle tests

Corresponding standard : (ESA PSS-01-612 / Mil STD 883 – Method 1010, "B")

Evaluation stage : 500 cycles : -55/+125°C

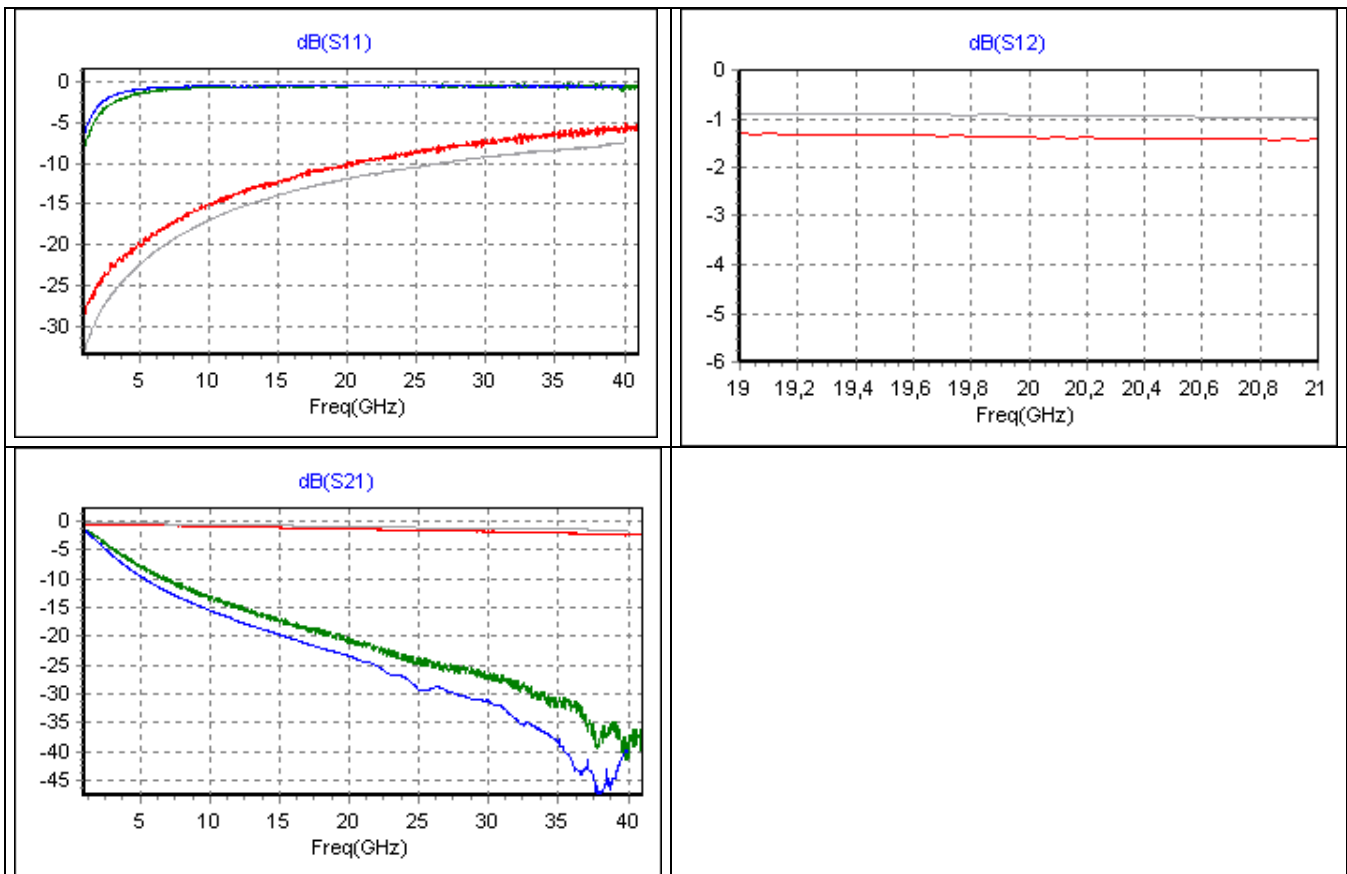


**Figure 59 : Impact of 500 cycles (-55; 125 °C) on S parameter of switch ref. S65 from wp3.1 taken at 2 locations. Before ageing (red (up state), green (down state)) and after ageing (grey (up state), blue (down state))**

<b>Non hermetic RF MEMS</b>	<b>Ref: ASP-06-BO/PH/EA-45</b>		
	DATE : 1/03/06	ED/REV :V10	PAGE : 72 / 89

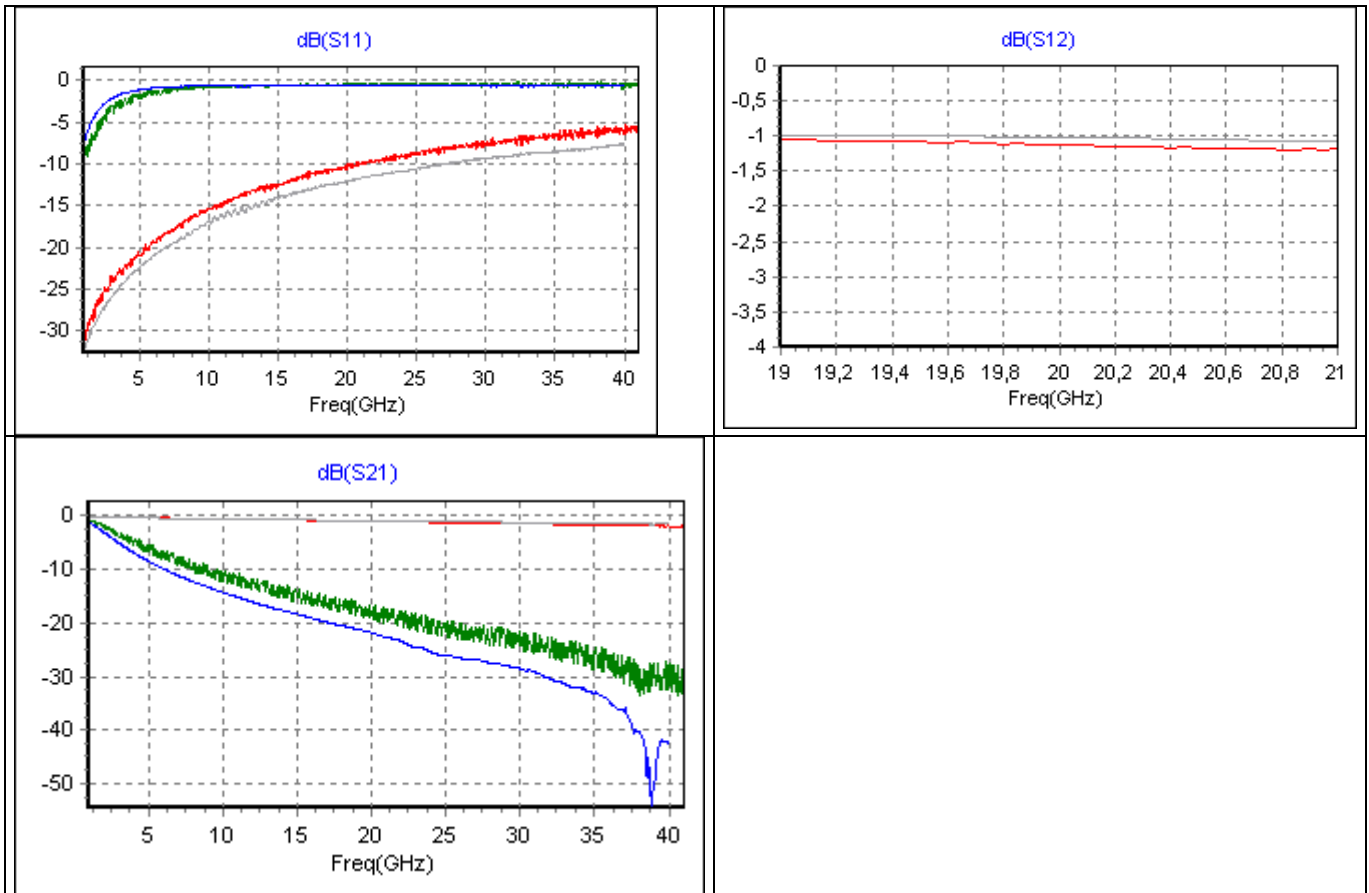


**Figure 60 : Impact of 500 cycles (-55; 125 °C) on S parameter of switch ref. S55 from wp3.1 taken at 2 locations. Before ageing (red (up state), green (down state)) and after ageing (grey (up state), blue (down state))**

500 rapid thermal cycling (-55/125 °C) have not affected the s parameter of the tested switches that are representative of the IRCOM capacitive switch technology using Al<sub>2</sub>O<sub>3</sub> as dielectric. What is shown in Figure 59 is that insertion loss in up state are somewhat improved from 1.4 dB to 0.9dB at 20 GHz. This can be partly explained by improved return loss improving from -10 dB to -12 dB after ageing. After visual inspection, we have noticed a slight warpage of the membrane, explaining the impact on the return loss in up state and the increase in the pull-in moving from 22.5 volts to 70 volts.

### **10.3.2. Thermal storage tests**

Corresponding standard : (ESA PSS-01-612 / Mil STD 883 – Method1008, "B")

First assessment stage : 260 h @ 125°C

# Non hermetic RF MEMS

Ref: ASP-06-BO/PH/EA-45

DATE :  
1/03/06

ED/REV :V10

PAGE :  
73 / 89

The obtained results are summarized in the following measured typical s parameter taken before and after temperature storage at 125 °C under Nitrogen flow.

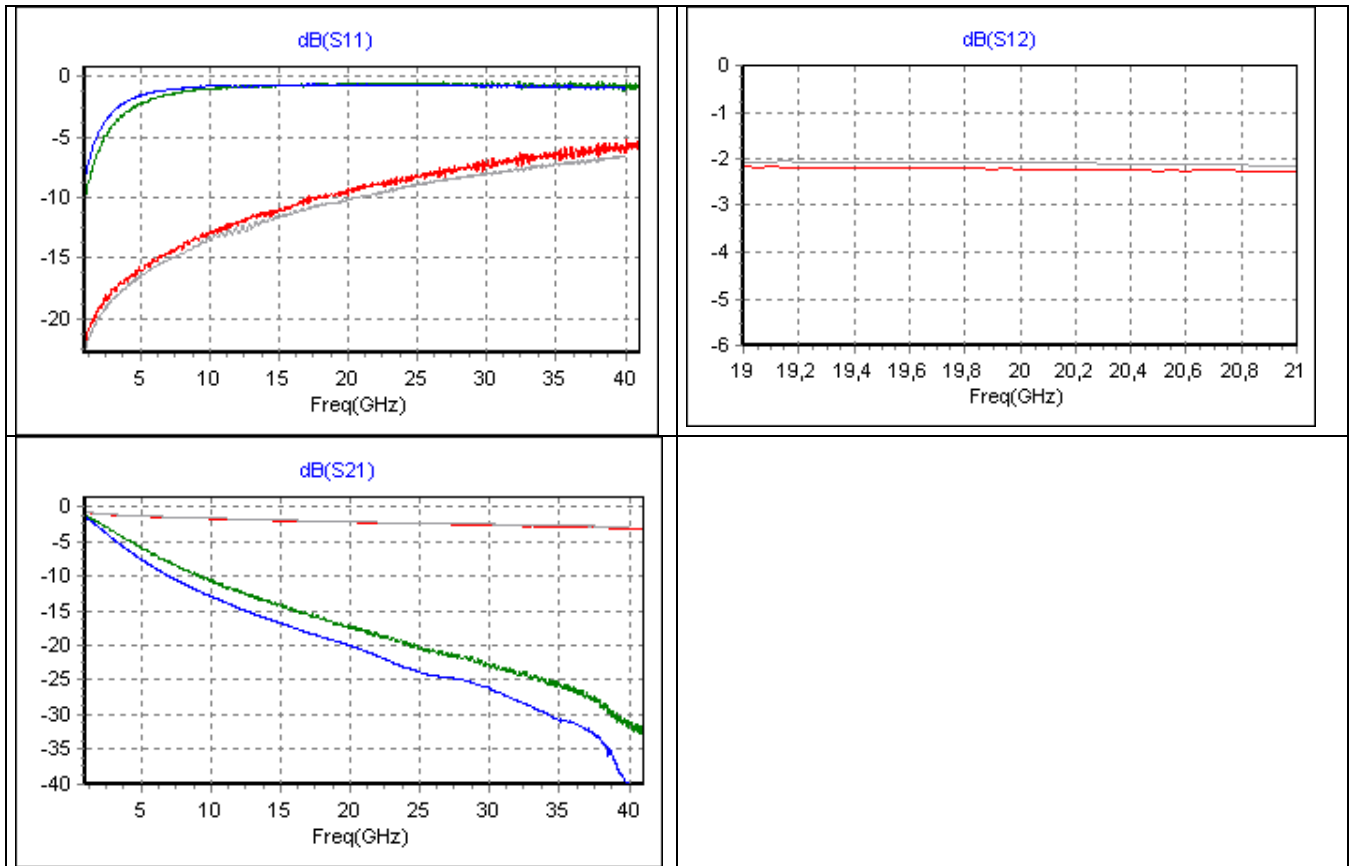
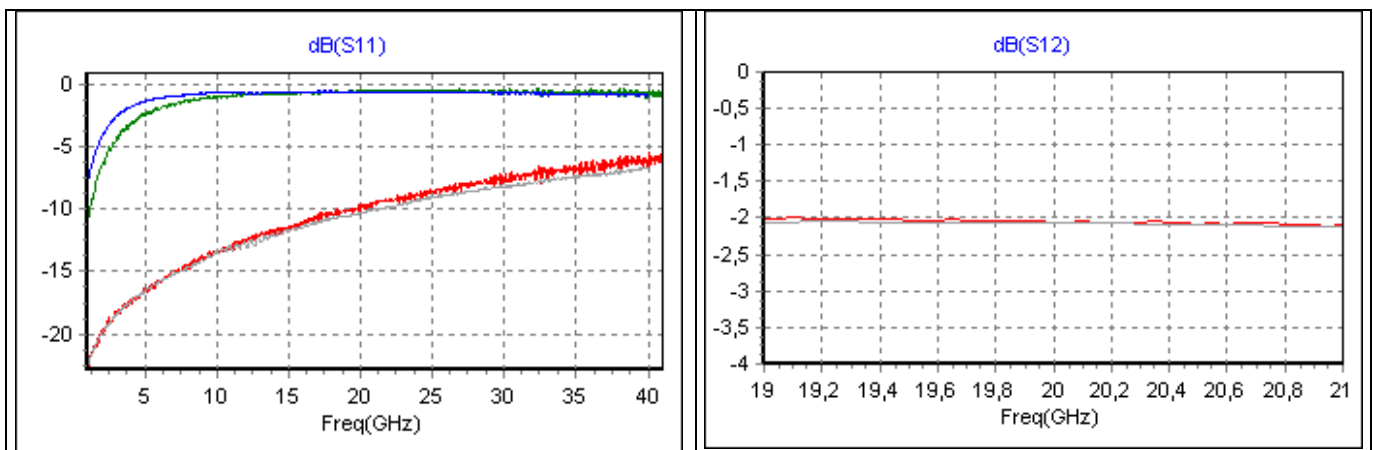


**Figure 61 : Impact of 260 hrs storage at 125 °C on S parameter of switch ref. S65 from wp3.3 taken at 2 locations. Before ageing (red (up state), green (down state)) and after ageing (grey (up state), blue (down state))**



<b>Non hermetic RF MEMS</b>	<b>Ref: ASP-06-BO/PH/EA-45</b>		
	DATE : 1/03/06	ED/REV :V10	PAGE : 74 / 89

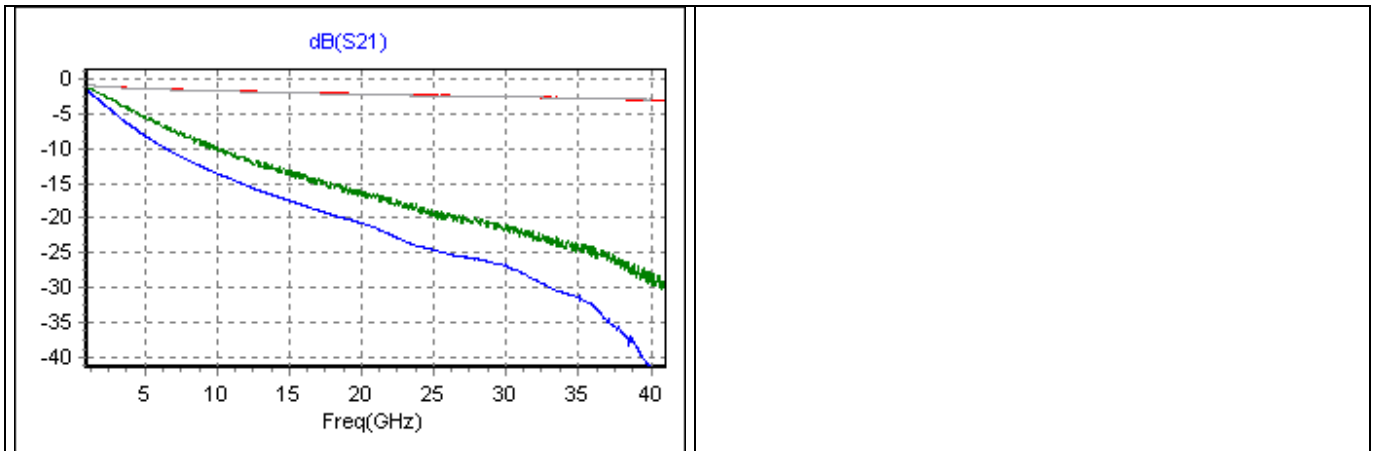


**Figure 62 : : Impact of 260 hrs storage at 125 °C on switch ref. S55 from wp3.3 taken at 2 locations. Before ageing (red (up state), green (down state)) and after ageing (grey (up state), blue (down state))**

Thermal storage during 260 hours at 125 °C have not affected the switches characteristics. The impact on the insertion loss in the up state can be considered to be within measurement accuracy. In this case, the shape of the membrane remains visually unchanged. Isolation is slightly changed because the measurement have been taken at a slightly higher biasing condition, increased by unwanted 10 %. Measured pull-in voltage was about 35 V for S65 structures and 42 V for stiffer S55 membranes.

As a conclusion, we can say that this type of ageing condition have not affected the electrical and mechanical behavior of the tested switches.

This aging condition has no effect on the dielectric charging phenomenon, which still remains very important for thin Al<sub>2</sub>O<sub>3</sub> dielectric (200 nm).

### **10.3.3. Electrical endurance tests**

#### *10.3.3.1. dielectricless switches*

We have performed accelerated life time test on the most promising technology developed within this contract (dielectricless switches),. As a simple but very efficient test, we have applied a monopolar biasing condition during a given period of time, with s parameter taken before and after stress. The results are presented in the curve below.

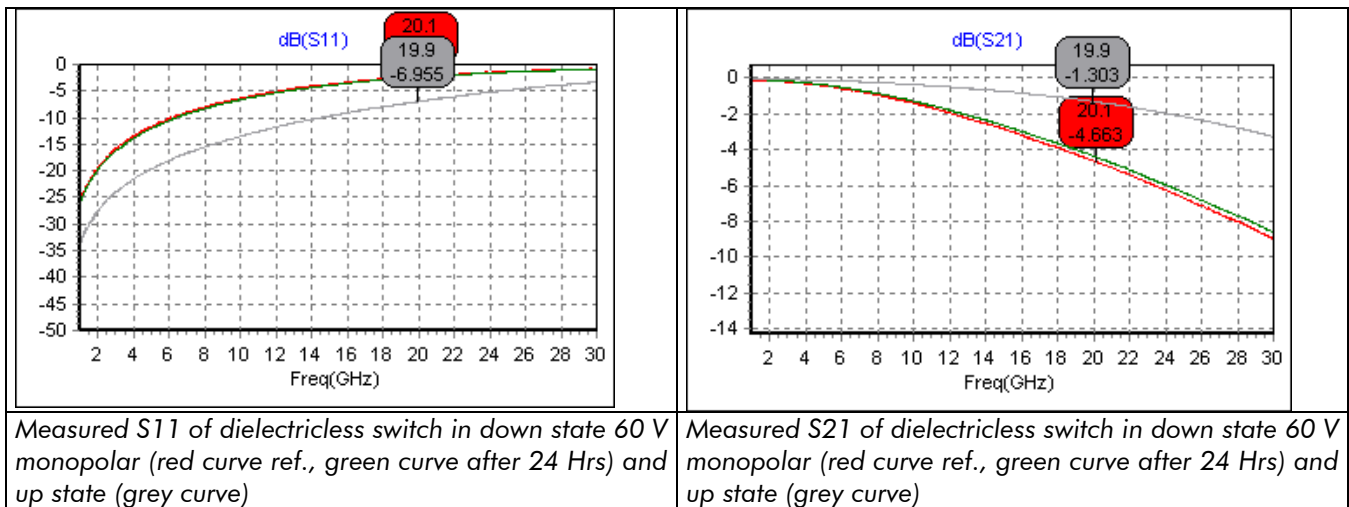


**Figure 63 : Aging test applied onto dielectricless switches from wp4.1**

It shows that no effect can be noticed after a 60 V monopolar stress step of 24 Hrs. It shows that the dielectric charging are not an issue anymore with that type of capacitive switch. The slight difference observed in down state is believed to be due to mechanical stress release within the membrane. The behavior in up state is unchanged. Compared to published data in the field of capacitive MEMS where most of the cumulated life time in down position are less than one hour, the result obtained above are state of the art, at least at European level.

In order to confirm that the switches remained not affected by applied monopolar biasing condition, we have measured C(V) curves before and after DC stress step.

In order to assess the reliability of air based dielectric RF-MEMS structures, we made very simple test using unipolar excitation. The dielectricless switches have been tested in open air, on a conventional probe station. The switch has been tested using a conventional microwave test set, and the transmission was recorded using a schottky detector and a digital oscilloscope. Our test equipment allowed to have data acquisition at regular rates (every 20 minutes was typical). The low frequency excitation voltage is a unipolar triangular signal. On conventional capacitive switches, this type of excitation usually leads to rapid failure of the switch, with permanent stiction within several minutes.

Our dielectricless based structure was subjected to this type of excitation and the C(V) characteristics were recorded after 24 hours cycling at 1Hz. No significant drift has been observed in the C(V) characteristics, as shown on the figures below.

<b>Non hermetic RF MEMS</b>	<b>Ref: ASP-06-BO/PH/EA-45</b>		
	DATE : 1/03/06	ED/REV :V10	PAGE : 76 / 89

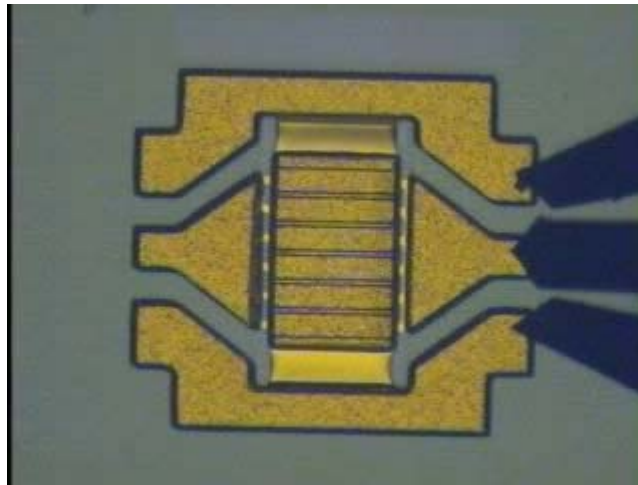
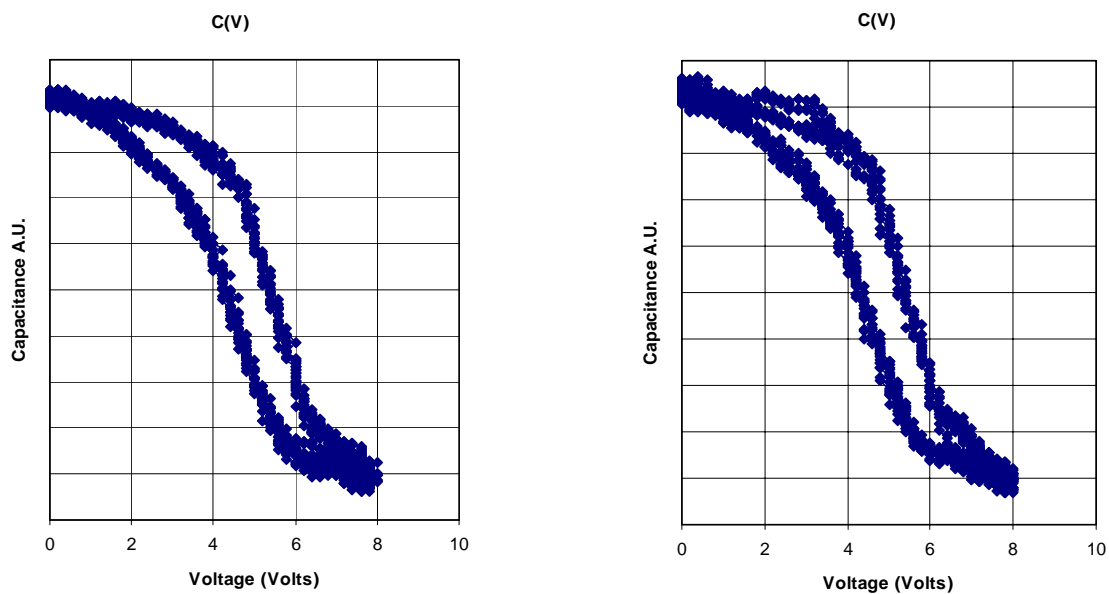


**Figure 64 : Typical dielectricless MEMS capacitive switch (wp4.1)**



(a) Initial C(V) characteristic

(b) After 24 Hours cycling (1Hz)

**Figure 65 : 1/C(V) characteristics of wp4.1 (dielectric less switch) before and after endurance On/Off testing**

### 10.3.3.2. $Al_2O_3$ dielectric switches

In the curves below we have stressed S35 switch with bipolar biasing conditions with a monitoring of the up and downstate capacitance until the device life time is reached. For the

<b>Non hermetic RF MEMS</b>	<b>Ref: ASP-06-BO/PH/EA-45</b>		
	DATE : 1/03/06	ED/REV :V10	PAGE : 77 / 89

device under test (S35, Al<sub>2</sub>O<sub>3</sub> 400 nm PECVD1), we have obtained a life time of 10<sup>6</sup> cycles at a frequency of 300 Hz which is close to best published results in Europe for capacitive switches [1].

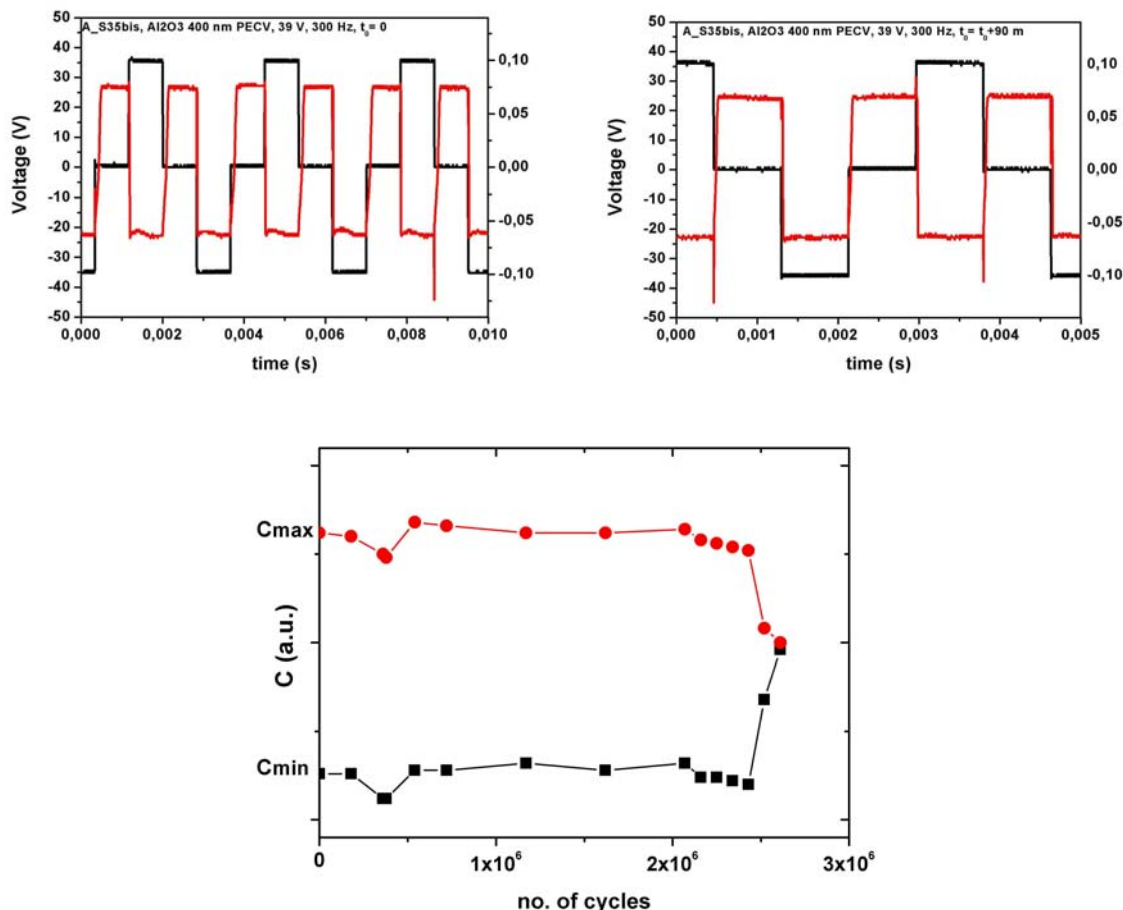


**Figure 66: Life time determination on 400 nm Al<sub>2</sub>O<sub>3</sub> PECVD, 39 V amplitude, square waveform, bipolar and ambient atmosphere at various frequencies. Determination of life time i.e. Cmin (C up) and Cmax (C down) evolution vs number of cycles**

[1] De Wolf I, van Spengen W.M., Modlinski R., Jourdain A., Witvrouw A. Fiorini P. and Tilmans H." Reliability and failure analysis of RF MEMS switches." Proc. 28th ISTFA 2002, pp. 275-281.

<b>Non hermetic RF MEMS</b>	<b>Ref: ASP-06-BO/PH/EA-45</b>		
	DATE : 1/03/06	ED/REV :V10	PAGE : 78 / 89

### 10.3.4. Total dose radiation test

#### 10.3.4.1. Test plan

Several steps are necessary to assess on dose radiation sensitivity :

- Electrical characterization that will serve as basis for radiation sensitivity. The testing was done on selected device, to avoid youth related degradation as much, as possible.
- Radiation at various stage (10 krad, 23.4 krad, 47 krad and 87 krad)
- Electrical characterization after radiation (Dwell time was set to <6 hours except for last radiation dose level) including C-V curves from which pull-in and pull-out are derived and for some piece of interest, S parameter measurements if accessible at ESA
- Annealing with duration and temperature to be compliant with the maximum allowed temperature by the MEMS switch which is less than 80 °C.
- Electrical characterization after annealing; including C-V curves from which pull-in and pull-out are derived

#### 10.3.4.2. Description of the pieces to be irradiated

After screening test performed by IRCOM, the wafer was diced in pieces (WP) that were mounted on golden coated brass, using room temperature curing resin. The wafer pieces (wp) were then numbered for tracing and ready to be mounted on the wp holder, manufactured specifically for this experiment. This stable vertical plate was compatible with DC probe mounting.

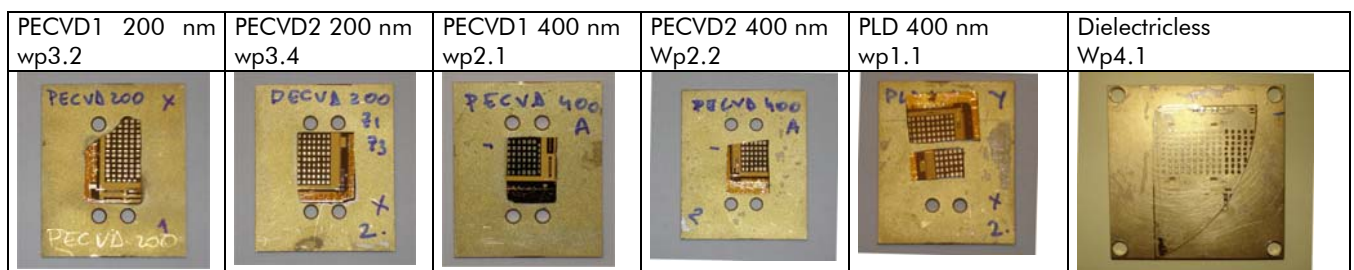


**Figure 67 : picture of the wp ready to be irradiated**

<b>Non hermetic RF MEMS</b>	<b>Ref: ASP-06-BO/PH/EA-45</b>		
	DATE : 1/03/06	ED/REV :V10	PAGE : 79 / 89

### 10.3.4.3. Test conditions

#### 10.3.4.3.1. General conditions

Radiation tests were done on 3 pieces including one unbiased piece. One reference piece is kept out of radiation chamber. Due to strong charging effect on dielectric switches, most of them are left un-biased.

#### 10.3.4.3.2. Radiation test conditions

Radiation test is performed under the following conditions :

Radiation source :                   Co60  
rate :            10 rad/min  
Temperature :     RT  
Total dose target: up to 100 krad

The radiation chamber based on a Co source is illustrated in the figure below.



**Figure 68 : backside view of the ESTEC Co Source radiation chamber**

<b>Non hermetic RF MEMS</b>	<b>Ref: ASP-06-BO/PH/EA-45</b>		
	DATE : 1/03/06	ED/REV :V10	PAGE : 80 / 89

We specify below the biasing condition of the RF MEMS switches under test :

- Most of the RF MEMS switches were left un-biased
- Except for some selected pieces where On/Off cycling conditions were applied (bipolar and monopolar)

The RF MEMS devices were not packaged so to avoid impact of packaging on the device life time. As a result, most of the devices were left un-biased. Some were biased using On/Off biasing conditions using DC probes as shown in the picture below. With our test set up and using specific GS DC probes, we were able to bias up to 4 switches at a time.

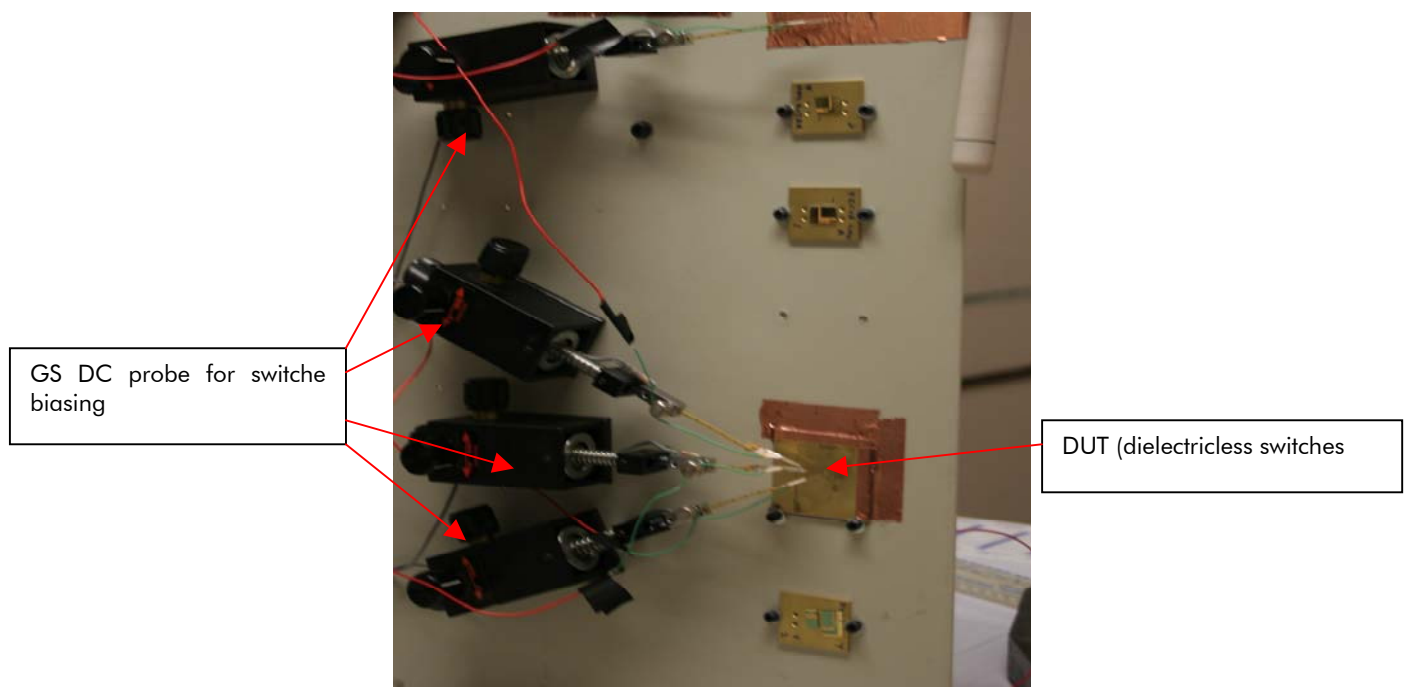


**Figure 69 : biasing configuration during irradiation phase**

#### 10.3.4.3.3. Screening

In the case of RF MEMS, burn-in condition are still not well defined. The goal of these test is to reject samples having process and youth related failure. These tests were done at IRCOM and were used to select the right switches to be further stressed.

- Note that applied biasing during screening and radiation phase are the same.

<b>Non hermetic RF MEMS</b>	<b>Ref: ASP-06-BO/PH/EA-45</b>		
	DATE : 1/03/06	ED/REV :V10	PAGE : 81 / 89

- Temperature : RT

#### *10.3.4.3.4.Electrical characterization*

If we use our background on dose radiation testing of ASICs, the intermediary measurements shall not exceed 2 hours. During each phase, we will have one reference sample in order to discriminate on measurement set-up and device handling/transport impact, actual stress applied to the devices.

The parameter to be measured are the following :

- 1/C(V) curves from which we can deduce Pull-in and Pull-out voltage
- S parameter measurements in up and down state at the end of the testing to confirm switch membrane integrity using S11 parameter in up-state and S21 parameter in down state. S parameter measurements have been extensively done at T0, so that they will be done after radiation if available at ESA ESTEC.

#### *10.3.4.3.5.Annealing*

Annealing is applied after completion of total dose radiation tests and first electrical test assessment. The idea is to apply temperature constraints that would not deteriorate the switch structure. The annealing temperature will be set to 70 °C with a duration of 1 week max. The idea there is to analyze the effect of annealing on the evolution of the pull-in and pull-out voltage. This topic was not fully covered because of time constraints and lack of proven standards, but some results obtained and presented in the last section of this report really opens some perspectives.

#### *10.3.4.4.Test results*

A radiation report will be available for ESA external diffusion. Nevertheless, we have reported herein all the results of this total dose radiation test campaign in the following.

##### 1/C(V) test conditions :

All 1/C(V) curves were taken (before and after irradiation) with a triangular waveform @ 50 and 200Hz to limit dielectric charging induced stresses. Note that all the ref. 1/C(V) curves have been performed at IRCOM. In order to check the capability of the system we have installed at ESA-ESTEC Labs, we have characterized few ref. switches to check on measurement system impact on these 1/C(V) curves.

<b>Non hermetic RF MEMS</b>	<b>Ref: ASP-06-BO/PH/EA-45</b>		
	DATE : 1/03/06	ED/REV :V10	PAGE : 82 / 89

Switches using Al2O3 as a dielectric :

As a reminder, we have summarized the main intrinsic mechanical characteristics switch S35 which had high yield in our fabrication process and is used very often in the assessment of the developed technologies.

L(μm)	W (μm)	w (μm)	K1 (N/m)	K2 (N/m)	Vp1 (V)	Vp2 (V)	f01 (kHz)	f02 (kHz)
280	120	80	21.8	42.9	28.44	39.91	50.48	70.83

Switch S35, g0= 2.2 μm, membrane thickness t= 0.5 μm, residual stress σ=50 and 100 Mpa

**table 10 : S35 mechanical characteristics**

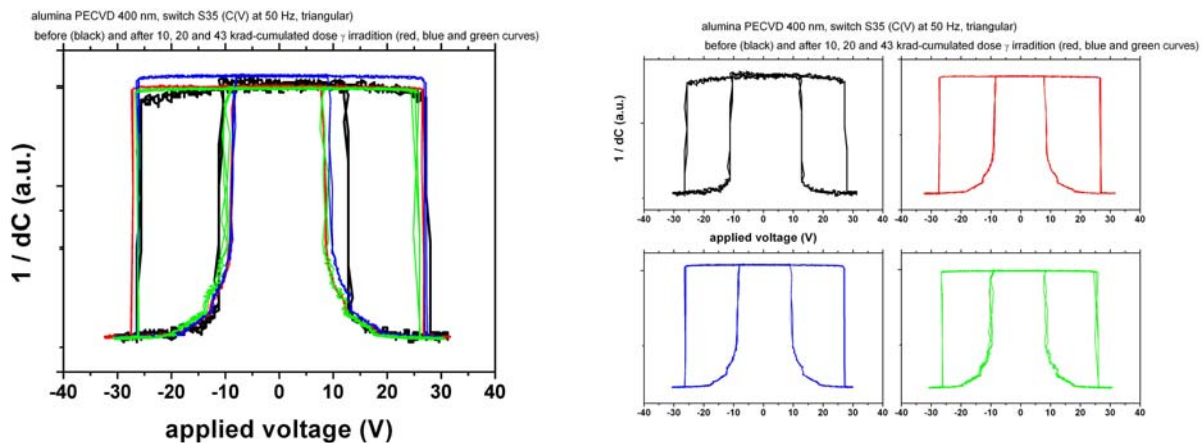


**Figure 70 : 1/C(V) of switch ref. S35 with alumina PECVD (wp2.2) (400 nm) – irradiated with a total dose of 43krad, unbiased conditions, test performed without annealing**

The curves illustrated in Figure 70 shows typical response of fully working switch with thin membrane and Al2O3 while actuating the switch with a bipolar triangular shape biasing condition. The down and up state cycle are recorded and perfectly centered due to symmetric charge injection into the dielectric.

V/ cumulated dose	0 krad (ref)	10 krad*	20 krad	43 krad
V <sub>pull-in</sub> (V)	27.3	26.47	27.2	25
V <sub>pull-out</sub> (V)	12	7.7015	8.6	7.3

\* the values may be shifted since for this specific 1/C(V) measurement the applied voltage was slightly higher than for the other measurements (1.58 X40 Vpp instead of 1.5 X40 Vpp)

**table 11 : Evolution of the V<sub>pull-in</sub>/V<sub>pull-out</sub> values (S35 switch)**

In the table shown above, the impact of total dose radiation on the tested RF switches with Al2O3 PECVD is summarized. The V<sub>pull-in</sub> remains within less than 10 % of the maximum value.

The  $V_{pull-out}$  decreases by about 40 % after the first 10 krad and then remains constant. One can assume that this can be due to residual carriers that may vanished with proper annealing. Note also that during the experiment the pads could not be grounded, this could also explain this voltage drop. The  $V_{pull-out}$  is also a more sensitive detection means for dielectric charging stiction mechanisms than that of  $V_{pull-in}$  because of the pull out forces generated that are lower.

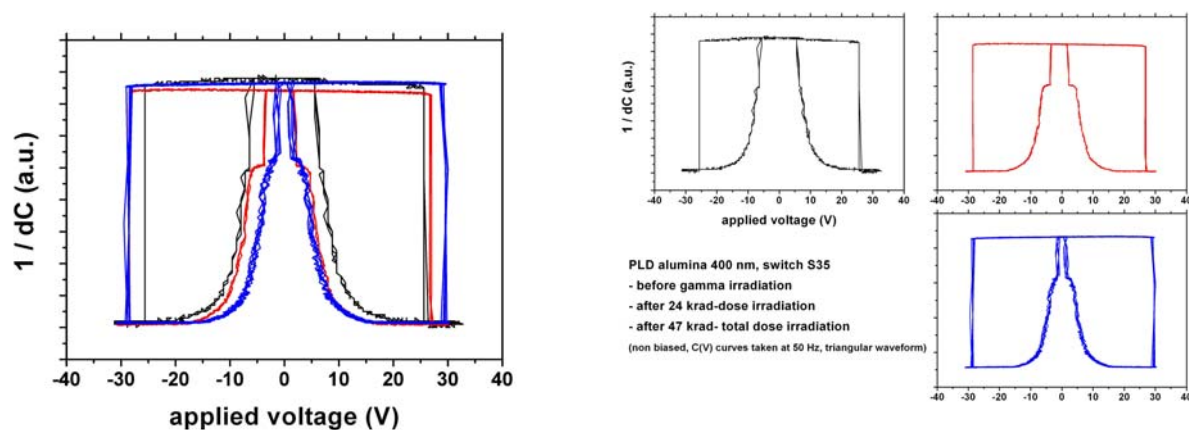


**Figure 71 : 1/C(V) of switch ref. S35 with Alumina PLD (wp1.1) (400 nm) – irradiated with a total dose of 47krad, unbiased conditions, test performed without annealing**

The 1/C(V) curves shows a quite unstable behaviour for the pull-out of the switch (<5V ) showing the starting point for a stiction phenomenon. The ref measurements shows also this weak  $V_{pull-out}$  relevant to the poor quality of the PLD Al<sub>2</sub>O<sub>3</sub> dielectric compared to the  $V_{pull-out}$  of 12 V for the same switch but with PECVD Al<sub>2</sub>O<sub>3</sub>. This point is also confirmed in previous paragraphs.

V/ cumulated dose	0 krad (ref)	24 krad	43 krad
$V_{pull-in}$ (V)	25.6	26.8	28.6
$V_{pull-out}$ (V)	5.6	1.6	1.2

**table 12 : Evolution of the  $V_{pull-in}/V_{pull-out}$  values (S35 switch):**

The table 12 shows that if the  $V_{pull-in}$  voltage remains constant after total dose irradiation test, note that the  $V_{pull-out}$  voltage drops dramatically to 1.6 Volts confirming degradation of the switch due to stiction relevant to dielectric charging.

Switches using air as a dielectric :

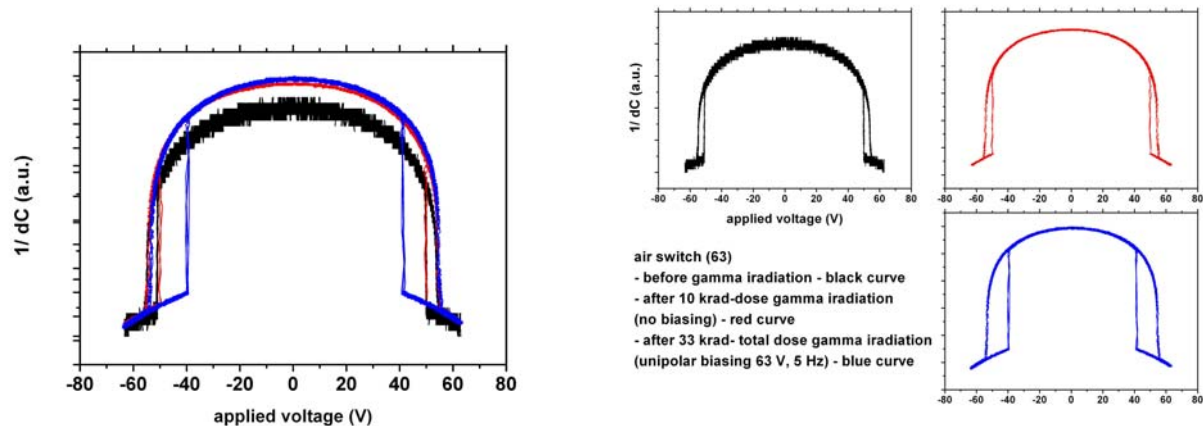


**Figure 72 : 1/C(V) of dielectricless switch (wp4.1) ref. S63 irradiated with a total dose of 33 krad, unbiased conditions, test performed without annealing**

The 1/C(V) is interesting because it shows that  $V_{pull-in}$  and  $V_{pull-out}$  are equal up to a low radiation dose of 10 Krad, where it is unchanged compared to reference. At 33 krad total dose, we can see a small shift of the  $V_{pull-out}$  due to either a mechanical aging of the membrane or residual carrier in the substrate which was not grounded during irradiation.

V/ cumulated dose	0 krad (ref)	10 krad*	33 krad**
$V_{pull-in}$ (V)	~50	~50	50
$V_{pull-out}$ (V)	-	-	-

\*no biasing

\*\* unipolar biasing 63 V, ~5 Hz for the last 23 krad dose (40 hours totak cycling, 720 060 cycles at 5 Hz equivalent to 11.42 hours in the down state)

**table 13 : Evolution of the  $V_{pull-in}/V_{pull-out}$  values ( dielectricless switch ref 63):**

#### 10.3.4.5. Summary

In the table below, we have summarized the results obtained on the switches stressed by total dose irradiation.

<b>Non hermetic RF MEMS</b>	<b>Ref: ASP-06-BO/PH/EA-45</b>		
	DATE : 1/03/06	ED/REV :V10	PAGE : 85 / 89

Device description/ switch type	Radiation total dose (krad)	Biasing condition	Measurements	Notes
PECVD 1 (400 nm) wp2.1			1/C(V) measurements @	
S33, S34, S35	88.3	non-biased	0, 46.9 and 88.3 krad	
S43, S45	88.3	non-biased	0, 46.9 and 88.3 krad	
S51, S55	88.3	non-biased	0, 46.9 and 88.3 krad	
PECVD 2 (400 nm) wp2.2				
S41	10.026 +74.813	biased (160 Vpp, 50 Hz, triangular)	failed, HS	
S33, S34, S35, S43, S45, S54	84.839	non-biased	0, 10, 20, 43 and 84.8 krad	
PLD (400 nm) wp1.1				
S44, S54	10.026+ 78.274	biased (160 Vpp, 50 Hz, triangular)	failed, HS	
S33, S35, S51, S64	88.3	non-biased	0, 24, 46.9 and 88.3 krad	
Switch air wp4.1				
S52, S63, S69	74.813	First 10.028 krad, non-biased, than biased with uni-polar square waveform, 63 V, ~ 5Hz	0, 10, 33 and 74.8 krad	
S68, S58	74.813	non-biased	0, 10, 33 and 74.8 krad	

#### 10.4. CONCLUSION ON RF MEMS SWITCH RELIABILITY ASSESSMENT AND PERSPECTIVES

In this section a test plan was presented and applied to the relevant RF MEMS switches which consisted of PLD and PECVD Al<sub>2</sub>O<sub>3</sub> dielectrics with 2 dielectric thicknesses and dielectricless switches. The test plan included thermal storage, thermal cycling, accelerated aging and radiation total dose testing. Based on s parameter measurements, and fast S<sub>21</sub> (V) charging curve, we have been able to study precisely the impact of the various stress applied on the switch intrinsic properties. It consisted of electrical (RF transmission) properties and mechanical properties ( $V_{pull-in}$  and  $V_{pull-out}$ ).

Thermal stress test flow was applied using 2 standards :

- Thermal storage (260 hrs – 125°C) on 200 nm Al<sub>2</sub>O<sub>3</sub> PECVD switches has clearly shown a minor impact on the switch : on similar device S parameter remain unchanged.

<b>Non hermetic RF MEMS</b>	<b>Ref: ASP-06-BO/PH/EA-45</b>		
	DATE : 1/03/06	ED/REV :V10	PAGE : 86 / 89

- Thermal cycling (-55°C, +125°C; 10°C/min, 500 cycles) on 200 nm Al<sub>2</sub>O<sub>3</sub> PECVD, if the devices remain functional, the pull-in voltage increased from 40 V to 70 V DC with improvement on the insertion loss in the up-state.

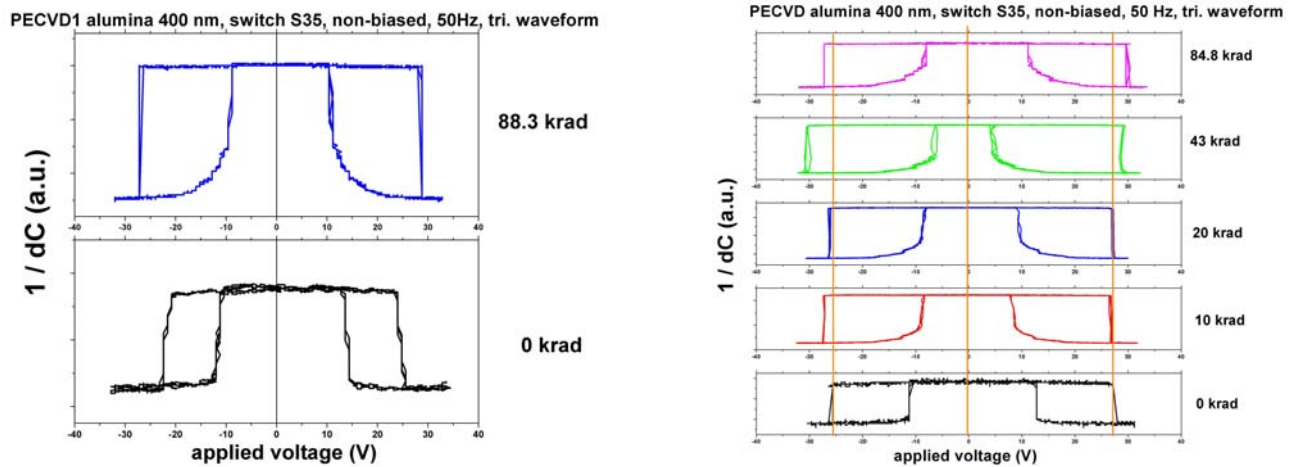
In both of the above cases the switches remained functional with either improved or same electrical properties.

We have also performed endurance testing, on the best device based on 400 nm thick Al<sub>2</sub>O<sub>3</sub> PECVD 400 nm and Dielectricless.

- For Al<sub>2</sub>O<sub>3</sub> dielectric switches, we have determined a life time of less than one hour cumulated time in down state which is limited by charging
- For Dielectricless switches we could not observe any failure relevant to charging effect. We anticipate some higher order failure mode due to mechanical fracture or strain that will appear at very high number of cycle but could not be observed within this study. We know that mechanical failure due to creep could appear and could be accelerated with higher stress of temperature on the membrane, but was not deeply analyzed within this study.

Reliability under gamma rays radiation is the topic on which we have spent the most efforts. All the type of switches (PLD and PECVD 400 nm Al<sub>2</sub>O<sub>3</sub> switches and dielectricless switches) have been stressed with and without biasing conditions. What we can extract as the main driver for these tests are the following :

- The dielectric with the worst charging signature such as 400 nm PLD Al<sub>2</sub>O<sub>3</sub> has shown failure related to stiction at a total dose of 88 krads. This result was obtained with unbiased condition.
- The dielectric (Al<sub>2</sub>O<sub>3</sub> 400 nm PECVD) with the best charging signature remain functional up to 88 krads with slight variation of the  $V_{pull-in}$  and  $V_{pull-out}$  that could be due to charge building up during irradiation. It shows that after a certain period of annealing time up to 168 hrs at 25 °C, this deviation is reduced. When on/off biased during irradiation the device goes to failure, because the actual life time without radiation of the device is too short for test duration. Total dose irradiation could though shorten this life time, but this could not be directly proven during the present study.



(a)  $1/C(V)$  curves before and after total dose radiation, using exact same characterization set-up (ref. PECVD1 Al<sub>2</sub>O<sub>3</sub> thickness 400 nm)

(b) Evolution of the  $1/C(V)$  curves along the total dose irradiation test campaign. Last testing point was done after 1 week annealing at 25 °C (ref. PECVD2 Al<sub>2</sub>O<sub>3</sub> 400 nm)

**Figure 73 :  $1/C(V)$  curves before and after several total dose irradiation steps of 400 nm thick Al<sub>2</sub>O<sub>3</sub> PECVD based switches**

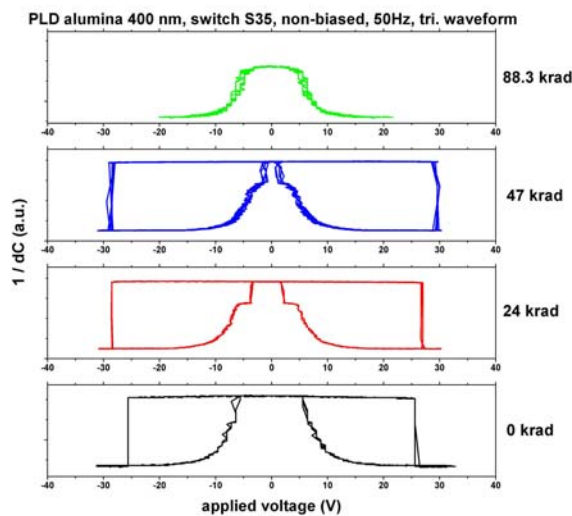


**Figure 74 :  $1/C(V)$  curves before and after several total dose irradiation steps of 400 nm thick Al<sub>2</sub>O<sub>3</sub> PLD based switches**

- After gamma ray irradiation of dielectricless switches, we could not see any failure on the device tested with or without uni-polar stress condition. These devices are very robust and promising for a space use because they have been demonstrated to be not sensitive to total dose radiation test up to **74.8 krad** while operating with On/Off uni-polar biasing. Under these conditions, we have demonstrated up to  $3 \cdot 10^6$  cycles at a frequency rate of 5 Hz. Several device have been tested with same conclusions.

<b>Non hermetic RF MEMS</b>	<b>Ref: ASP-06-BO/PH/EA-45</b>		
	DATE : 1/03/06	ED/REV :V10	PAGE : 88 / 89

- We have found some perspective for further research for total dose sensitive devices (PLD 400 nm). We have noticed some failure recovery after annealing (1 week at 25 °C) on some switches. This open some new ways for investigation on the impact on gamma rays on RF MEMS devices, trying to understand what exactly happen within the dielectric. This is illustrated by the figure below.

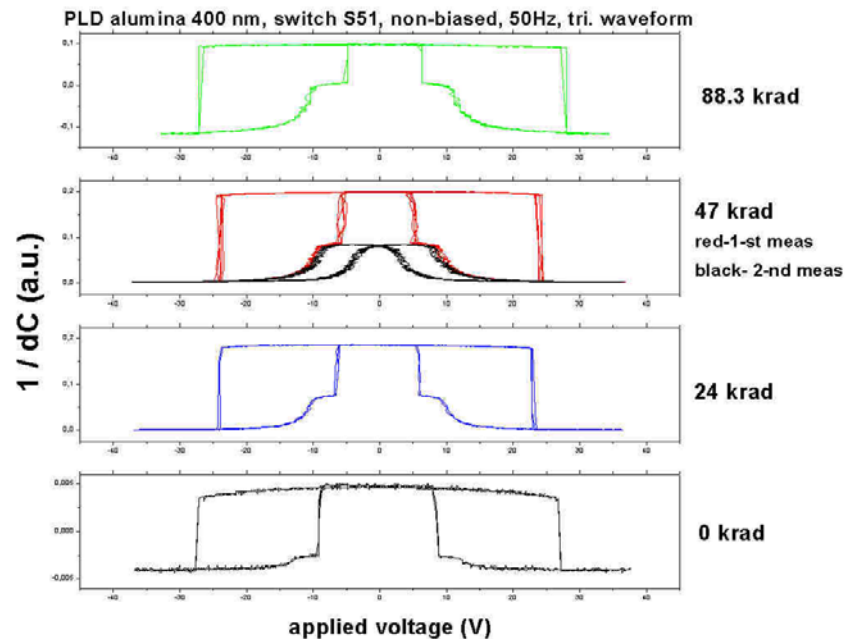


**Figure 75 : Example of switch recovery after annealing (168 H 25°C) and failure noticed after 47 krad total dose**

## 11. GENERAL CONCLUSION

### Report structure

This final report has first described the context of RF MEMS application within satellite payloads, followed by the specifications and conceptual design of the  $\mu$ switches that have been fabricated within the study. We have also presented and developed capacitive switch design methodology based on two approaches. The first one relayed on standard shunt capacitive switches on coplanar wave (CPW) transmission lines using stiff bridges and various dielectrics. The dielectrics are deposited using two deposition system processes pulsed laser deposition (PLD) for Teflon, diamond like carbon (DLC) and Al<sub>2</sub>O<sub>3</sub>, and plasma enhanced chemical vapor deposition (PECVD) for Al<sub>2</sub>O<sub>3</sub>. Process flow relevant to PLD and PECVD were also presented and discussed.

Another approach which is very innovative and promising, was based on dielectricless capacitive switches for which reliability concerns, such as dielectric charging have been suppressed.

<b>Non hermetic RF MEMS</b>	<b>Ref: ASP-06-BO/PH/EA-45</b>		
	DATE : 1/03/06	ED/REV :V10	PAGE : 89 / 89

Prior to reliability study, device selection was made in order to only test device for which process repeatability was clearly explained which dielectric and/or process sequence is applicable or not.

Finally, a test plan was presented and applied to the relevant RF MEMS switches which consisted of PLD and PECVD Al<sub>2</sub>O<sub>3</sub> dielectrics with 2 dielectric thicknesses and, air as a dielectric. The test plan included thermal storage, thermal cycling, accelerated aging and radiation total dose testing. Based on s parameter measurements, and fast S<sub>21</sub> (V) charging curve, we have been able to study precisely the impact of the various stress applied on the switch intrinsic properties. It consisted of electrical (RF transmission) properties and mechanical properties ( $V_{pull-in}$  and  $V_{pull-out}$ ).

Technology and process assessment :

Technology wise this study has helped us to select the most promising material and processes to enable high reliability switches with reduced environmental and packaging constraints.

Firstly, in order to reduce dielectric charging problems, we have investigated the dielectric quality impact on switch reliability. The alumina thin film quality was assessed through AFM roughness tests, OH- contamination through FT-IR and breakdown voltage. The alumina layer deposition (obtained by PLD or PECVD) was optimized especially from the point of view of thickness and composition (in the case of PECVD deposition). We have then established design rules for the Al<sub>2</sub>O<sub>3</sub> layer thicknesses : 400 nm thick film is definitely the best for any kind of Al<sub>2</sub>O<sub>3</sub> layer, because it makes the breakdown voltage far enough from the actual pull-in voltage of the switch. We also found out PECVD process more reproducible than PLD process, because this latter system had still to go through some more industrial optimization.

In order to reduce mechanical stiction phenomenon, we have studied of protective layers thin films of PTFE and tetrahedral carbon (ta-C) were fabricated on top of the alumina layers. They are supposed to increase the hydrophobic characteristics of the alumina dielectric and the switch resistance in humid environments. However, it was noticed that the PTFE layers deposited by PLD presented a high roughness, which could potentially influence- via the sacrificial layer- the membrane shape (which should be as smooth as possible for a perfect contact with the dielectric during on-state actuation). Based on these findings, this PTFE protection coating was then given up.

For the thin ta-C (20 nm) deposited by PLD on top of the alumina layers (~220 nm thickness) it was observed that the fabricated switches were drastically damaged once the actuation voltage is applied. The phenomenon was explained by a strong electrical conduction mechanism in the thin ta-C layer (similar to the field emission from the same type of material) under the strong electrical field applied to the switches. This was verified and confirmed by including the same type of sandwich layer (alumina+ ta-C) in MIM-type capacitances (with gold electrodes) implemented in a microwave coplanar waveguide (CPW) line (Figure 40) and by performing I(V) measurements on these structures. It remains at this stage not physically understood. This promising approach was also given up.

Lastly, in order to remove any effect of dielectric charging, we have designed and validated dielectricless switches. These switches look very promising for future space relevant application assuming that the corrugated membrane process is controlled and that the finding to improve Con/Coff ratio is further validated.

<b>Non hermetic RF MEMS</b>	<b>Ref: ASP-06-BO/PH/EA-45</b>		
	DATE : 1/03/06	ED/REV :V10	PAGE : 90 / 90

Reliability assessment :

Thermal stress test flow was applied using 2 standards :

- Thermal storage (260 hrs – 125°C) on 200 nm Al<sub>2</sub>O<sub>3</sub> PECVD switches has clearly shown a minor impact on the switch : on similar device S parameter remain unchanged.
- Thermal cycling (-55°C, +125°C; 10°C/min, 500 cycles) on 200 nm Al<sub>2</sub>O<sub>3</sub> PECVD, if the devices remain functional, the pull-in voltage increased from 40 V to 70 V DC with improvement on the insertion loss in the up-state.

In both of the above cases the switches remained functional with either improved or same electrical properties.

We have also performed endurance testing, on the best device based on 400 nm thick Al<sub>2</sub>O<sub>3</sub> PECVD 400 nm and Dielectricless switches.

- For Al<sub>2</sub>O<sub>3</sub> dielectric switches, we have determined a life time of less than one hour cumulated time in down state which is limited by charging
- For dielectricless switches we could not observe any failure relevant to charging effect. We anticipate some higher order failure mode due to mechanical fracture or strain that will appear at very high number of cycle but could not be observed within this study .We know that mechanical failure due to creep could appear and could be accelerated with higher stress of temperature on the membrane, but was not deeply analyzed within this study.

Reliability under gamma rays radiation is the topic on which we have spent the most efforts. All the type of switches (PLD and PECVD 400 nm Al<sub>2</sub>O<sub>3</sub> switches and dielectricless switches) have been stressed with and without biasing conditions. What we can extract as the main driver for these tests are the following :

- The dielectric with the worst charging signature such as 400 nm PLD Al<sub>2</sub>O<sub>3</sub> has shown failure related to stiction at a total dose of 88 krad. This result was obtained with unbiased condition.
- The dielectric (Al<sub>2</sub>O<sub>3</sub> 400 nm PECVD) with the best charging signature remain functional up to 88 krad with slight variation of the  $V_{pull-in}$  and  $V_{pull-out}$  that could be due to charge building up during irradiation. It shows that after a certain period of annealing time up to 168 hrs at 25 °C, this deviation is reduced. When on/off biased during irradiation the device goes to failure, because the actual life time without radiation of the device is too short for test duration. Total dose irradiation could though shorten this life time, but this could not be directly proven during the present study.
- After gamma ray irradiation of dielectricless switches, we could not see any failure on the device tested with or without uni-polar stress condition. These devices are very robust and promising for a space use because they have been demonstrated to be not sensitive to total dose radiation test up to **74.8 krad** while operating with On/Off uni-

<b>Non hermetic RF MEMS</b>	<b>Ref: ASP-06-BO/PH/EA-45</b>		
	DATE : 1/03/06	<b>ED/REV :V10</b>	<b>PAGE :</b> 91 / 91

polar biasing. Under these conditions, we have demonstrated up to  $3 \cdot 10^6$  cycles at a frequency rate of 5 Hz. Several device have been tested with same conclusions.

- For total dose sensitive devices (PLD 400 nm), we have noticed some failure recovery after annealing (1 week at 25 °C) on some switches. This open some new ways for investigation on the impact on gamma rays on RF MEMS devices, trying to understand what exactly happen within the dielectric. This is illustrated by the figure below.